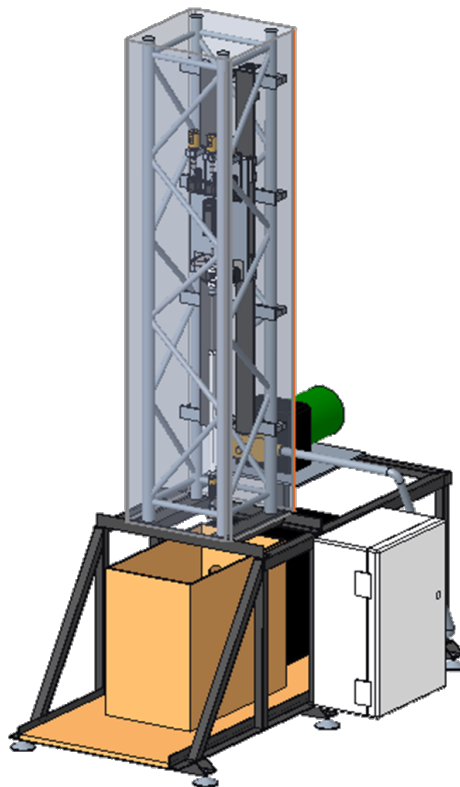




TU Clausthal
Clausthal University of Technology



Drillbotics® -Phase 1 Design Report
International University Competition
2023/2024 Group B (Physical Rig)

Clausthal University of Technology
Institute of Subsurface Energy Systems
Date: December 30nd, 2023

Table of Contents

List of Figures	V
List of Tables	VII
List of Abbreviations	VIII
Symbol register	IX
Guidelines taken into account	X
1 Introduction and Objectives	1
2 Team and workflow	3
3 Rig Design	8
3.1 Machine Bed	8
3.2 Rock Sample Receiver	9
3.2.1 Magnetic Field Analysis	10
3.3 Traverse	11
3.4 Top Drive	12
3.5 Rig Electronics and Power Supply	13
4 Circulation System	15
4.1 Rig Plumbing and Mud Handling	15
4.2 Cutting Transport Calculation	16
4.3 Pressure Loss Calculation	22
5 Hoisting System	28
5.1 Force Calculations	28
5.2 System Stability and Improvements	29
5.2.1 Calculation of Bending Moment	29
6 Rotation System	31
6.1 Drill Motor	31
6.2 Rotary Table	32
6.3 Collet chuck joint	32

6.4	Drillpipe	32
6.4.1	Limit Calculations	33
6.4.2	Buckling Limit Calculation	33
6.4.3	Burst Limit Calculation	35
6.4.4	Torsional Limit Calculation	35
6.5	Drill Bit	36
7	Steering System	37
7.1	Downhole Steering Unit	37
7.2	Surface Actuation Unit	37
7.3	Internal mesurment unit	39
7.4	Maximum Inclination	40
8	Mechatronic System Architecture	41
8.1	CAN Bus	41
8.2	Can bus timing	42
8.3	Actuator Modules	43
8.3.1	Motor Module	43
8.3.2	Rotary Table Module	44
8.3.3	Relay Module	44
8.3.4	Hoisting Module	45
8.3.5	IMU Module	46
8.3.6	Flow-meter Module	47
8.3.7	WOB/Hookload Module	49
8.3.8	Steering Module	50
8.3.9	Depth Module	50
8.3.10	Clock	51
8.3.11	E-Stop Module	51
8.4	Sensor Calibration	52
8.4.1	IMU	52
8.4.2	Strain gauge	53
8.4.3	Absolute depth measurement unit	54
8.5	Development and Design of PCB	55
9	Network Architecture	58
9.1	Modular Setup and Intra-Module Communication	59

9.2	CAN-Bus Translator and MQTT Broker	60
9.2.1	CAN-Bus Translator	60
9.2.2	MQTT Broker	61
9.3	Client Setup	62
9.4	Response time and latency	63
9.4.1	Setup	63
9.4.2	Evaluation	63
10	Software Architecture	65
10.1	Connection Handling	66
10.1.1	Multi-Threading and Thread-Safe Programming	67
10.2	Digital Rig Counterparts	67
10.3	Rig Component Manager	69
10.4	The State Machine	70
10.4.1	Default State	71
10.4.2	Initiation State	71
10.4.3	Park State	73
10.4.4	Drilling State	73
10.4.5	Survey State	74
10.4.6	Steering State	76
10.5	The Commander	81
10.6	Engineering Control Interface:	82
10.7	GUI	84
10.8	Logger	85
10.9	Drilling Performance Optimizations	86
10.9.1	Mechanical Specific Energy	86
10.9.2	ROP Surface Plot Generation	87
11	Test and Evaluation	89
11.1	Setup	89
11.1.1	Calibration	89
11.2	Evaluation	92
11.2.1	Initial Observations and Drilling Process	92
11.2.2	Commander Performance and State Transitions	92
11.2.3	Z-Axis Motor Error	94
11.2.4	Trajectory	96
11.2.5	Additional Observations	96

12 End of Well Report	99
12.1 Third-Party Interface	100
13 Further Rig Considerations	101
13.1 Power Consumption	101
13.2 Rig Handling and Transportation	101
13.2.1 Design for Mobility	101
13.2.2 Quick Release Couplings	101
13.2.3 Transport Configuration	101
13.2.4 Weight Specifications	102
13.3 Rock Sample Handling	102
13.4 Rig Upscaling	102
13.4.1 Innovative Transmission Methods	102
13.4.2 Torque Transmission and Limitations	103
13.4.3 BHA Inclination and Steering	103
13.5 Funding Plan and Sponsorship Update for 2023/24	104
13.5.1 New Organizational Structure	104
13.5.2 Sponsorship Acquisition Phase	104
13.5.3 Current Sponsorship Status	104
13.5.4 Financial Overview	104
13.6 Acknowledgement	106
14 Safety Consideration and Risk Analysis	107
14.1 Safety Plan	107
14.1.1 Safety Protocols and Training	107
14.1.2 Physical Barriers and Protective Measures	107
14.1.3 Communication and Emergency Response	107
14.1.4 Human Factor	107
14.1.5 Risk Assessment and Continuous Improvement	108
14.1.6 Technical safety	109
14.1.7 Human safety	112
14.1.8 Communication safety	117
15 Appendix	118
15.1 A: Data and Assumptions	118
A Bibliography	125

List of Figures

3.1	Rig Base First Level	8
3.2	Rig Base Second Level	9
3.3	Rock sample receiver with coil	10
3.4	Rig Traverse Backside	11
3.5	Rig overview	11
3.6	Top-Drive Cage	12
3.7	TN-S network	14
4.1	Mud Handling	15
4.2	Slip velocity derived by Moore ´s correlation	17
4.3	Slip velocity derived by Moore ´s correlation	18
4.4	Borehole schematic	20
4.5	Connection for Hoses and Cable	21
4.6	Fluid-flow schematic	22
4.7	Fanning chart	26
5.1	Hoisting System	28
5.2	Bending Moment on Spindle	30
6.1	Design value K variation	34
6.2	Diamond Coated Drill Bit	36
7.1	3D-view of the BHA	38
7.2	Side view of the BHA showing the geometrical minimal steering radius	38
7.3	Cross-section view of the BHA schowing the steering mechanism and most internal components.	39
7.4	BHA	40
8.1	CAN bus schematic	41
8.2	Quick data schematic	42
8.3	Can time diagram	43
8.4	Motor control unit	44
8.5	Rotary table control unit	44
8.6	Relais switching unit schematic	45
8.7	Hoisting system control unit schematic	45

8.8	Electrical schematic of the Sensor Unit	46
8.9	Flow-Meter and Pressure-sensor schematic	47
8.10	Flow-Meter and Pressure-sensor UML	48
8.11	WOB Measurement module schematic	49
8.12	Wheatstone full and half bridge	49
8.13	Steering module	51
8.14	IMU Calibration Concept Visualization	52
8.15	Calibration Device	53
8.16	KiCad Circuit Diagram	55
8.17	KiCad PCB Diagram	56
8.18	Finished PCB	56
9.1	Network Architecture	58
9.2	Modular Setup	60
9.3	MQTT Broker	61
9.4	Recorded dead time of the rig	64
10.1	Connection Handling	66
10.2	Rig Manager	69
10.3	Test-Trajectory with 20 Surveys	71
10.4	Initiation Procedure	72
10.5	Drilling Procedure	74
10.6	Survey Procedure	75
10.7	Steering Procedure	76
10.8	Projection in TF -coordinate and reference-coordinate system	78
10.9	High side Visualization	79
10.10	Pad-Force decomposition	81
10.11	Automation of the State machine	82
10.12	Engineering Control Interface	83
10.13	GUI	84
10.14	Logging Process	85
10.15	Example of a ROP Surface Plot	88
11.1	Accelerometer Data and Corresponding Angle	90
11.2	Comparison Original Pitch and Analytic Pitch	91
11.3	Duration Distribution	93
11.4	Drilled Trajectory	96

List of Tables

3.1	Rig components' dimensions	9
4.1	Pump power requirement rotary drilling	27
6.1	Buckling limit according to K variation	35
9.1	Hookload Module	59
9.2	Dead Time and Recorded Time for Each Case	64
10.1	WOB Component Setup	68
11.1	Constants from the Testwell Setup	89
11.2	Duration's spent in each drilling state	94
14.1	Technical safety	111
14.2	Human safety	116
14.3	Communications safety	117
15.1	Drilling hole and rock data	118
15.2	Rig Specifications	118
15.3	Overview of Data and Actuator	119
15.4	Drilling fluid data	119
15.5	Drill pipe data	120
15.6	Stabilizer / downhole BHA data	120
15.7	Bit data	120
15.8	Calculation Results	121

List of Abbreviations

ADC	Automated Drilling Control	APH	Automated Pipe Handling
BHA	Bottom Hole Assembly	bb1	Barrel
BHP	Bottom Hole Pressure	BLDC	Brushless DC Motor
BOP	Blow Out Preventer	CAD	Computer Aided Design
CAN	Controller Area Network	CSV	Comma-Separated Value
DHM	Down Hole Motor	DP	Drill Pipe
FEMM	Finite Element Method Magnetics	FFT	Fast Fourier Transformation
Fifo	First In, First Out	GUI	Graphical User Interface
IMU	Inertial Measurement Unit	IMU	Internal Measurement Unit
IoT	Internet of Things	ISR	Interrupt Service Routine
JSON	JavaScript Object Notation	KOP	Kick Off Point
LAN	Local Area Network	LSB	Least Significant Bit
LWD	Log while Drilling	MD	Measured Depth
MPD	Managed Pressure Drilling	MQTT	Message Queuing Telemetry Transport
MPT	Mud Pulse Telemetry	MWD	Measurement While Drilling
NOV	National Oilwell Varco	PF	Pad Force
PFV	Pad Force Vector	PID	Proportional-Integral-Derivative
PLC	Programmable Logic Controller	PCB	Printed Circuit Board
PTB	Push the Bit	PTV	Projected Target Vector
QoS	Quality of Service	RCD	Rotating Control Device
ROP	Rate of Penetration	RPM	Revolutions Per Minute
RT	Rotary Table	RPI	Raspberry Pi
SMD	Surface Mount Device	SWOB	Setpoint WOB
TD	Total Depth	TF	Tool Face
TP	Target Point	TV	Target Vector
TVD	True Vertical Depth	UI	User Interface

Symbol register

A	Area	α	Azimuth
B	Magnetic flux density	β	Beta (Angle/Phase Offset)
Δ	Change/Difference	γ	Inclination
e	Euler's Number	F	Force
g	Gravitational Acceleration	h	Height
I	Current	i	Imaginary Unit
j	Imaginary Unit	KD	Controller Constant
KI	Controller Constant	KP	Controller Constant
l	Length	m	Mass
N	Number of turns	μ	Friction Coefficient/Micro
μ_0	Vacuum permeability	μ_r	Relative permeability
Φ	Magnetic flux	P	Pressure
π	Pi (3.14159...)	ρ	Density
q	Complex Rotation	q^*	Conjugate Complex
τ	Tau (Torque)	θ	Steering Angle
θ_c	Corrected Steering Angle	t	Time
Θ	Magnetomotive force	V	Volume
x, y, z	Cartesian Coordinates		

Guidelines taken into account

Guidelines

i. Student Biographies

Included in Chapter: **2**, Page **4**

ii. A description of your safety plan that is appropriate for the project

Included in Chapter: **14**, Page **107** and in Chapter **3.5**, Page **13**

iii. Engineering sketches or drawings of the rig concept, mechanical and electrical and auxiliary systems, if any, that explain your design assumptions

Along the whole report as an example the full BHA setup is shown in Figure **3, 3**,

iv. Include any design notes and calculations regarding rig, drillstring and other limitations for the particular modules used in your models.

Cutting transport Calculation given in Chapter: **4.2**

Pressure Loss Calculation given in Chapter: **4.3**

Whole DP-Calculations are given in Chapter: **6.4**

v. A block diagram/flowchart of the modeled control system architecture. Describe the key features. The response time of measurements, data aggregation and control algorithms should be estimated. Explain how individual measurements are used in the control code. Are they all given equal weight, and if not, what criteria is used to assign importance?

Included in Chapter: **10** and Page: **58**

vi. Since this is a directional drilling problem, be sure to include how downhole data is used for steering and other drilling aspects? Judges are looking for a description of the principles being applied to directionally steer the wellbore and hit the required targets with the intent to score the maximum number of points.

Trajectory is explained in Chapter: **10.4.2**

Exact calculations for the Steering are given in Section: **10.4.6**

vii. Proposed user interface/data display that shows the drilling progress in real time.

An example of the GUI and Engineering Interface is shown on Page: **82-84**

viii. Cost estimate and funding plan

Funding Plan and Price list are given in Chapter: **13.5**

ix. Key features for any models/modules and control software. What drilling dysfunctions are addressed?

Included in Chapter **8.3**

x. Proposed data handling, i.e., inherent time delays and uncertainty.

Included in Chapter: **8** and in Section **9.4**

xi. The Phase I design report should include a discussion regarding the major design concept as modeled (mechanical and otherwise) with respect to the feasibility for use on today's working rigs? If not, what would be needed to allow implementation?

Included in Chapter: **13.4**

1 Introduction and Objectives

The 2023 Drillbotics® competition marks the eighth consecutive year that a team from Clausthal University of Technology (TU Clausthal), Germany, is participating. This year, TU Clausthal has chosen again to compete in Group B, the physical rig challenge. According to the 2023 Drillbotics® competition guidelines, the objective of this category is "to design and build a miniature drilling rig that can autonomously drill a directional well through a homogeneous rock sample according to a specified plan." Drilling automation is increasingly gaining interest from the oil and gas industry, equipment manufacturers, and research organizations. Automating and digitizing the drilling process is believed to enhance safety during operations, reduce drilling time, increase accuracy in data acquisition, improve well placement and quality, and lower costs. In automated drilling systems, operating parameters are optimized by acquiring relevant data, analyzing it, and adjusting the parameters without human intervention. Ideally, the system would reach tier three automation, a stage where it can make decisions and act autonomously. The purpose of this report is to present a well-conceived design plan for a small-scale drilling robot that incorporates key features commonly encountered in the field. The design emphasizes the implementation of innovative ideas and solutions not typically used in conventional drilling processes, particularly for the demands of directional drilling. This approach utilizes an automated process that, from a human intervention perspective, requires only the activation of the start button. The proposal is structured into several chapters, which are outlined as follows:

Introduction and Objectives

The Introduction and Objectives of this report sets the objectives of the proposal and the project. A brief description of the proposal content is explained herein.

Team and workflow

Team members, as well as supervising and advising staff, are introduced here. Also, workflow and distribution of workload is described.

Mechanical Rig Design

This chapter explains the rig structure design, the machine bed, the fluid system, the hoisting system, the rotation system, the steering system, the sled, and the top drive system. The rig's dimensions are listed. Further, calculations for pressure loss and cutting transport are presented.

Mechatronic System Architecture

Within this chapter the mechatronic system, the used sensors, the different actuators and as well the bus system that distributes the operational data will be described. Also, the calibration of the sensors before the drilling operations are discussed.

Network Architecture

This chapter describes the setup of the network, which facilitates remote operations and enables work distribution among different parties. The architecture is designed to ensure efficient communication, data transfer, and collaboration across various locations, while maintaining high levels of reliability. It outlines the technical specifications, hardware and software components.

Software Architecture

The software architecture section delves into the complete state machine utilized for operating the rig, detailing the defined states and transitions. It also presents the Automated Instance, which enables autonomous operation of the rig. Additionally, this section covers aspects related to logging, data management, and the interfaces that facilitate interaction between different software components and users.

Test and Evaluation

This chapter details the early tests conducted and highlights potential improvements and critical malfunctions that could arise during operation.

End of Well Report

This chapter includes the data acquisition and structure that will be generated after the well is drilled, and it will detail how this data is processed for potential improvement.

Further Rig Considerations

This chapter includes the anticipated total power consumption of the rig, a funding and budgeting plan, a calculation for the rig's shipping weight and a discussion how the rig's design concept could be upscaled.

Safety Consideration and Risk Analysis

This chapter discusses the risks and potential harmful events that could occur during the test. Precaution and mitigation plan are set to prevent undesirable events, including the rig structure design and drilling automation system. This report is an update of the previous design report submitted for the Drillbotics® international university competition 2023.

2 Team and workflow

This year, the TU Clausthal's Drillbotics® team will once again be working under the supervision of senior researchers from the Drilling and Production Department at the Institute of Subsurface Energy Systems. The team is also receiving assistance from the SPE (Society of Petroleum Engineers) Student Chapter e.V. Since 2023, the TU Clausthal Drillbotics team is an integral part of the TUC-SPE Student Chapter e.V., with all its members belonging to the SPE.



TUC Drillbotics®
learning & creation

Supervisors:

Prof. Dr. Philip Jaeger

Erik Feldmann, M.Sc

Dr. –Ing. Carlos Andres Paz Carvajal

One staff member of the drilling and production department of the Institute of Subsurface Energy Systems, who was himself three times a participant in previous Drillbotics® competitions, will serve as advisor to the current team.

Advisors:

Wolfgang Hollstein, M.Sc.

Dominik Orgel, M.Sc.

The competition team of the TU Clausthal consists of five students from different engineering backgrounds.

Student Team:

Charalampos Soilemezidis

Previously attained degree: B.Sc. in Energy and Resources
Current degree: M.Sc. in Petroleum Engineering
Expected graduation date: Fall 2025
Role and responsibilities: Teamleader, Administrative, Electronics, Software, IT

Ali Alkhawaja

Current degree: B.Sc. in Geo-Energy Systems
Expected graduation date: Winter 2024
Role and responsibilities: Administrative, Drilling Technology

Kanaan Al-Masarain

Current degree: B.Sc. in Mechanical Engineering
Expected graduation date: Fall 2024
Role and responsibilities: Mechanic, Steering-Tool Specialist

Farouk Jamali

Current degree: B.Sc. in Mechanical Engineering
Expected graduation date: Winter 2024
Role and responsibilities: Mechanics, Network, IT

Nils Hamlet

Current degree: B.Sc. in Computer Science
Expected graduation date: Winter 2024
Role and responsibilities: Network, IT, AI

Liban Ahmed Yusuf

Previously attained degree: B.Sc. in Petroleum and Natural Gas
Current degree: M.Sc. in Petroleum Engineering
Expected graduation date: Summer 2025
Role and responsibilities: IT, AI

Based on the previous experiences of teams from Clausthal University of Technology in the Drillbotics® competition, it has been observed that distinct distribution of workload and clear communication among team members are crucial for success. Consequently, when working on a project of this scale with a relatively small team, setting clear objectives and splitting the workload become essential. This season, a strategic decision was implemented, requiring every team member to approach the project in an interdisciplinary manner. This means that specific tasks are distributed among two or more team members, allowing for a comprehensive overview of the entire project and more effective error prevention. For instance, the tasks in the rig mechanics were divided between two people, programming was handled by two individuals, administrative activities were shared among three members, and responsibilities related to mechatronics and automation were evenly distributed between two members. To further enhance this approach, smaller tasks are defined in work packages and made public throughout the institute. This initiative allows students who are interested in specific tasks, but not necessarily in participating entirely in the competition, to opt for these individual tasks. This method not only facilitates greater student engagement but also enriches the project with diverse inputs. Each year a total of 10 work packages is planned for release some work packages are presented in Figure 2 and 2, upon accomplishment an certificate will be issued. The team leader plays a crucial role in ensuring smooth communication between team members and tracking overall progress. Regular team meetings are scheduled on Friday, supplemented by smaller working groups that meet frequently during the week. These weekly team meetings enable all team members and the advisor to maintain an up-to-date understanding of the project's status. Any uncertainties are discussed with the advisor, allowing for efficient resolution. For efficient project management and progress monitoring, the team utilizes an online cloud-based platform. This system enables team members to work from home, ensuring flexibility and continued productivity.

TODO

WORK PACKAGE

TITEL : Development of Vibration Measurement Unit for the Rig

WOPA.Nr: 0003

CONTEST YEAR: 2023/2024

ISSUED BY: C. SOILEMEZIDIS

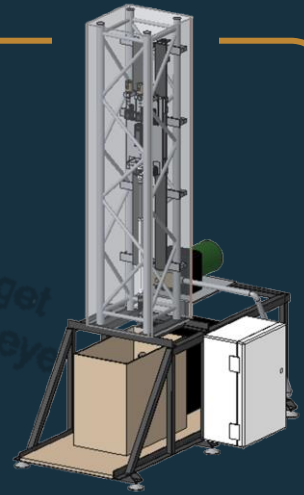


Supervisor: M.Sc. Wolfgang Hollstein
E-Mail: who11@tu-clausthal.de

Advisor: B.Sc. Charalampos Soilemezidis
E-Mail: cso19@tu-clausthal.de



Drillbotics® is a prestigious international university competition where teams from around the globe collaborate to design and develop an autonomous directional drilling rig. This challenge merges engineering expertise with innovation, aiming to revolutionize the drilling industry while promoting collaboration and hands-on experience.



OBJECTIVE

DEADLINE: 31st February 2024

To design, develop, and integrate a vibration measurement unit that can effectively monitor and measure vibrations in the drillstring.

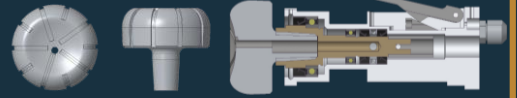
DESCRIPTION

The student will embark on a project to create a specialized vibration measurement unit for the rig. The process begins with familiarizing oneself with Kicad, a software essential for PCB design. Under guidance, the student will draft and refine the PCB layout tailored for the specific requirements of the rig's measurement unit. Concurrently, the student will delve into basic C programming, crafting code to enable the measurement unit's functionality. This unit will be equipped with a dedicated sensor, whose primary role is to detect and quantify vibrations in the drillstring. Throughout the project, the student will receive valuable advice on the design nuances of the module and best practices in coding for optimal performance.

OUTCOME

Upon project completion, the rig will be equipped with a fully operational vibration measurement module, offering real-time insights into drillstring vibrations. The student, having gone through this comprehensive exercise, will be adept at using Kicad for PCB design and will have foundational knowledge in programming microcontrollers using C.

CONTACT



drillbotics@tu-clausthal.de

Student Work Packages

Students interested in hands-on experience and applying their academic knowledge are encouraged to take on these work packages. If you're keen to express interest, apply for a work package, or seek more details, please contact us. It's up to you to decide whether the task aligns with your skills and interests. If you lack experience in the highlighted fields (in BLUE), seize the opportunity to learn with us. Don't worry; the primary requirement is motivation. This journey is all about learning and growing.

Certificate of Completion for Work Packages

Upon successful and timely completion of the designated work package, and if the specified outcomes are met, a certificate will be issued to the individual responsible for the task. This certificate stands as an official recognition of the individual's diligence, skill, and commitment to the project.

Complexity grade

1. 20h	3. 60h	5. 100h
2. 40h	4. 80h	6. >100h



Complexity grade

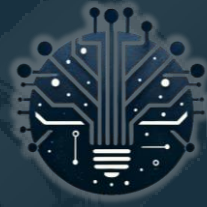
6
5
4
3
2
1



TUC Drillbotics®
learning & creation



MECHANICAL



ELECTRICAL



ADMINISTRATIV



PROGRAMMING



AI



DESIGN

TODO

WORK PACKAGE

TITEL : Design and Manufacturing of BHA and Drill Pipe Stabilizers

WOPA.Nr: 0007

CONTEST YEAR: 2023/2024

ISSUED BY: C. SOILEMEZIDIS

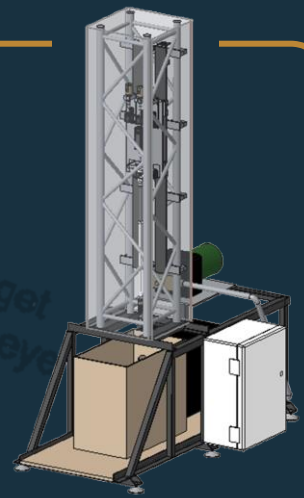


Supervisor: M.Sc. Wolfgang Hollstein
E-Mail: who11@tu-clausthal.de

Advisor: B.Sc. Charalampos Soilemezidis
E-Mail: cso19@tu-clausthal.de



Drillbotics® is a prestigious international university competition where teams from around the globe collaborate to design and develop an autonomous directional drilling rig. This challenge merges engineering expertise with innovation, aiming to revolutionize the drilling industry while promoting collaboration and hands-on experience.



OBJECTIVE

DEADLINE: 31st December 2023

To conceptualize, design, and oversee the manufacturing process of new BHA and drill pipe stabilizers.

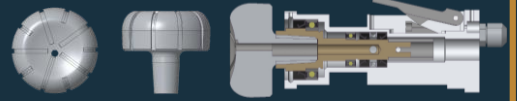
DESCRIPTION

The task at hand revolves around the pivotal role of constructing new BHA and drill pipe stabilizers. The student's responsibilities kick off with selecting appropriate materials for the components. Utilizing Creo, the student will draft the design blueprints for the stabilizers. Once the design phase is concluded, the student will manage the manufacturing workflow. While the drill pipe stabilizers can benefit from 3D printing techniques, the BHA necessitates a metal-based material. A significant challenge to address during the project is the wear process the stabilizers undergo, especially in directional sections of the borehole.

OUTCOME

Upon completion, the rig will be fortified with newly designed and manufactured BHA and drill pipe stabilizers. The student will have developed expertise in material selection, CAD design using Creo, 3D printing applications, and oversight of the manufacturing process. Additionally, they will gain insight into the wear challenges associated with directional drilling.

CONTACT



drillbotics@tu-clausthal.de

Student Work Packages

Students interested in hands-on experience and applying their academic knowledge are encouraged to take on these work packages. If you're keen to express interest, apply for a work package, or seek more details, please contact us. It's up to you to decide whether the task aligns with your skills and interests. If you lack experience in the highlighted fields (in BLUE), seize the opportunity to learn with us. Don't worry; the primary requirement is motivation. This journey is all about learning and growing.

Certificate of Completion for Work Packages

Upon successful and timely completion of the designated work package, and if the specified outcomes are met, a certificate will be issued to the individual responsible for the task. This certificate stands as an official recognition of the individual's diligence, skill, and commitment to the project.

Complexity grade

1. 20h	3. 60h	5. 100h
2. 40h	4. 80h	6. >100h



Complexity grade

6
5
4
3
2
1



TUC Drillbotics®
learning & creation



MECHANICAL



ELECTRICAL



ADMINISTRATIV



PROGRAMMING



AI



DESIGN

3 Rig Design

3.1 Machine Bed

The TUC-Drillbotics drilling rig has undergone significant improvements compared to its previous iterations. Overall, the rig consists of a machine bed, which serves as the base for various subsystems. This bed is constructed from 4x4 steel tubing and measures 1m in height, 2m in length, and 1m in width. The design objective was to create a base that is as compact as possible. The machine bed is supported by six feet, allowing the total chargeable weight to be evenly distributed. The overall weight of the rig is 250 Kg (551 lbs.), and the chargeable weight is 500 Kg (1102 lbs.). This results in a weight of approximately 83 Kg per foot. Each foot has an area of 29cm², leading to a weight distribution of 2.93 kg/cm², which is acceptable for most indoor facilities and does not require special safety equipment to prevent floor damage. The base plate is constructed from wood, reinforced with a thin metal sheet screwed on top of it. Figure 3.1 illustrates the placement of different components on this base. The main cabinet, containing all power supplies, opens to the side, allowing for easy maintenance without disassembling other rig components. The rock sample receiver is located on top of the steel plate. This decision was made because the receiver is equipped with lubricated sliding shins, enabling easy movement of the receiver even when loaded with a rock sample. Therefore, a harder base was necessary to minimize scratching and damage to the wood. The pre-charge pump, as well as the filter and buffer tank, are mounted on the wooden base.

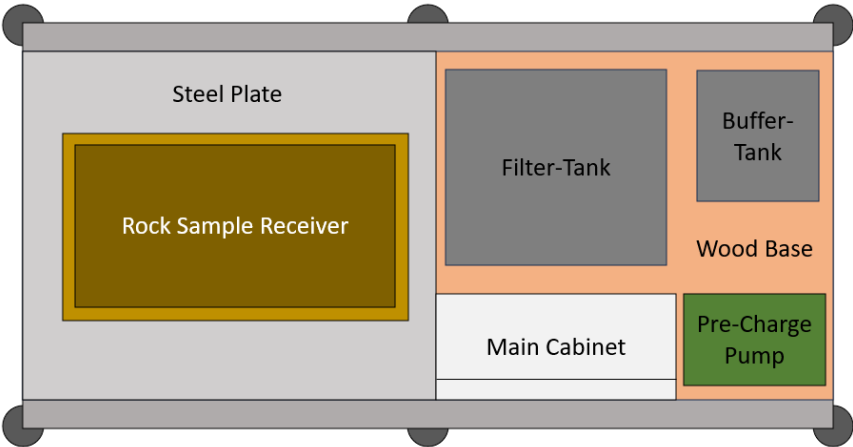


Figure 3.1: Rig Base First Level

The second level of the base plate accommodates the high-pressure pump, the emergency switch, and the first large control cabinet, as depicted in Figure 3.2.

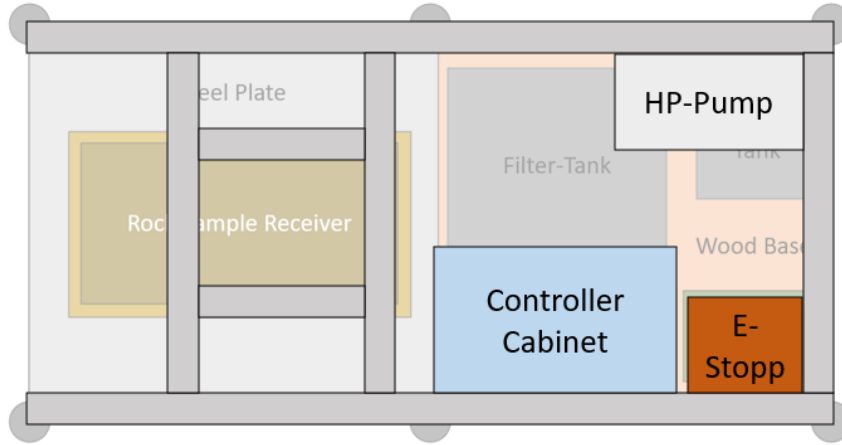


Figure 3.2: Rig Base Second Level

Component	Height (cm)	Length (cm)	Width (cm)	Volume (L)
Rock sample receiver	60	68	38	155
Mounting System	100	200	100	
Traverse System	200	40	40	
Topdrive	50	35	35	
Transport Mode	140	200	100	
Drilling Mode	300	200	200	

Table 3.1: Rig components' dimensions

3.2 Rock Sample Receiver

The rock sample receiver (**Figure 3.3**) of this year's rig is a simple cuboid. As illustrated in the image beneath this section, the rock sample will be hoisted into it. The sampling receiver is connected to the mud filtration system to separate the drilling fluid into its different components. Unlike last year's installation, this year's receiver will feature a mounted beam with a centralizer tube on top to stabilize the BHA before it completely enters the rock sample. A reliable measurement of the earth's natural electromagnetic field to determine azimuth is challenging due to electromagnetic noise and interference from nearby electrical devices and motors. To mitigate this, two square coils, each with 185 windings of copper

wire and a diameter of 1 mm, will be placed on the outer walls of the rock sample receiver. The length of each side of the square coils is 400 mm. These coils are designed to create a stronger magnetic field, providing a better environment for the magnetometer and ensuring reliable azimuth measurements.

The coils are self-made, and the electric resistance for each coil is calculated as follows:

$$R = \frac{\rho \times l}{A} = \frac{17.86 \times 10^{-6} \Omega \cdot \text{m} \times (0.4 \text{ m} \times 4 \times 185)}{\pi \times \left(\frac{0.5 \text{ mm}}{2}\right)^2} \approx 6.722 \Omega \quad (3.1)$$

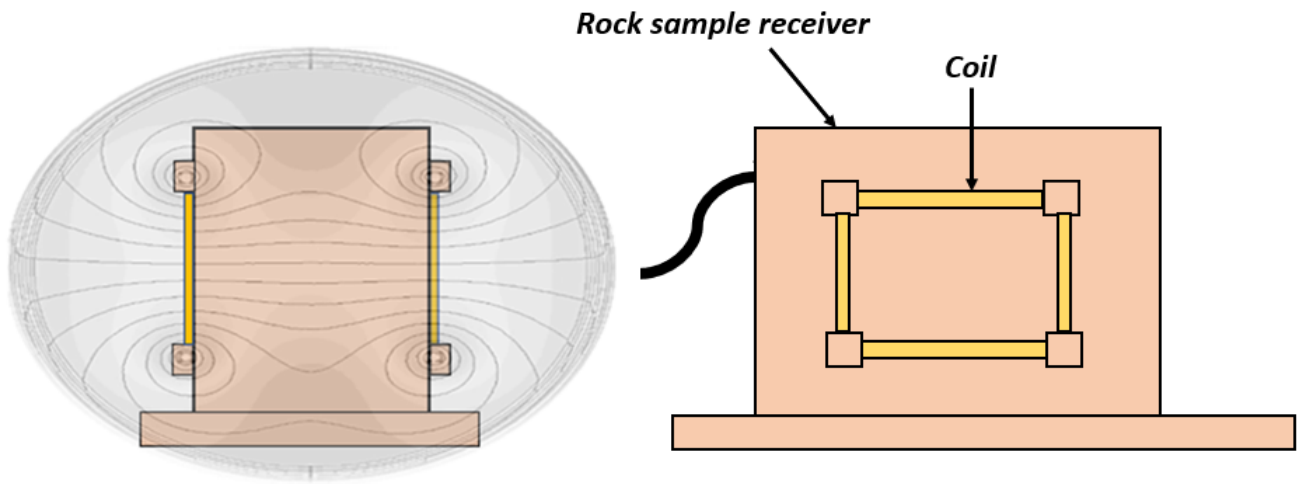


Figure 3.3: Rock sample receiver with coil

3.2.1 Magnetic Field Analysis

Following the installation of the square coils on the rock sample receiver, an analysis of the generated magnetic field (B) was conducted. The coils are powered by a 24V source and connected in series. Each coil has 185 windings of copper wire with a diameter of 1 mm and a square shape with a side length of 400 mm. The magnetic field strength at the center of the coils was calculated using the formula:

$$B = \frac{2\sqrt{2}\mu_0 I N}{\pi a} \quad (3.2)$$

where μ_0 is the magnetic constant ($4\pi \times 10^{-7} \text{ T} \cdot \text{m/A}$), I is the current, N is the number of turns, and a is the side length of the coil. The calculated field strength was approximately 0.934 mT (milliteslas). The Earth's magnetic field strength varies by location but typically

ranges from 25 to 65 μT (microteslas). The magnetic field generated by the coils is significantly stronger than the Earth's magnetic field, approximately 18 times the average Earth's field strength. The magnetic field's interaction with different materials - wood, air, and rock - was evaluated based on their relative permeabilities. The field strength in air and wood remained approximately the same as the initial value, 0.934 mT, due to their relative permeabilities being close to 1. However, the field strength in rock, with a relative permeability of 10^{-3} , was significantly reduced. The exact reduction in field strength within the rock can be calculated based on its permeability and thickness.

Note: These calculations assume uniform magnetic properties of the materials and do not account for complex factors like material inhomogeneities or geometrical considerations of the setup.

3.3 Traverse

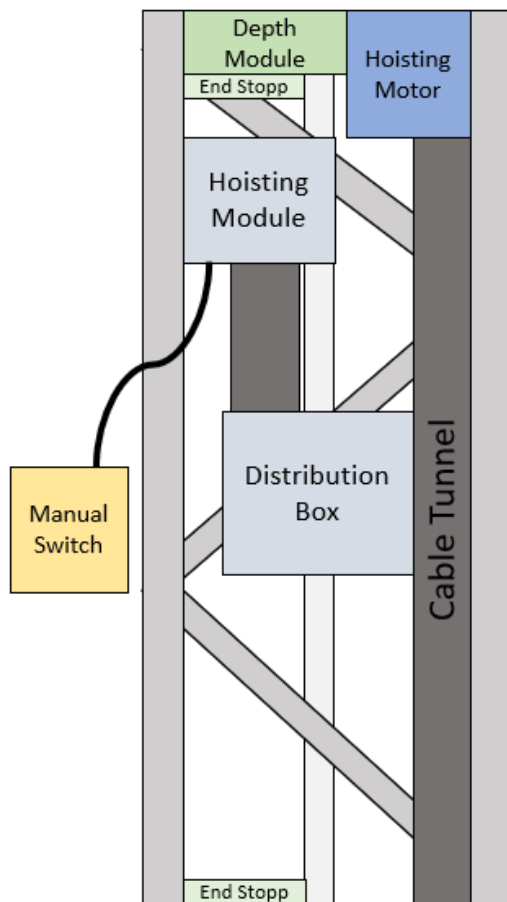


Figure 3.4: Rig Traverse Backside



Figure 3.5: Rig overview

Moving from the machine bed to the traverse, the latter contains most of the rig's electronics, motors, and actuators. It is designed to be detachable for transportation or when dealing with larger rocks that do not fit in the rock sample receiver. With the traverse upright, the rig reaches a total height of 3m. The rig setup is done manually by at least three persons. The traverse is secured using four bolts, hammered in for a secure fit and reinforced with retaining rings. The backside of the mast functions as a second distribution node and mounting place for the hoisting motor and module, depth module, stops, and cable tunnels, as shown in Figure 3.4.

3.4 Top Drive

Figure 3.5 displays the CAD model from the previous year, which has not been updated yet. However, the base structure remains the same. Shifting the focus from the mast to the top drive, all necessary components of the top drive have been added step by step to the base sledge. This resulted in a very chaotic and unorganized setup. Since the development has reached a stage where no major changes are expected for the upcoming year, the entire top drive is going to be redesigned as a complete cage for easy attachment and detachment. The redesigned cage will contain the same components, but they will be reorganized for better efficiency. It will include the rotary table motor and gearbox, the drilling motor, and the corresponding ESC, the surface pulley system for pad actuation downhole, a designated electric distribution node, a filter case, a place for all top drive modules, and cooling fans. The cage is currently under development, but a schematic is presented in Figure 3.6. Once successfully completed, this will mark a significant milestone as it would represent a ready-to-use small-scale directional drilling box. The objective of the box is not only to organize the setup but also to make it easily detachable. This allows the whole rig to be subdivided into the machine bed, the traverse,

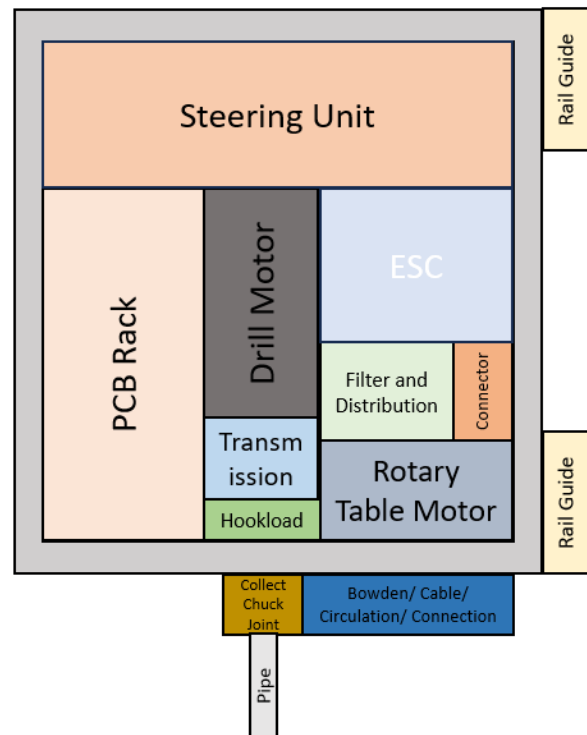


Figure 3.6: Top-Drive Cage

the Top-Drive cage, and the drill pipe, including the BHA.

3.5 Rig Electronics and Power Supply

The electronics of the rig are housed in a switch-cabinet located under the rig table, safeguarded against water ingress. To ensure safety, multiple FI circuit breakers are installed, designed to interrupt the power supply immediately in case of any failure. The rig employs a **TN-S network**, complying with **DIN VDE 0100** German standards. This network is chosen for its safety, characterized by separately laid **PE (Protective Earth)** and **N (Neutral)** conductors, ensuring reliable disconnection in case of faults.

Furthermore, all personnel involved with the mini-rig system received training in electrical engineering, emphasizing adherence to the 5 safety rules as per **DIN VDE 0105**. The rig is activated using a Main-switch located on the right side of the switch-cabinet, directly linked to the primary FI-circuit breaker. This breaker disconnects all three phases during a failure, with three additional separate FI-circuit breakers for independent phase monitoring. An emergency switch, accessible within reach and conforming to **EN ISO 13850** standards, is installed for immediate shutdown in case of human or system errors. This switch is distinct from a second emergency stop, which sends a signal through the BUS system to cease all moving or active components.

The rig's power supply is structured as follows:

- **400V 3-Phase Power:** Two phases are dedicated to powering the pumps, while the third phase supports various electrical components:
 - A **5V power pack** for modules and microelectronics.
 - A **12V power pack** for relays inside the cabinet.
 - A **24V power pack** for powering smaller stepper motors, including the Hoisting motor and the rotary table.
 - A **48V power pack** designated for the drilling motor.
- To minimize electrical noise, particularly from motors, most power supplies are equipped with individual ground lines, preventing noise transfer.
- Each motor is further filtered using a common-mode choke to reduce electromagnetic interference.

A process-flow diagram illustrating the connections of individual components is provided on **Page 58**. Please note that this is a process-flow diagram and not a circuit diagram.

The main computer, along with the human-machine interface, is positioned at a safe distance from the rig to ensure safety during operation.

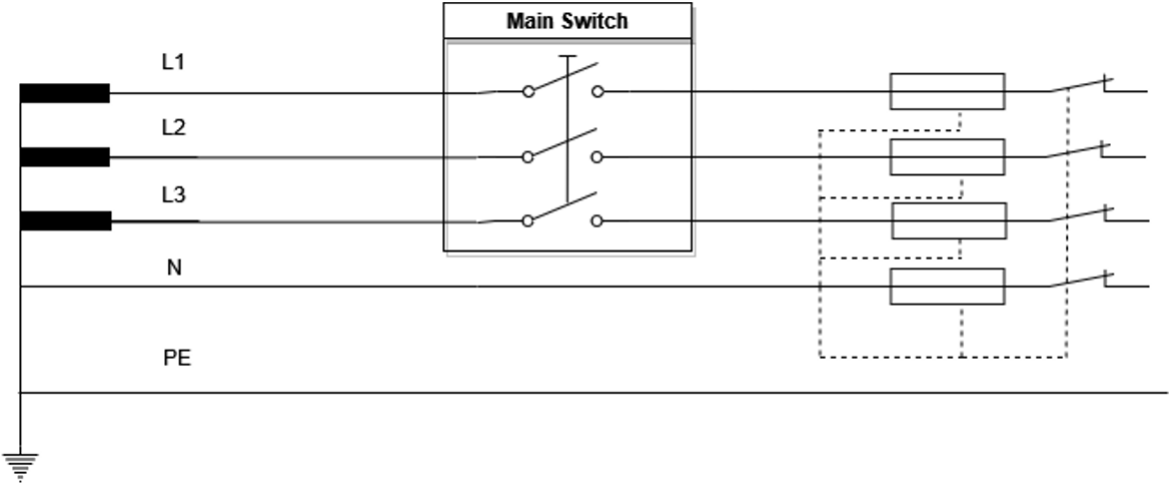


Figure 3.7: TN-S network

4 Circulation System

4.1 Rig Plumbing and Mud Handling

A drilling mud preparation container is installed adjacent to the drilling sample container. Behind the filter, a pump is connected, generating the necessary pressure for drilling. The pump setup comprises a pre-charging pump (providing 2-3 bar pre-pressure) that feeds into a positive displacement pump with a maximum pressure capacity of 120 bar. Between both pumps, a flow meter is installed to measure the amount of fluid fed to the positive displacement pump. Further details about the flow meter are discussed in **Chapter 8.3.6**. The drilling mud is conveyed through a cooper hose running parallel to the drill pipe, leading into the Bottom Hole Assembly and then directed to the bit, exiting through its nozzles. The returning drilling mud is processed by a two-chambered separation tank system. Initially, the mud is drawn from the rock sample receiver into the first mud tank, where heavier components are separated due to gravitational force, allowing only the liquid components to enter the subsequent filtering tank. The system's slow flow rate provides ample time for separating solid and liquid components of the mud. The final tank, equipped with a pump, reinjects the filtered drilling mud into the hose. Filtration packs within the mud tanks, consisting of plastic granules, enhance the mud handling system's filtration performance. Water, without additives, is used as the drilling mud. Opting for other substances would lead to higher environmental impacts and necessitate a comprehensive sealing and leakage prevention strategy. Additionally, there is no perceived need for additives or oil-based mud in the given application. The design of the circulation system is based on cutting transport and pressure loss calculations, presented in the subsequent sub-chapters. The values used for these calculations can be found in the **Appendix**.

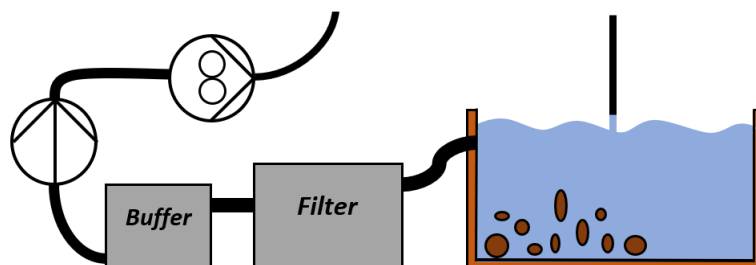


Figure 4.1: Mud Handling

4.2 Cutting Transport Calculation

The following section sets the flow rate calculation required for the drilling operation with a Newtonian fluid. References are **PhD u. Liu (2011)** and **Aadnoy (2006)** The minimum flow rate of the mud v_{mud} must be greater than the terminal slip velocity $v_{rittinger}$ expressed in **equation 4.1**.

$$v_{mud} > v_{rittinger} \quad (4.1)$$

The slip velocity can be calculated by Moore's correlation for a vertical well. The slip velocity of a small spherical particle settling (slipping) through a Newtonian fluid under laminar flow condition, v_{slip} is given by Stoke's law **4.5**.

$$\begin{aligned} v_{slip} &= \frac{g * (\rho_s - \rho_w) * d_s^2}{\mu_w * 18} \\ &= \frac{9.81 \text{ m s}^{-2} * 0.000\,000\,01 \text{ m} * (2650 \text{ kg m}^{-3} - 1000 \text{ kg m}^{-3})}{18 * 0.001 \text{ Pa s}} \\ &= 0.5394 \text{ m min}^{-1} \\ &(\text{ = } 0.0295 \text{ ft s}^{-1}) \end{aligned} \quad (4.2)$$

Where:

- d_s : Diameter of cutting
- ρ_s : Density of the cutting solid
- ρ_w : Density of the drilling fluid (Water)
- μ_w : Viscosity of the drilling fluid (Water)

Stokes law could be used already to determine the slip velocity, as the Particle Reynolds number is smaller than one. The Particle Reynolds number Re_p is calculated as follows **4.6**.

$$\begin{aligned} Re_p &= \frac{\rho_w \cdot v_{slips} \cdot d_s}{\mu_w} \\ &= \frac{1000 \text{ kg m}^{-3} * 0.008\,99 \text{ m s}^{-1} * 0.0001 \text{ m}}{0.001 \text{ Pa s}} \\ &= 0.899 \end{aligned} \quad (4.3)$$

The friction factor f is taken as 44.49 according to Moore's correlation **4.3**, with that in mind, the empirical equation **4.4** that applies for particle Reynolds numbers smaller than 3, can be used. This equation only works in field units, so in the following it will be switched

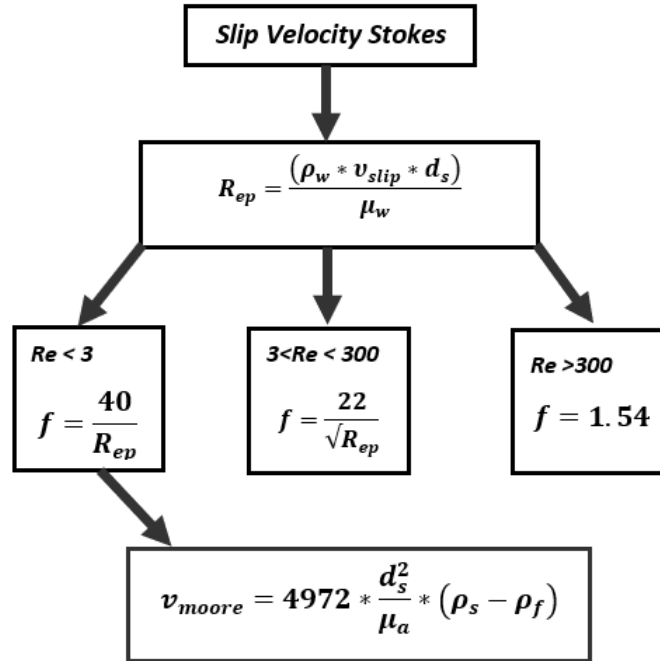


Figure 4.2: Slip velocity derived by Moore's correlation

from SI units to Oil-field units. This method is used to get a closer approximation to the actual slip velocity by including the friction factor.

$$\begin{aligned}
 v_{moore} &= 4972 * \frac{d_s^2 * (\rho_s - \rho_w)}{\mu_w} \\
 &= 4972 * \frac{0,000016 * (26,55 - 8,34)}{1} \\
 &= 1.448 \frac{\text{ft}}{\text{min}} \\
 &= (0.441 \frac{\text{m}}{\text{min}})
 \end{aligned} \tag{4.4}$$

The slip velocity is quite low. This is attributed to the approximation of the cuttings' diameter. Previously, a grinding action was primarily employed to bore through the sample, leading to small cuttings of less than 0.1 mm in size. Due to the structure of the bit, it is highly unlikely to generate cuttings larger than 0.1 mm. However, to ensure accuracy, the slip velocity is calculated for **cuttings as large as 1 mm**.

$$\begin{aligned}
 v_{slipB} &= \frac{g * (\rho_s - \rho_w) * d_s^2}{\mu_w * 18} \\
 &= \frac{9.81 \text{ m s}^{-2} * 0.000\,001 \text{ m} * (2650 \text{ kg m}^{-3} - 1000 \text{ kg m}^{-3})}{18 * 0.001 \text{ Pa s}} \\
 &= 53.49 \text{ m min}^{-1} \\
 & (= 2.95 \text{ ft s}^{-1})
 \end{aligned}
 \tag{4.5}$$

$$\begin{aligned}
 Re_{pB} &= \frac{\rho_w * v_{slipsB} * d_s}{\mu_w} \\
 &= \frac{1000 \text{ kg m}^{-3} * 0.899 \text{ m s}^{-1} * 0.0001 \text{ m}}{0.001 \text{ Pa s}} \\
 &= 899
 \end{aligned}
 \tag{4.6}$$

For the bigger cutting diameter ($Re_{pB} > 1000$) the friction factor becomes constant as turbulent flow is approached. This leads to Rittingers equation ($f=1.54$).

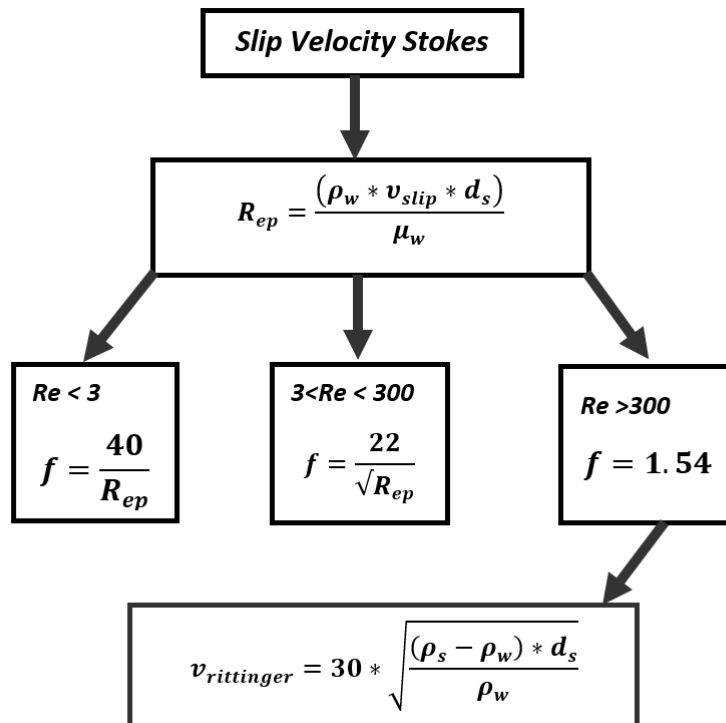


Figure 4.3: Slip velocity derived by Moore's correlation

$$\begin{aligned}
v_{rittinger} &= 30 * \sqrt{\frac{(\rho_s - \rho_w) * d_s}{\rho_w}} \\
&= 30 * \sqrt{\frac{(2.65 \text{ g cm}^{-3} - 1 \text{ g cm}^{-3}) * 0.1 \text{ cm}}{1 \text{ g cm}^{-3}}} \\
&= 7.30 \text{ m min}^{-1} \\
& (=0.399 \text{ ft s}^{-1})
\end{aligned} \tag{4.7}$$

Therefore, the mud velocity must be at least as high as 0.399 ft s^{-1} .

A flow rate of 1.85 gpm (7 L min^{-1}) is pumped by the rig pump. The annular velocity v_a is calculated by following formula:

$$\begin{aligned}
v_a &= \frac{Q}{2,448 * (d_h^2 - d_d^2)} \\
&= \frac{1.85 \text{ gpm}}{2,448 * (2.22 \text{ in} - 0.15 \text{ in})} \\
&= 0.3650 \text{ ft s}^{-1} \\
& (=6.675 \text{ m min}^{-1})
\end{aligned} \tag{4.8}$$

Where:

- Q : Flow rate of drilling fluid
- d_h : Diameter of Borehole in inch
- d_p : Diameter of Drill pipe in inch

It can be seen that the annular velocity is smaller than the slip velocity, ($v_a < v_{rittinger}$) which would make an effective cutting transportation impossible. When it is taken into account that a major part of the cross-sectional area, between the drill pipe and the borehole, is going to be taken away by the hoses cables and the drilling fluid supply (as it won't flow through the DP), the difference between inner and outer diameter gets smaller, and therefore the annular velocity gets higher.

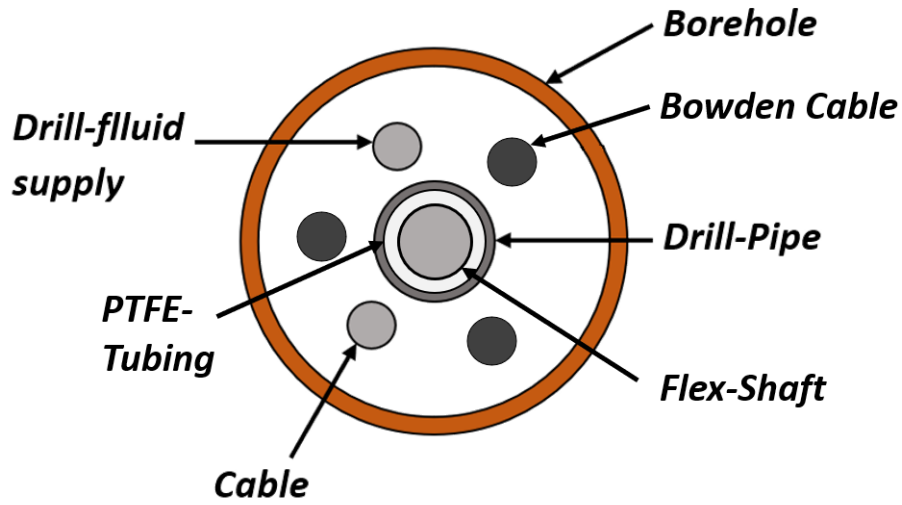


Figure 4.4: Borehole schematic

$$\begin{aligned}
 A_{BO} &= \frac{\pi}{4} * (1,5in)^2 = 1,767in^2 \\
 A_{DP} &= \frac{\pi}{4} * (0,4in)^2 = 0,126in^2 \\
 A_{BC} &= \frac{3 * \pi}{4} * (0,2in)^2 = 0,094in^2 \\
 A_{FS} &= \frac{\pi}{4} * (0,314in)^2 = 0,077in^2 \\
 A_C &= \frac{\pi}{4} * (0,314in)^2 = 0,077in^2 \\
 A_I &= A_{DP} + A_{BC} + A_{FS} + A_C = 0,374in^2 \\
 d_{dneu} &= \sqrt{\frac{A_I}{\frac{\pi}{4}}} = 0.70 \text{ in}
 \end{aligned} \tag{4.9}$$

$$\begin{aligned}
 v_{a,neu} &= \frac{Q}{2,448 * (d_h^2 - d_{d,neu}^2)} \\
 &= \frac{1.85 \text{ gpm}}{2,448 * (2.22 \text{ in} - 0.7 \text{ in})} \\
 &= 0.50 \text{ ft s}^{-1} \\
 & (=9.2 \text{ m min}^{-1})
 \end{aligned} \tag{4.10}$$

For efficient hole-cleaning during drilling, it is empirically recommended to maintain a

transport ratio above 50%. The transport ratio is calculated as follows,

$$\text{Transport ratio} = \frac{v_{a,neu} - v_{rittinger}}{v_{a,neu}} * 100 = 20\% \quad (4.11)$$

resulting in a determined value of 20%. However, this is only applicable in the highly unlikely scenario where the cutting size exceeds 1 mm. In various test wells, cuttings were analyzed, and due to the grinding action, the initial estimate of a 0.1 mm cutting size holds valid. In case of 0.1 mm cutting size the transport ratio would increase to approximately 95%.

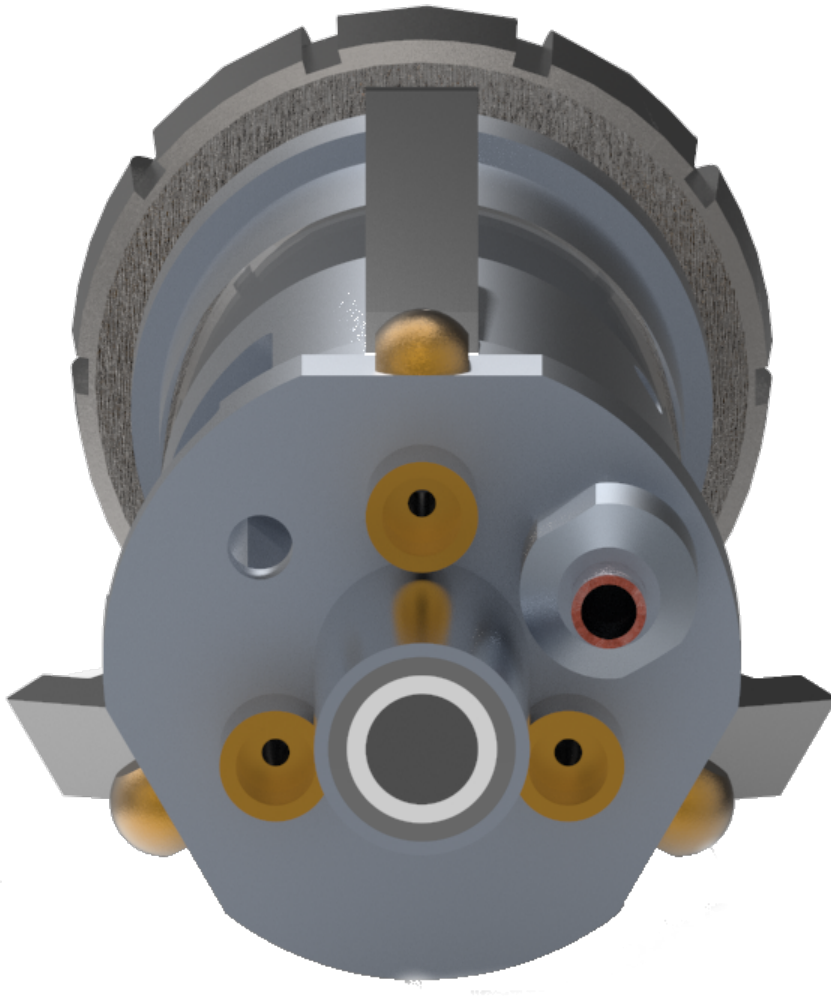


Figure 4.5: Connection for Hoses and Cable

4.3 Pressure Loss Calculation

The following section sets the calculation for conventional, rotary drilling pump. Assuming the Newtonian fluid (water) flows inside the hose around the drill string until it gets to the BHA where it connects to the drill pipe and exits through the bit, which cause the biggest drop in pressure. The pressure loss inside the hose along the drill pipe until it connects to the BHA is neglected. A small overview of how the fluid flows is shown in **Figure: 4.6**.

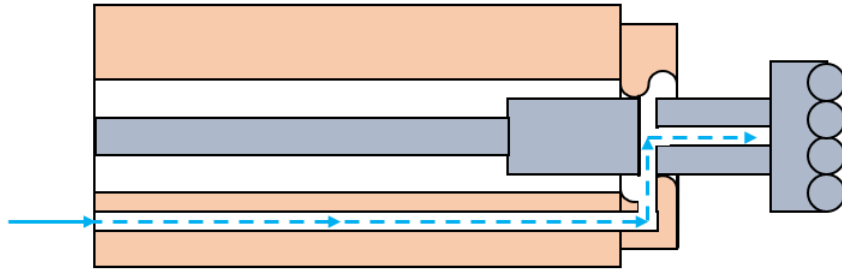


Figure 4.6: Fluid-flow schematic

First the velocity of the fluid in the Flow line v_d is determined:

$$v_d = \frac{Q}{2.448 * id_H^2} = \frac{1,85gpm}{2.448 * 0,15^2in} = 33.5 \text{ ft s}^{-1} \text{ (102 m/s)} \quad (4.12)$$

Where:

Q : Flow rate of drilling fluid

Based on that, the Reynolds number is determined:

$$Re = \frac{928 * \rho_f * v_d * id_p}{\mu_w} = \frac{928 * 8.33ppg * 33.5 \text{ ft s}^{-1} * 0.15 \text{ in}}{1cp} = 38844 \text{ (Turbulent)} \quad (4.13)$$

The Required friction factor f can be calculated by the following formula:

$$f = 0.25 \left(\log_{10} \left(\frac{k}{3.7 * id_p} + \frac{5.74}{Re^{0.9}} \right) \right)^{-2} = 0,25 * \left(\log_{10} \left(\frac{0.0006in}{3.7 * 0,15in} + \frac{5.74}{38844^{0.9}} \right) \right)^{-2} = 0.031 \quad (4.14)$$

Where:

k : Roughness of the flow line (assumed with 0,0006in)

Re : Reynolds number

The pressure loss in the flow line inside the BHA parallel to the drill string, P_s is calculated as follows:

$$P_s = \frac{f * \rho_w * v_d^2 * L_{Flowline}}{25.8 * id_p} = \frac{0.0301 * 8.33ppg * 33,5^2 ft s^{-1} * 3.14 in}{25.8 * 0.15 in} = 228 \text{ psi} \quad (15.72 \text{ bar}) \quad (4.15)$$

Where:

f : Fanning friction factor

$L_{Flowline}$: Length of the drill string

i_{dp} : Internal diameter of the Flow line

In the next part, the losses in the hollow rotating part right beneath the Steering unit as well as the losses inside the small section where the fluid flows through the DP, have to be calculated.

First, the Losses inside the Hollow part are determined.

$$v_{ho} = \frac{Q}{2,448 * id_{ho}^2} = \frac{1,85gpm}{2,448 * 0,118^2 in} = 54.27 \text{ ft s}^{-1} \quad (16.49 \text{ m s}^{-1}) \quad (4.16)$$

Where:

v_{ho} : Velocity of the drilling fluid inside the hollow part

id_{ho} : Internal diameter of the hollow part

Reynolds Number:

$$Re = \frac{928 * \rho_w * v_{ho} * id_{ho}}{\mu_w} = \frac{928 * 8.33ppg * 54.27 \text{ ft s}^{-1} * 0,118in}{1cp} = 49503 \quad (Turbulent) \quad (4.17)$$

Friction factor:

$$f = 0.25([\log_{10}(\frac{k_{ho}}{3.7 * id_{ho}} + \frac{5.74}{Re^{0.9}})])^{-2} = 0,25 * ([\log_{10}(\frac{0.0039in}{3.7 * 0,118in} + \frac{5.74}{49503^{0.9}})])^{-2} = 0.051 \quad (4.18)$$

Where:

k_{ho} : Roughness of the hollow part (0.0039in)

Pressure Losses:

$$P_{ho} = \frac{f * \rho_w * v_{ho}^2 * L_{ho}}{25.8 * id_{ho}} = \frac{0.051 * 8.33ppg * 54,27^2 \text{ ft s}^{-1} * 0.35 \text{ in}}{25.8 * 0.118 \text{ in}} = 143.84 \text{ psi} \quad (9.9 \text{ bar}) \quad (4.19)$$

Where:

L_{ho} : Length of the hollow part

Now, only a small section inside the DP remains:

$$v_{dp} = \frac{Q}{2,448 * id_{dp}^2} = \frac{1,85gpm}{2,448 * 0,27^2in} = 10.36 \text{ ft s}^{-1} \quad (3.13 \text{ m s}^{-1}) \quad (4.20)$$

Reynolds Number:

$$Re = \frac{928 * \rho_w * v_{dp} * id_{dp}}{\mu_w} = \frac{928 * 8.33ppg * 10.36 \text{ ft s}^{-1} * 0,27in}{1cp} = 21623 \quad (Turbulent) \quad (4.21)$$

Friction factor:

$$f = 0.25([\log_{10}(\frac{k_{dp}}{3.7 * id_{dp}} + \frac{5.74}{Re^{0.9}})])^{-2} = 0,25 * ([\log_{10}(\frac{0.0039in}{3.7 * 0,27in} + \frac{5.74}{21623^{0.9}})])^{-2} = 0,045 \quad (4.22)$$

Pressure Losses:

$$P_{dp} = \frac{f * \rho_w * v_{dp}^2 * L_{dp}}{25.8 * id_{dp}} = \frac{0.051 * 8.33ppg * 10.36^2 \text{ft s}^{-1} * 1.3 \text{ in}}{25.8 * 0.275 \text{ in}} = 8.35 \text{ psi} \quad (0.6 \text{ bar}) \quad (4.23)$$

Finally, the previously calculated losses are summed up to acquire the BHA pressure losses:

$$P_{dp} + P_{ho} + P_s = P_{BHA} = 380 \text{ psi} \quad (26.2 \text{ bar}) \quad (4.24)$$

There is one nozzle at the bit with diameter d_n . For that reason, the total area of nozzle, A_n is calculated as follows:

$$A_n = \frac{\pi}{4} * d_n^2 = \frac{\pi}{4} * 0.118 \text{ in}^2 = 0.01 \text{ in}^2 \quad (0.645 \text{ cm}^2) \quad (4.25)$$

Then, the pressure loss at the bit, P_{bit} can be estimated by following calculation:

$$P_{bit} = \frac{Q^2 * \rho_f}{12031 * A_n^2} = \frac{1.84 \text{ gpm}^2 * 8.33 \text{ ppg}}{12031 * 0.01 \text{ in}^2} = 22.43 \text{ psi} \quad (4.26)$$

The jet impact force, F_j of the bit is:

$$F_j = 0.01823 * C_d * Q * \sqrt{\rho_f * P_{bit}} = 0.01823 * 0.95 * 1.85 \text{ gpm} * \sqrt{8.33 \text{ ppg} * 22.43 \text{ psi}} = 0.43 \text{ lbf} \quad (4.27)$$

Where:

C_d : Discharge coefficient (assumed value 95%)

The jet velocity of the bit, v_{bit} is:

$$v_{bit} = \frac{Q * 144}{448.8 * A_n} = \frac{144 * 1.85 \text{ gpm}}{448.8 * 0.01 \text{ in}^2} = 59.35 \text{ ft s}^{-1} \quad (17.98 \text{ m s}^{-1}) \quad (4.28)$$

Further, the pressure loss in the annulus, P_a is calculated as follows:

$$P_a = \frac{1,4327 * 10^{-7} * \rho_f * L_{rock} * v_{a,neu}^2}{d_h - d_{d,neu}} = \frac{1,4327 * 10^{-7} * 8,33 \text{ ppg} * 1,97 \text{ ft} * 27,6^2 \frac{\text{ft}}{\text{min}}}{0,125 \text{ ft} - 0,05 \text{ ft}} = 0,02 \text{ psi} \quad (4.29)$$

The annular velocity was calculated as 28 ft min^{-1} . As this is not very fast, the pressure loss in the annulus is negligible. the total downhole pressure loss $P_{downhole}$ is the sum of the following.

$$P_{downhole} = P_{bit} + P_{BHA}(+P_a) = 22.43psi + 380psi = 402.43psi \quad (27 \text{ bar}) \quad (4.30)$$

It is assumed that the pump will be connected with the hose line (made from rubber material) to the standpipe with roughness 0.0006 in . The pressure loss in the hose, P_H is calculated by following schematic as applied for the pressure loss calculation before:

$$v_H = \frac{Q}{2,448 * id_H^2} = \frac{1,85gpm}{2,448 * 0,5^2in} = 3.02 \text{ ft s}^{-1} \quad (0.92 \text{ m s}^{-1}) \quad (4.31)$$

$$Re = \frac{928 * \rho_w * v_H * id_H}{\mu_w} = \frac{928 * 8.33ppg * 3.02 \text{ ft s}^{-1} * 0,5in}{1cp} = 11678 \quad (Turbulent) \quad (4.32)$$

Then, the ratio of the roughness of the pipe divided by the inner diameter of the pipe k_H/id_H calculated to determine the friction factor on the Fanning chart, as shown in Figure ?? :

$$\frac{k_H}{id_H} = \frac{0.0006 \text{ in}}{0.5 \text{ in}} = 0.0012 \quad (4.33)$$

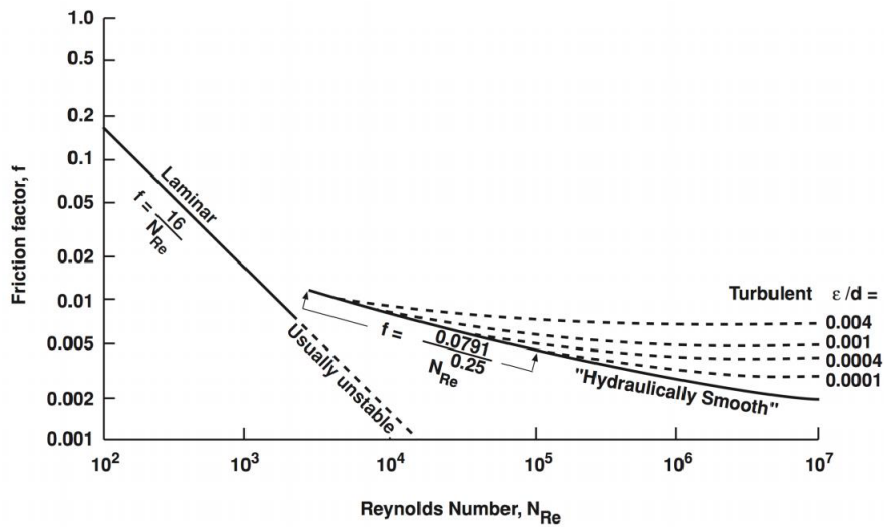


Figure 4.7: Fanning chart

Based on the Fanning chart, see **Figure 4.7**, the friction factor, f is approximately 0.007.

The pressure loss inside the hose, P_H is:

$$P_H = \frac{f * \rho_w * v_H^2 * L_H}{25.8 * id_H} = \frac{0.007 * 8.33ppg * 3.02^2 ft s^{-1} * 7.5 in}{25.8 * 0.5 in} = 0.3 psi \quad (0.02 bar) \quad (4.34)$$

The pressure loss through the hose is negligible, which brings the total pressure loss along the entire system to $P_{system}=P_{downhole}$ or 402.43 psi. If additional atmospheric pressure and the hydro static-pressure are added, the pressure which the pump has to deliver can be determined.

$$\begin{aligned} P_{pump} &= P_{system} + P_{atm} + \frac{\rho_w * (v_H - v_a)^2}{2} + \rho_f * g * H_{rig} \\ &= 402.43psi + 14.5 + \frac{8.33ppg * 7.48 * (3.02^2 - 0.46^2) \frac{ft}{sec}}{2 * 32.174 \frac{ft}{sec} * 144} + \frac{8.33ppg * 7.48 * 32.174 \frac{ft}{sec}^{-2} * 7.5}{32.174 \frac{ft}{sec}^{-2} * 144} \\ &= 422.86psi \quad (28.7bar) \end{aligned} \quad (4.35)$$

$$P_{umpHP} = \frac{P_{pump} * Q}{1714} = \frac{422.86psi * 1.85gpm}{1714} = 0,45HP \quad (4.36)$$

It is assumed that the efficiency of the pump is 85%, therefore the requirement of the horsepower pump is 0.46 HP. The following **Table 4.1** shows the variation of the pump power requirement according to the flow rate variation:

Table 4.1: Pump power requirement rotary drilling

Flow ratevariation (gpm)	Flow rate variation (Lpm)	Transport ratio (%)	Pump Pressure (bar)	Pump (HP)	Pump (kW)
1.32	5	70	4.82	0.05	0.04
1.84	7	83	8.19	0.12	0.09
2.64	10	85	15.3	0.34	0.25
3.43	13	88	24.89	0.72	0.53

5 Hoisting System

The primary responsibility of the hoisting system is to raise or lower the drill string. In the employed small-scale setup, where Weight on Bit cannot be applied through drill collars, the hoisting system is also designed to apply a downward force. This year, the hoisting system has been upgraded with a more powerful electric stepper motor, capable of providing up to $1.2 \text{ N} \cdot \text{m}$ of torque and reaching speeds of up to 1600 RPM. However, the main functionality remains the same: the stepper motor powers a trapezoidal threaded spindle to move the top drive up and down. Early tests indicated that a sufficiently high WOB, especially during steering operations, is crucial. Consequently, a gear ratio of 4:1, coupled with a 4mm lead screw pitch, was implemented. The hoisting system can be actuated either manually with the remote switch or through the user interface, where movement speed and distance can be adjusted as desired.

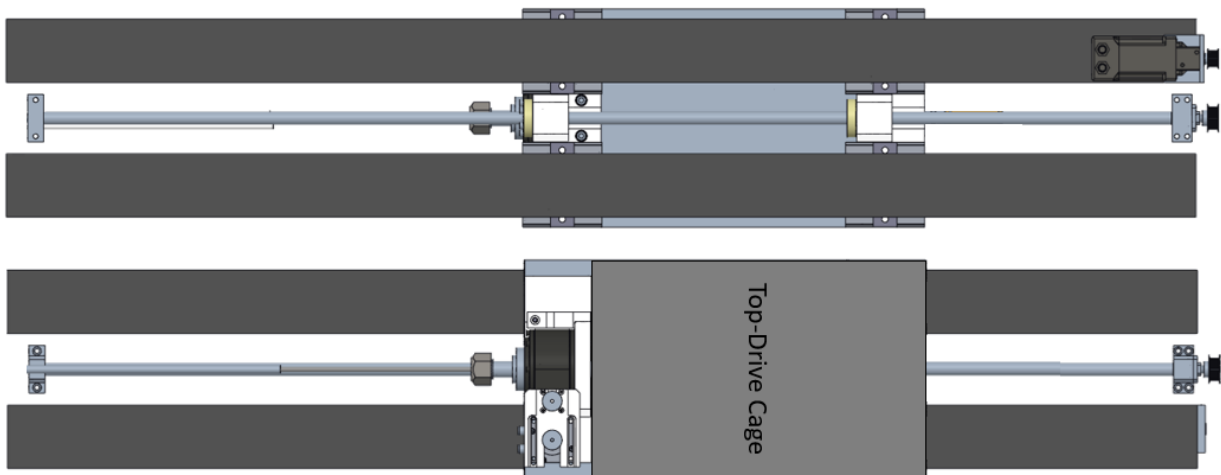


Figure 5.1: Hoisting System

5.1 Force Calculations

To calculate the lifting and pushing forces of the hoisting system, consider the following:

Lifting Force: Given the motor's torque of $1.2 \text{ N} \cdot \text{m}$ and a gear ratio where the motor turns 4 times for one spindle turn, the effective torque is calculated as:

$$\text{Effective Torque} = \text{Motor Torque} \times \text{Gear Ratio} = 1.2 \text{ N} \cdot \text{m} \times 4 = 4.8 \text{ N} \cdot \text{m} \quad (5.1)$$

Using a spindle with a 4mm lead screw pitch (or 0.004m), the lifting force can be determined by:

$$\text{Lifting Force} = \frac{\text{Effective Torque}}{\text{Lead Screw Pitch}/(2\pi)} = \frac{4.8 \text{ N} \cdot \text{m}}{0.004 \text{ m}/(2\pi)} \approx 7539.82 \text{ N (768Kg)} \quad (5.2)$$

Pushing Force: Considering the weight of the top drive (40 kg), the pushing force is calculated as:

$$F_{push} = F_{lift} + W_{topdrive} \quad (5.3)$$

where $W_{topdrive}$ is the weight of the top drive converted to Newtons ($W_{topdrive} \times 9.81$). The pushing force is 7932.22 N which correlates to about 808 Kg.

5.2 System Stability and Improvements

Adjacent to the spindle, two tracks are mounted to the traverse, serving as guiding rails for the Top-Drive. In the current setup, the Top-Drive has two nuts attached to the spindle, one at the bottom and one at the top. The Top-Drive features guiding rails at each corner. However, since the bottom two guiding rails are not rigidly connected to the upper two, a lever effect is created. To address this, the Top-Drive cage will have two beams connecting the lower and upper guiding rails. This modification aims to reduce the flexibility of the Top-Drive and enhance its stability. The bending moment exerted on the track, particularly during the withdrawal of the drill string, presents a significant mechanical challenge. This issue becomes critical when the Bottom Hole Assembly becomes stuck, and the powerful motor attempts to extract it from the hole. In such scenarios, the entire rock sample, weighing approximately 300 kg, could be lifted out of the rock sample receiver. Ideally, this situation should be prevented by a controller monitoring the hook load. However, in case of malfunction, it is essential to ensure that no damage occurs to the vital rig components. This necessitates an estimation of the loads that the hoisting system must handle.

5.2.1 Calculation of Bending Moment

The bending moment exerted on the tracks can be calculated using the formula:

$$M = F \times d \quad (5.4)$$

where M is the bending moment, F is the force (weight of the rock sample), and d is the lever arm distance (distance from the force application point to the Track). With a force of

300 kg (approximately 2943 N, considering $g = 9.81 \text{ m/s}^2$) and a lever arm distance of 86.25 mm (0.08625 m), the bending moment is:

$$M = 2943 \text{ N} \times 0.08625 \text{ m} \approx 253.83 \text{ N} \cdot \text{m} \quad (5.5)$$

This high bending moment necessitates the adoption of the two-nut design to distribute the load more evenly and reduce the risk of damaging the guiding or the track

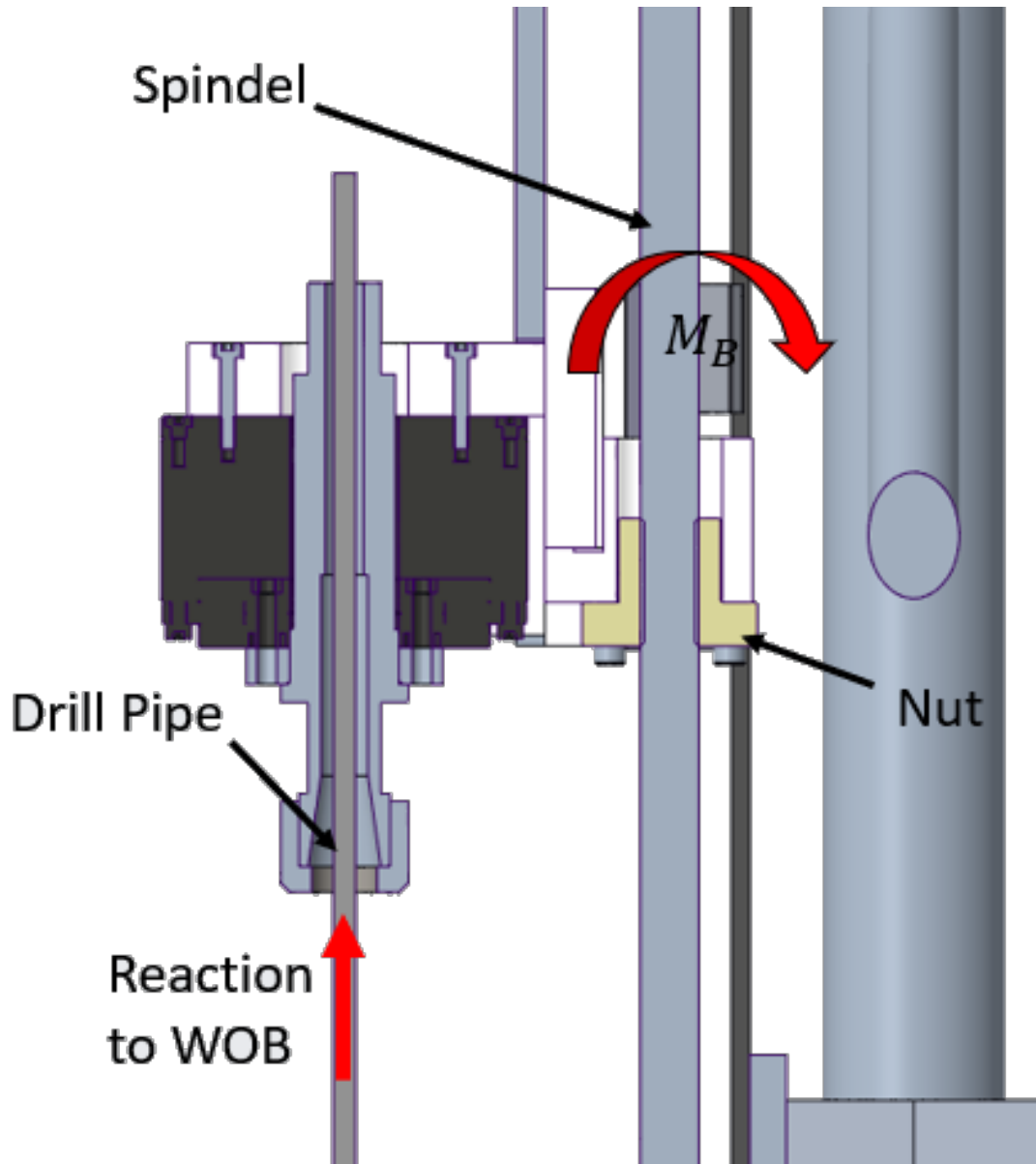


Figure 5.2: Bending Moment on Spindle

6 Rotation System

6.1 Drill Motor

In the past, the team often experienced issues where the servo motor, previously used as a drill motor, would enter an error state. Several causes were identified for this. Firstly, the motor was designed for precise positioning and had relatively high torque at very low speeds. This meant that the torque necessary to maintain the required position was insufficient at the target speed. Additionally, the motor had a monitoring system for the target position, which would detect an error due to torque spiking and oscillation of the flex shaft. Since the type of drilling we are considering does not require precise knowledge of the drill bit's rotational position, this function is unnecessary. Consequently, the decision was made to switch to a brushless DC motor from the modeling industry. This motor is essentially a permanently excited synchronous motor, powered by three-phase alternating current supplied by a miniature inverter (electronic speed controller, or ESC). The ESC employs Hall sensors to detect the rotor's position and commutates the alternating current and the magnetic field generated by the stator accordingly. The ESC used in this case also provides telemetry data, including motor current, speed, and temperature. A target speed is set as the input, which the ESC strives to maintain. The maximum speed is dependent on the supply voltage, which is why a 48 V power supply unit was installed. The current setup is capable of turning up to approx. 3000 rpm and providing a torque of approx 1.3 Nm, which is calculated as follows:

Given:

- Current, $I \approx 10 \text{ A}$
- Voltage, $V = 48 \text{ V}$
- Rotational Speed, $\text{RPM} \approx 3000$

Calculate Electrical Power: (P_{elec}):

$$P_{elec} = V \times I = 48 \text{ V} \times 10 \text{ A} = 480 \text{ W} \quad (6.1)$$

Mechanical Power (P_{mech}):

$$P_{mech} = P_{elec} \times \eta = 480 \text{ W} \times 0.85 = 408 \text{ W} \quad (6.2)$$

Angular Velocity (ω) from RPM:

$$\omega = \text{RPM} \times \frac{2\pi}{60} = 3000 \times \frac{2\pi}{60} \approx 314.16 \text{ rad/s} \quad (6.3)$$

Torque (τ):

$$\tau = \frac{P_{mech}}{\omega} = \frac{408 \text{ W}}{314.16 \text{ rad/s}} \approx 1.30 \text{ Nm} \quad (6.4)$$

During testing, there were attempts to use the motor current as an additional input for the hoisting system's controller. However, the signal-to-noise ratio was found to be very poor. Consequently, there is now consideration of using a motor designed for higher speeds. This change aims to improve the signal quality and enable operation at higher speeds.

6.2 Rotary Table

The rotary table, originating from one of the early designs, is utilized to rotate the Bottom Hole Assembly along with the drill pipe. However, since all BHA systems require cabling, continuous rotation using the rotary table is not feasible. Continuous rotation would result in the cables being wound up and potentially torn off. Nevertheless, the rotary table is employed during the setup phase, prior to the actual drilling process, for calibrating the BHA sensors and setting the precise azimuth. Over time, some play has developed in the shaft of the auger gear. This play causes the drill pipe holder to tilt and encourages the pipe to buckle. The current plan is to replace the existing Igus plastic gearbox with a more robust solution: a hollow shaft mounted on tapered roller bearings, coupled with a worm gearbox.

6.3 Collet chuck joint

The drillpipe is clamped via a collet chuck. This solution has proven itself in the past and will continue to be used.

6.4 Drillpipe

The rig featured an aluminum drill pipe that has an outer diameter of 10 mm and an inner diameter of 8 mm. The 1 m long pipe is constructed in one piece and hence does not need tool joints. The pipe is connected with the top drive via collet chuck joint and with the BHA using threaded, in-house manufactured adapter. Through the pipe runs the

before mentioned flexible shaft that has a diameter of 6 mm. A PTFE-tube (OD: 8 mm, ID: 6 mm) was used in the remaining space to reduce friction between the flexible shaft and the Aluminum pipe and to suppress any vibrations that developed during earlier drilling tests without that PTFE-tube. The flex shaft makes it possible to use a push-the-bit design with a static down hole steering unit. This has a fundamental advantages to a RSS. First of all, the static position of the BHA allows more precise control of the drilling tool. Since the BHA does not rotate, sensors and other instruments can be read more accurately and the data transmitted directly to the control unit. In this way, complex drilling operations such as drilling curves can be performed with greater accuracy. In addition, the use of a push-the-bit system can help reduce wear on the BHA and other drilling equipment. Since the BHA does not rotate with the drill pipe, it is subjected to less stress, which extends its life and reduces the need for frequent repairs or maintenance. All hoses and cables are attached to the outside of the DP. To accomplish a stable connection, 3D Printed clips that are screwed tightly around the DP with clip-in connections for the hoses, cables and fluid supply are used.

6.4.1 Limit Calculations

The drill pipe can be considered as one of the weakest parts in the entire string. This has been proven to be an critical factor influencing the drilling capability of the rig which lead to the decision to implement a steel drill pipe instead of the before used aluminum. The following calculated values for buckling, burst and torsion maxima, for a steel drill pipe are based on the scenario that no other forces are acting on the component for the calculation. The maximum values are good indicators, aiding in the selection of the appropriate equipment and parameters for the drilling robot, such as the maximum WOB for the hoisting system and high pump pressures for flushing. The used values can be found in the **Appendix**.

6.4.2 Buckling Limit Calculation

Buckling is characterized by a lateral deformation or failure of a structural member subjected to high axial compressive stress, where the compressive stress at the point of failure is less than the yield strength that the material can withstand. The critical buckling load limit of the steel drill pipe is calculated by the following Euler equation (assuming both pipe ends are pinned). First the moment of inertia is determined:

$$I = \frac{\pi}{64} * (d_p^4 - id_p^4) = \frac{\pi}{64} * (0,393in^4 - 0,315in^4) = 6.876 * 10^{-4}in^4 \quad (6.5)$$

Where:

d_p : Outside diameter of the drill pipe

id_p : Inside diameter of the drill pipe

Then the critical buckling load, P_{bcr} is calculated:

$$P_{bcr} = \frac{\pi^2 * E * I}{(K * L)^2} = \frac{\pi^2 * 2,901 * 10^{-7} * 6,8790 * 10^{-4}}{(1 * 36)^2} = 151.92 \text{ lbf} \quad (75,77 \text{ N}) \quad (6.6)$$

Where:

P_{bcr} : Critical buckling load

E : Modulus of elasticity of the steel drill pipe

I : Area moment of inertia

L : Length of the column

K : Column effective length factor

Based on the scenarios of buckling failure, there are several recommendations in respect to the effective length factor (K), as illustrated in **Figure 6.1** and **Table 6.1**. The variation of effective length factor is used to estimate the buckling load limit.

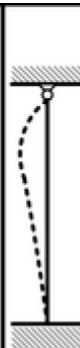
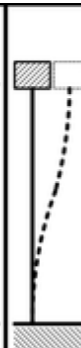
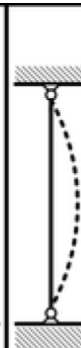
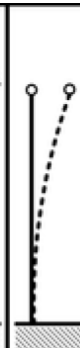
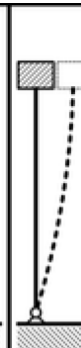
Buckled shape of column shown by dashed line						
Theoretical K value	0.5	0.7	1.0	1.0	2.0	2.0
Recommended design value K	0.65	0.80	1.2	1.0	2.10	2.0
End condition key		Rotation fixed and translation fixed				
		Rotation free and translation fixed				
		Rotation fixed and translation free				
		Rotation free and translation free				

Figure 6.1: Design value K variation

Table 6.1: Buckling limit according to K variation

K variation	Buckling load limit (lbf)	Buckling load limit (N)	Buckling load limit (Kg)
0,5	607,67	2703,05	275,63
0,7	310,04	1379,13	140,63
1	151,92	675,77	68,91
2	37,98	168,94	17,22

6.4.3 Burst Limit Calculation

Assuming the yield strength of the steel drill pipe is **31183 psi** (215 MPa) and a safety factor of **1.5**, the burst limit P_{burst} of the steel drill pipe can be estimated by following equation (Barlow equation):

$$P_{burst} = \frac{2 * Y_p * t}{d_p * Sf} = \frac{2 * 31183 \frac{N}{in^2} * 0,0787in}{0,393in * 1,5} = 8326.04psi \quad (574.06 \text{ bar}) \quad (6.7)$$

Where:

- Y_p : Yield strength of the drill pipe
- t : Wall thickness of the drill pipe
- d_p : Outside diameter of the drill pipe
- Sf : Safety factor

6.4.4 Torsional Limit Calculation

Assuming the maximum yield stress of the steel drill pipe is **31183 psi** (215 MPa). The maximum limit of torque T_{max} of the steel drill pipe can be estimated by following equation:

$$T_{max} = \frac{\pi}{16} * \sigma_{max} * \frac{(d_p^4 - id_p^4)}{d_p} = \frac{\pi}{16} * 31183 \frac{N}{in^2} * \frac{(0.393in^4 - 0,315in^4)}{0,393in} = 218.25in \text{ lbf} \quad (6.8)$$

Where:

- d_p : Outside diameter of the drill pipe
- id_p : Inside diameter of the drill pipe
- σ_{max} : Yield strength of the drill pipe

6.5 Drill Bit

The recently developed drill bit represents a notable advancement over its predecessor. Despite the rig maintaining a grinding action with high RPM, the decision was made to continue using diamond coating while significantly altering the design. For this purpose, the TUC team collaborated with engineers from **MICON Drilling** to construct a new drill bit. The primary objective was to reduce the height compared to the previous model, achieve a self-centering feature by introducing a conical angle in the center, and tilt the gauge to minimize friction on the gauge side. The new drill bit was coated with D356 diamonds, which were galvanized. This first use of the new drill bit resulted in a marked reduction in drill string vibration and a substantial increase in ROP, primarily due to decreased vibration. The new setup also demonstrated only minor hole size variations, less than 1 mm. The new drill bit measures 38 mm in diameter and 17 mm in height, measured from the exposed surface. It includes fluid pathways and is screwed in with an NPT 1/8 thread for circulation. The drill bit features only one nozzle; however, this is sufficient for hole cleaning due to the high RPM and small cutting size. In the operation of diamond-coated drill bits, determining the optimal Weight On Bit range is crucial. Using these drill bits with a very small WOB can cause the diamonds to lose their sharp edges and become polished, significantly reducing their cutting capability. Similarly, an excessively high WOB can lead to the diamonds breaking too rapidly. While this creates new edges, it can happen too quickly, potentially leading to diamond loss or areas on the bit losing their coating. The ideal operation is anticipated to be within the so-called 'micro-fracturing zone'. This is the WOB range where only minor chips are broken from the diamonds, thereby creating new sharp edges as the drilling process proceeds. To determine this zone, the drill bits are frequently analyzed with a microscope after usage under constant WOB to identify signs of micro-fracturing. So far, one drill bit has been used for approximately 2 meters and exhibited no to minor signs of wear. Further evaluation is required to determine the life expectancy for a single coating.

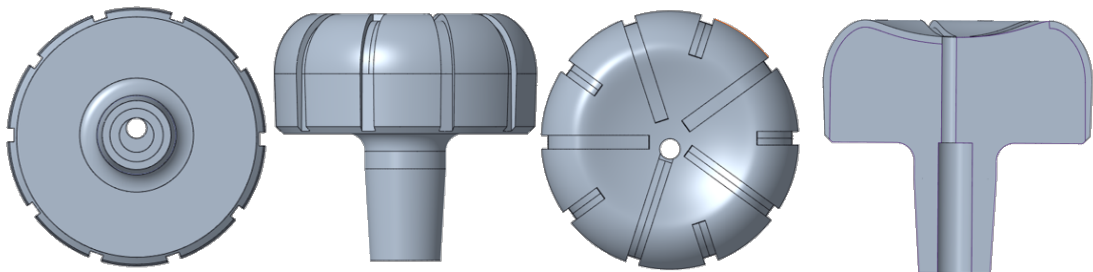


Figure 6.2: Diamond Coated Drill Bit

7 Steering System

7.1 Downhole Steering Unit

The Steering system comprises two primary components: the BHA and the surface steering units, which were completely redesigned with several optimization goals at the forefront of the new design. One significant objective was to enhance the steering capability of the BHA, allowing it to steer more tightly using less lateral force, given the employed 3-pad push-the-bit system. The geometrical steering radius is influenced by three factors: the outer diameter of the drilling bit and stabilizer, the outer diameter of the BHA housing, and the length of the BHA. The focus was on the latter two parameters since the diameter of the drill bit is regulated at 38mm in the competition regulations [Drillbotics Guidelines, 2022-2023]. The outer diameter of the BHA housing was reduced by 5mm, moving from 33mm in the previous year to 28mm this year. This reduction was made possible by developing a more space-efficient deployment mechanism for the pads. Additionally, the length of the BHA was reduced by almost 50%, from slightly above 140mm in the previous year [TUC Drillbotics - Phase 1 Design Report, 2022/2023] to 74mm this year (without drillbit). In the prior BHA design, separate housings for bearings, strain gauges, the steering pads, the IMU and the stabilizer were required, necessitating them to be secured with bolts and nuts that consume valuable space. This year, an effort was made to consolidate these components into a singular aluminum structure, see figure 7.1. Although this made the BHA more intricate and challenging to produce, it significantly reduced its length. Furthermore, the contact point between the pad and formation is now positioned farther from the stabilizer and nearer to the bit, offering greater mechanical leverage to deviate the drill bit. These enhancements have substantially decreased the geometrical steering radius from just over 1000 mm in the previous design to 220 mm, see figure 7.2.

7.2 Surface Actuation Unit

A notable difference from the design of the previous year is the actuation of the pads using the surface steering unit. The previous hydraulic system faced challenges like leakage and sealing issues due to the hydraulic actuation. In the current design, each pad possesses its own bowden cable (a steel cable that moves inside a sleeve), with a steering unit on the surface with the objective of pulling the respective bowden cable via a pulley. This pulley is

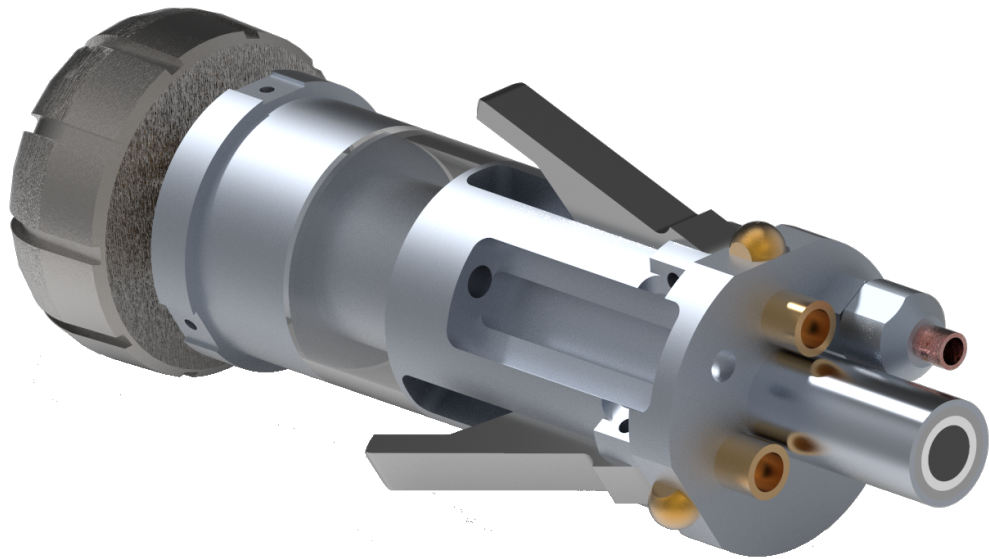


Figure 7.1: 3D-view of the BHA

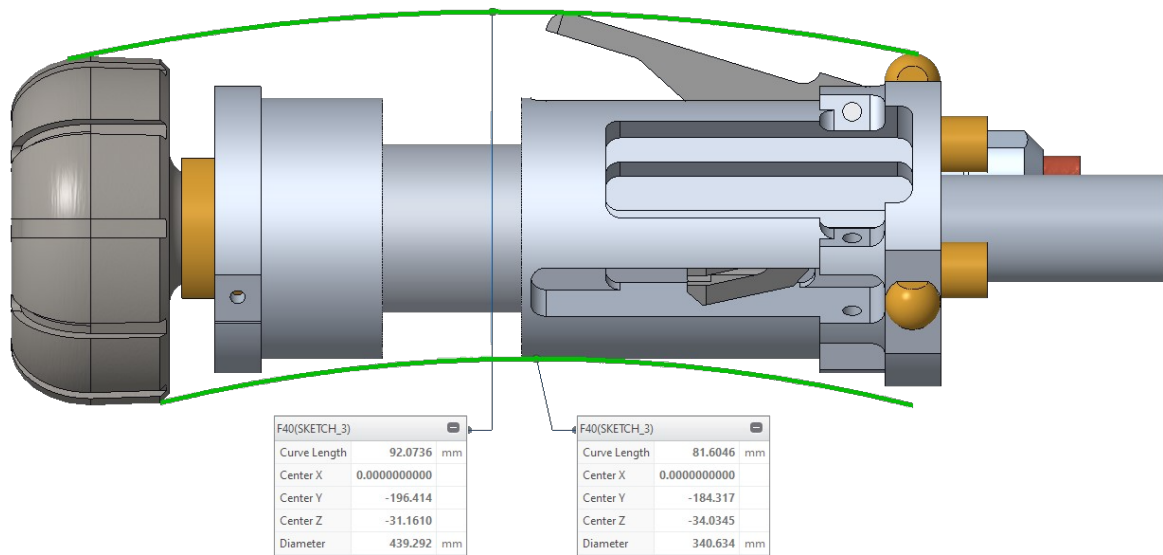


Figure 7.2: Side view of the BHA showing the geometrical minimal steering radius

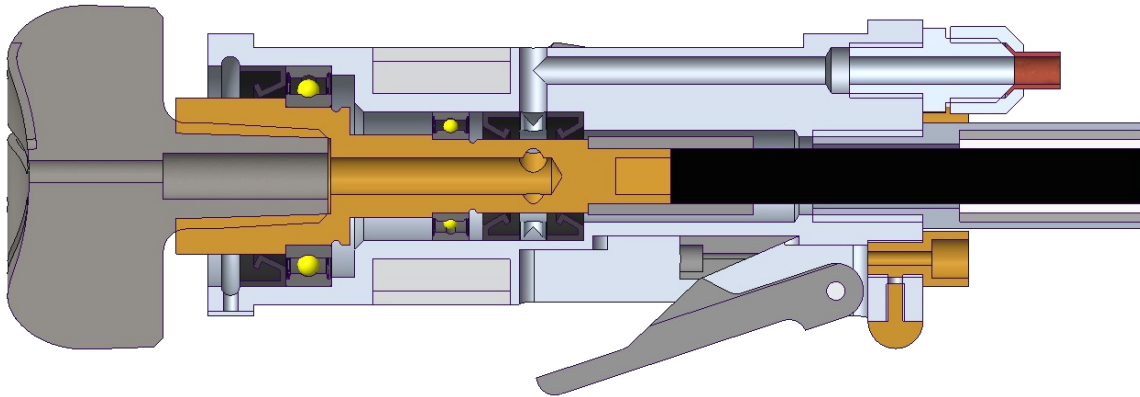


Figure 7.3: Cross-section view of the BHA showing the steering mechanism and most internal components.

operated by an electric motor, complemented by a gearbox to optimize the torque as well as a rotary encoder to ascertain the rotation of the pulley, which ensures precise measurement for the position of the wedge and the extent of wing deployment. The top end of the bowden cable is attached to a load cell, measuring the pulling force during steering, which currently has a threshold of 350 N. The pads are deployed by a sliding wedge, a modification that has proven to be significantly more effective than the previous mechanism. The former design had a lever arm actuated by a hydraulic piston, which had its set of challenges, such as nonlinearity between input and output force. The new sliding wedge design substantially diminishes this nonlinearity, resulting in an almost linear relationship between the input force (cable's pulling force) and the output force (pad's force on the formation), with an approximate ratio of 0.7. The pads can be deployed up to 23° , translating to a 10 mm deployment distance at the wing's tip. Each pad has two sliding surfaces: one between the wedge and the BHA housing, and another between the wedge and the wing's nose. These surfaces are treated with PTFE-coating to minimize friction and enhance the efficiency, see figure 7.3.

7.3 Internal measurement unit

The IMU in the BHA contains an accelerometer for inclination and vibrations measurements and a 3-axis magnetometer for azimuth measurements utilizing the artificial magnetic field generated outside the rock sample. In this way, it serves as the rig's MWD/LWD system, to enable orientation surveys. Combined with the steering algorithm this system ultimately enables directional drilling.

7.4 Maximum Inclination

Preliminary drilling tests were carried out with only one wing employed for steering. The objective was to determine the maximum build rate with only one wing in operation. For this test, the ROP was set to a constant value of 50 mm min^{-1} , and the wing force was held constant at 100 N after the KOP. Results indicated a build rate of about 4° per 100 mm, with a total deviation of approximately 22 mm from the starting position after drilling 360 mm.

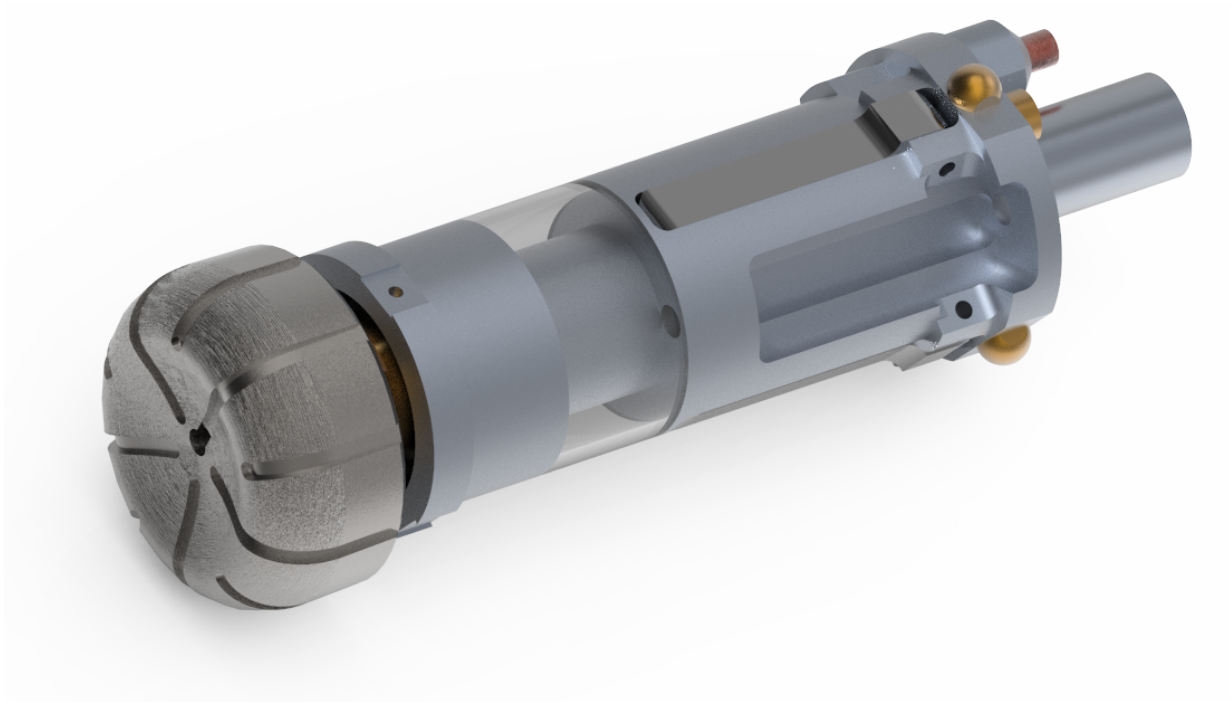


Figure 7.4: BHA

8 Mechatronic System Architecture

8.1 CAN Bus

A universal, error-resistant bus system is necessary, since many subsystems in the arrangement are required to communicate with each other without interference. Therefore, a decision was made in favor of the controller area network protocol, which is widely used in the automotive industry.

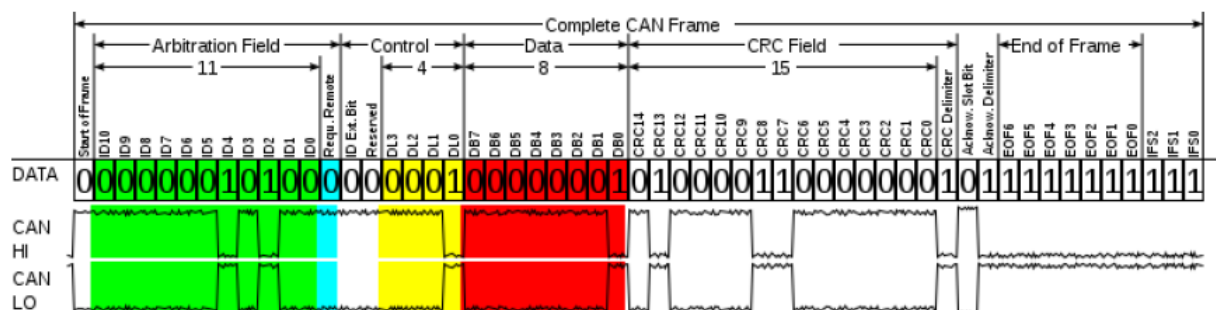


Figure 8.1: CAN bus schematic

The structure essentially consists of two redundant data lines, CAN High and CAN Low. To write a "one", the CAN High line goes to zero voltage while it is normally on supply voltage, the CAN Low line goes from zero voltage to supply voltage. To write a "zero", CAN High stays on supply voltage and CAN Low stays on zero voltage. This mechanism results in an opposing signal in which errors can easily be detected. In a CAN network, these two lines connect all participants. The electronics in the BHA and on the surface are also supposed to be connected in this way. Thus, actuators and sensors can exchange data with each other without a complicated algorithm. Synchronized processes can be organized in a decentralized way. In addition, several algorithms can retrieve data and place commands in the network independently. A practical example is an initialization, or an emergency stop command. A CAN message thus consists of several sections. In the beginning, there is the arbitration field which represents a sequential number. Depending on this number, only an individual module or all even modules are addressed. An emergency shutdown will have the number "1". Each module that does not receive this number will go into an error mode. This numbering also makes it possible to prioritize messages. If a sender wishes to send a message, it also listens to the bus lines simultaneously. If it randomly sends signals

simultaneously with a higher priority module, it automatically stops sending and waits for a new time window. Thus, important messages are exchanged very fast. The next data field of the CAN message determines the type of message. A distinction is made between data message, the message that transmits data from a module. The remote message requests data from a particular module and the error message signals to all participants that an error condition has been triggered. The overload message forces all participants to take a pause to stabilize the data traffic. Aligned behind it is the data field, which contains all the data that is to be sent. The CAN message is terminated by a CRC, a count sum to verify the correctness of the message. If this does not agree with the sum of the message, the message is considered unusable and the data is requested again.

8.2 Can bus timing

To transmit large amounts of data from many sensors as fast as possible, a data acquisition protocol was designed, as shown in **Figure 8.2**.

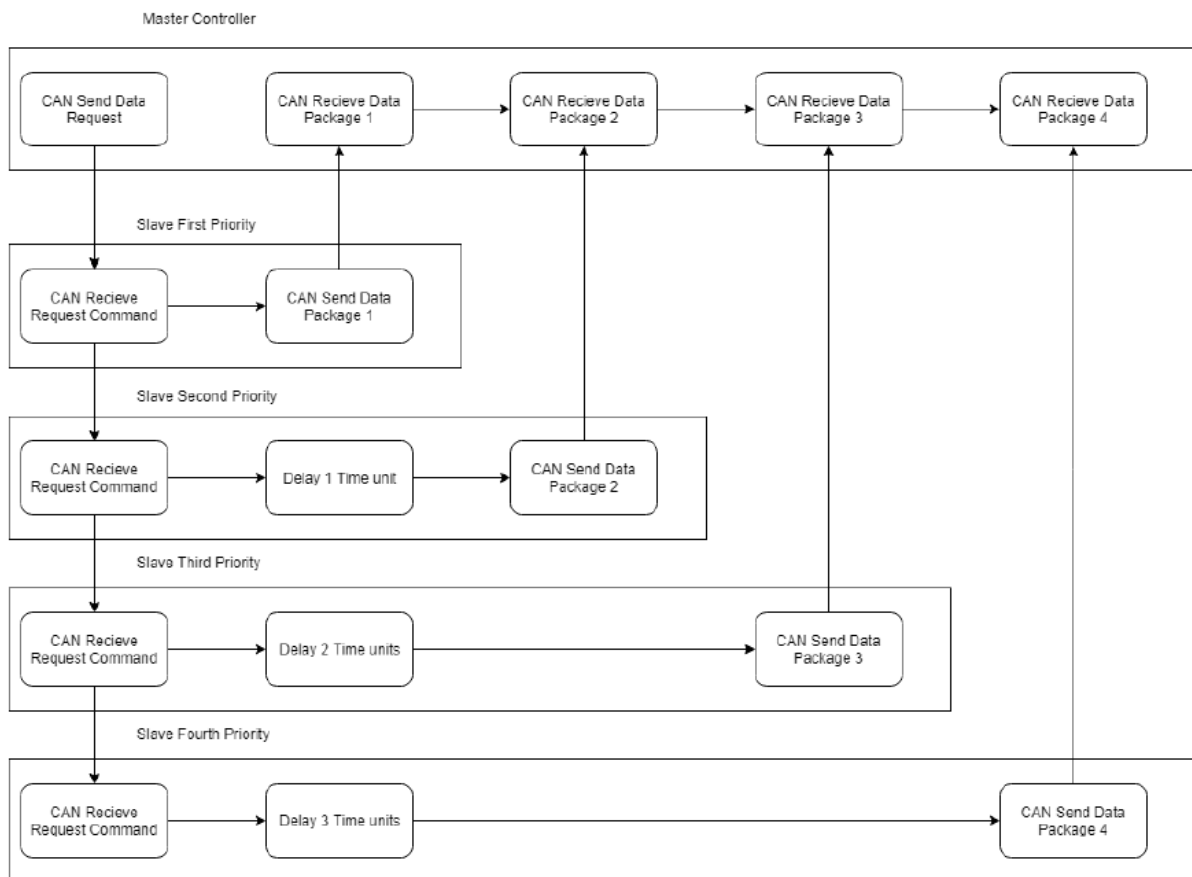


Figure 8.2: Quick data schematic

Normally an ECU would send a query message to a sensor and wait for a response. If this was received error-free, it would dedicate itself to the next sensor and again wait for an answer to the request. To avoid this waiting cascade, a trick is used. Each module that transmits data has a specific waiting time which corresponds to its own priority number. If a data acquisition message which is further noted as the clock message is send into the network, all modules, which have no data to send, pause their communication. All modules, at which data are to be queried, go into a "data sending mode" and wait for a specific time and, subsequently, send their data set. If this is successfully completed, the network returns to normal operation. Thus, the time required for the normal polling can be saved.

To accommodate network jitter and ensure a stable control loop for the hoisting module, an 'execute' message has been implemented. Considering the variable time required for computing and transmitting the drive message, the clock module additionally outputs an execute command 50ms after the clock message. When the hoisting module receives a drive command, it does not execute it immediately. Instead, it waits until the execute command is received. This approach guarantees that the time interval between the recording of the data and its execution remains consistent, allowing for a constant dead time of 50ms to be assumed. As shown in picture **Figure 8.3**.



Figure 8.3: Can time diagram

8.3 Actuator Modules

8.3.1 Motor Module

The motor control unit consists of a microcontroller unit, a electronic speed controller (ESC) and a sensed brush-less dc motor. The ESC itself is a open source Vesc 4.2, and it communicates via a Uart interface with the microcontroller. A custom Library enables the query of telemetry data like motor current, motor RPM and temperature. The microcontroller can send drive commands to the esc and sets a desired revolution speed. The Esc itself senses blockage through the attached hall sensors, so that it can commutate

the three phase current in sync with the permanent magnetic field of the rotor. If the motor or esc gets too hot it shuts down to prevent damage. **Figure 8.4**

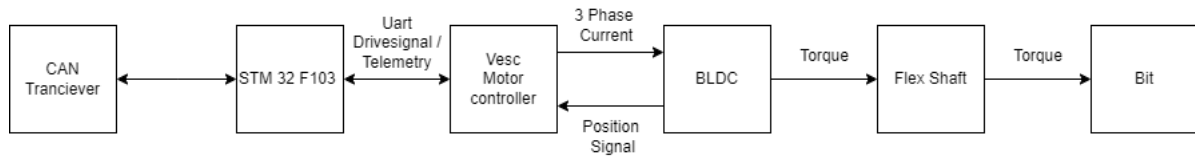


Figure 8.4: Motor control unit

8.3.2 Rotary Table Module

The rotary encoder control unit, as seen in the **Figure 8.5**, consists of a CAN transceiver and an ATmega 328p, which controls a stepper motor driver and assesses the absolute rotary encoder.

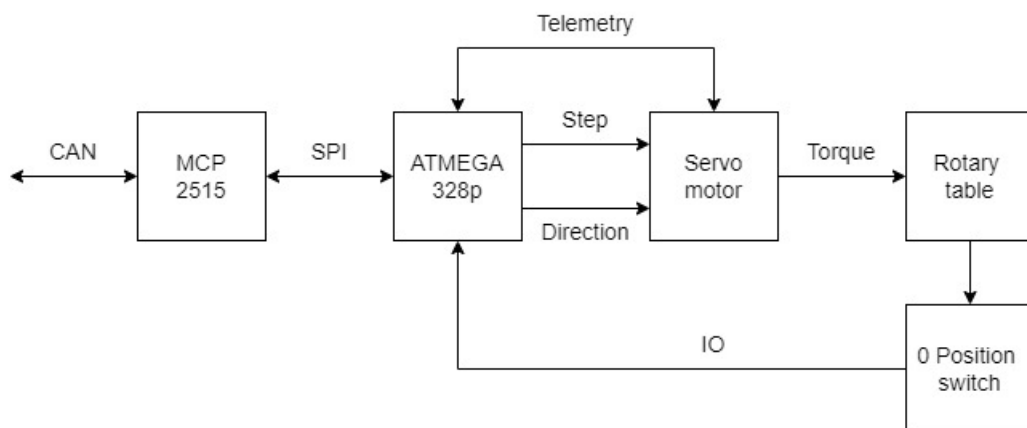


Figure 8.5: Rotary table control unit

The algorithm determines the current angle value and compares it with the desired angle. If a deviation is determined, the system moves in the opposite direction to correct the deviation to zero. As soon as the stepper motor moves, the motor current is additionally determined and compared with a previously defined maximum value. As soon as these values are exceeded, a warning message is generated.

8.3.3 Relay Module

The mechatronic system contains a CAN network controllable relay card which switches the pump. This unit consists of an ATMEGA 328p and a CAN transceiver as well as a relay card.

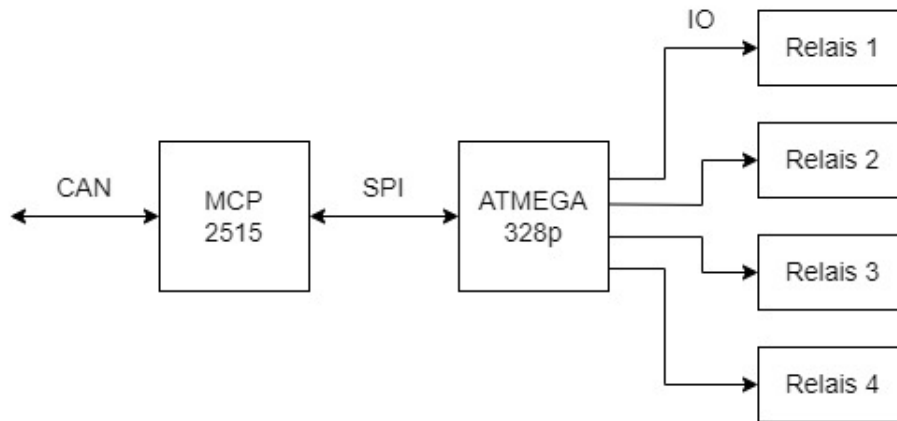


Figure 8.6: Relais switching unit schematic

8.3.4 Hoisting Module

This unit consists of a CAN transceiver and an ATMEGA 328p as well as switching inputs for the upper and lower limit switch of the hoist axis.

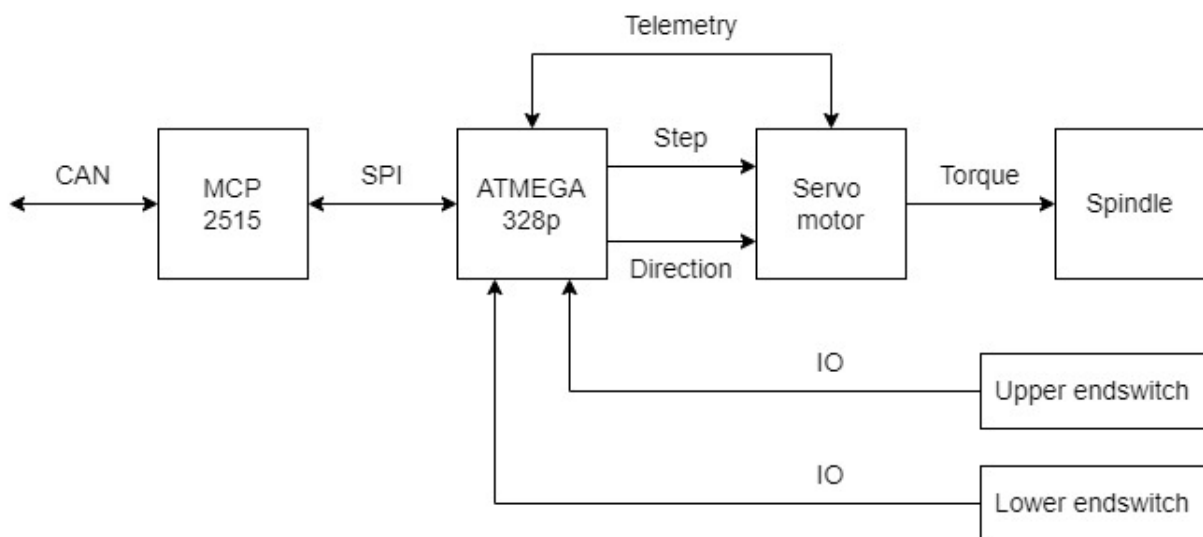


Figure 8.7: Hoisting system control unit schematic

The algorithm has in total two modes. In the first mode, N steps are driven in the pre-set direction. The second mode moves to a desired WOB and adjusts it with the hook load via the spindle. Since the controller has access to the data of the Downhole WOB module via CAN network, abnormal operating states can be determined by a comparison.

8.3.5 IMU Module

To be able to determine the actual drilled path the azimuth and inclination of the BHA has to be measured. The inclination is measured from the angle of the acceleration of gravity to the BHA, the azimuth is determined from the angle of the magnetic field of the magnetic coils to the BHA. These measurements are made in the MWD unit which consist of a magnetometer and an accelerometer (LSM303AGR). As shown in the **Figure 8.8**, one central microcontroller is used for each sensor. Communication between the sensors and controller is enabled via I2C. The information is processed by the STM32 and transmitted to the transceiver via CAN communication. This forwards the data to the bus via a CAN protocol. With this design, the magnetic range magnetometer can use the magnetic field strength outside the BHA. To ensure that the data is measured and transmitted as accurately as possible, a low pass filter is implemented. The sensor unit consists of three smaller circuit boards arranged inside the sensor ring. The system consists of a LDO that supplies the entire unit with power. For this purpose, a voltage regulator is installed to regulate the voltages for the electronics down to 3.3V respectively. This board is standardized and used for all sensors. The unit will be inserted in the notch alongside the BHA. In addition, a standardized 4 pin jst connector is used, which is intended for data transfer and programming the STM32.

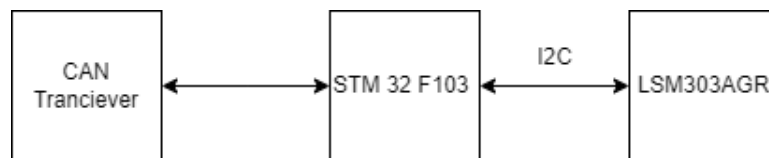


Figure 8.8: Electrical schematic of the Sensor Unit

The sensor unit in the lower notch of the BHA will be located over the drill bit. Since the BHA is constantly flooded, it is necessary to shield the sensors from water or make them waterproof. Therefore, the two sensor modules are framed with epoxy resin or silicone. The plugs are laid from the housing to the inside, where the cables are also guided along. Another sensor unit is placed at the upper end of the BHA. The two rings make it possible to better determine references and deflections of the entire BHA. Another identical sensor unit is attached to the drill pipe to measure the vibration of the drill string. This is done via an embedded optimized FFT to compute the time discrete signal into the frequency domain. These values are included in the control algorithm. This allows a maximum value to be set at a point that must not be exceeded. If the value is exceeded an alarm will go off and the RPM of the flexible shaft will be reduced. If an even higher threshold is reached, the drilling process will be stopped for safety considerations.

8.3.6 Flow-meter Module

To control a crucial part of the cutting transport, it has to be ensured that a certain flow rate is constant getting pumped through the bit. As mentioned before, there is a pre-charge pump that feeds in the high-pressure pump, so they deliver a combined flow rate. In order to precisely control and monitor the values of the pump control system, the flow meter and the pressure sensor are installed between both pumps. The flow meter consists of sensors that measure the flow rate of the liquid that passes through, it captures an accurate output with built-in visual confirmation of the flow rate in the pipe. The vane cells in the flow sensor output a square wave signal proportional to the flow rate. These serial rectangular signals are counted by the counter 74HC590 in a certain interval. The data from the serial input shift register are transferred to the output register and converted as a parallel output. After the high pressure pump, a pressure sensor was connected that works up to a maximum of 10V and records pressure up to a maximum of 400bar. The pressure sensor is connected to the ADS1115 analog-digital converter, which has an internal signal amplifier that forwards the converted signal to the ATmega328p and finally forwards it to the CAN-BUS. It also has an alarm function that issues a warning if the set maximum pressure value is reached or exceeded. The communication between the two sensors and the micro controller shown in **Figure 8.9** takes place via SPI.

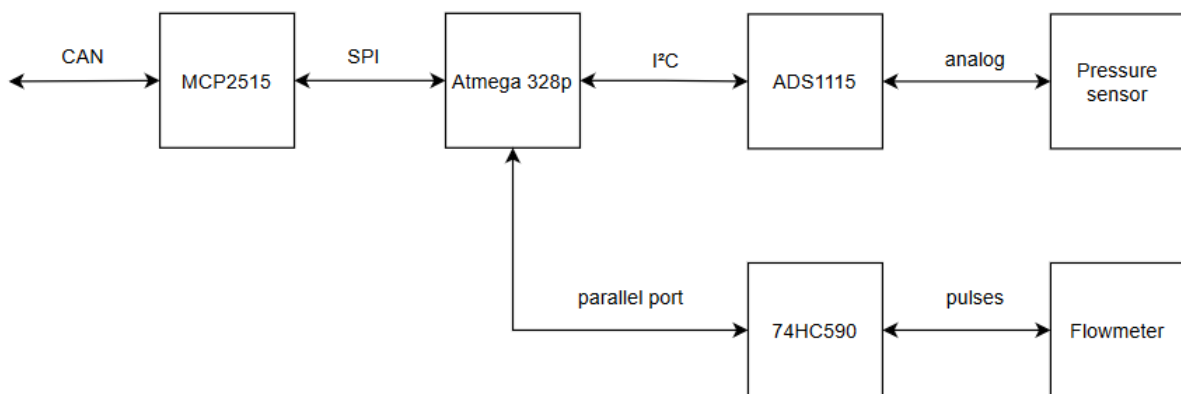


Figure 8.9: Flow-Meter and Pressure-sensor schematic

8.3.7 WOB/Hookload Module

The Down hole WOB is measured by a strain gauge inside the BHA. The Hookload is measured by a strain gauge glued to the mounting tube of the drill pipe. Both units have an Hx711 analog digital converter and a CAN transceiver which is controlled by a Atmega 328p micro controller. On request, the unit returns a WOB value or warning message if the set maximum value is reached or exceeded. In addition the units can receive a Tara command to set the output to zero.

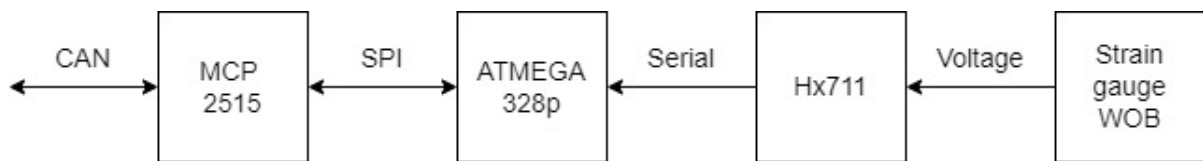


Figure 8.11: WOB Measurement module schematic

The measuring strips of the WOB unit are placed on the housing above the bit. The arrangement of the strain gauges is selected in such a way, that the influence of temperature and bending, as well as torsion, is compensated and the measuring bridge is only sensitive to strain. The measuring strips of the hook load sensor are configured in such a way that one Wheatstone bridge is measuring the axial strain and the other is measuring the torque. Due to the very small output values, an amplifier is needed. The HX711 has an internal signal amplifier which passes the amplified and converted output signal to the ATmega 328p and finally forwards it to the bus via CAN. In the sensor module, the measuring strips are mounted as a full bridge and half bridge as shown in **Figure 8.12**.

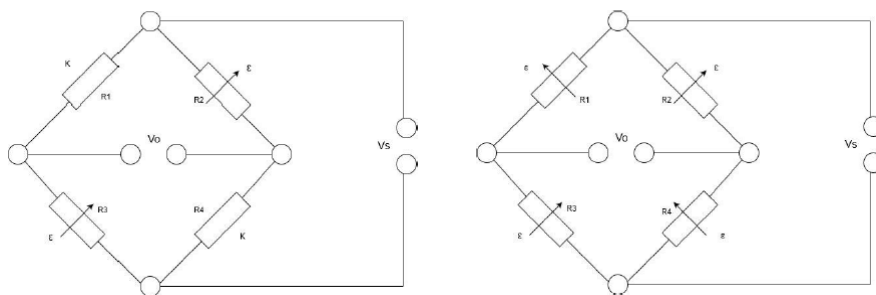


Figure 8.12: Wheatstone full and half bridge

On both controllers loops will run and query data permanently. For measuring normal elongation, the strain gauges are arranged as a diagonal bridge, each with 2 active and 2 passive measuring strips. This measures normal elongation independently of the bending strain. The strain is described by the following formula:

$$\epsilon = \epsilon_n = \frac{1}{2} * \frac{4}{k} * \frac{V_0}{V_s} \quad (8.1)$$

Where k is the K-factor of the measuring strips V_s and V_0 are the adjacent voltages. The equation can calculate the change in length that can be compared with the previously determined real values to find the critical values.

To measure the torsion, the strain gauges are installed as a full bridge, with four superimposed strips offset by 45° . The principle is like that of the half bridges and is described by the following formula:

$$\epsilon = \epsilon_d = \frac{1}{4} * \frac{4}{k} * \frac{V_0}{V_s} \quad (8.2)$$

8.3.8 Steering Module

The Steering Module comprises an STM32 Microcontroller paired with an MCP2515 CAN interface. This controller is linked to three full-bridge drivers, which in turn are connected to geared DC motors. The controller is capable of driving these motors forward and backward through a PWM signal that regulates motor current. Attached to the motor spindle is a mechanism that spools the inner Bowden cable, facilitating its movement up and down to the Bottom Hole Assembly (BHA).

To accurately determine the shaft's angle, and consequently the deployment of the wing, a magnetic rotary absolute encoder is affixed to the shaft. It is also crucial to detect whether the wing is in contact with the formation. For this purpose, the outer hull of the Bowden cable is connected to a load cell, which measures the force exerted through the spool **Figure 8.13**. In order to apply a precise force vector in the correct direction, the module executes a gradual deployment of the wings. The incoming drive command, specifying the percentage of deployment for each wing, is divided into 30 steps. At each step, the controller ensures that the force does not exceed a predetermined upper limit and advances all wings to the next step. Progression to the subsequent step occurs only if all wings have reached the current step. This procedure ensures that the force vector is applied accurately and in the intended direction.

8.3.9 Depth Module

To ensure consistency during power loss, the team decided to incorporate a redundant method for measuring the true vertical depth. The module is equipped with an MCP2515 and an ATMEGA328P microcontroller. For depth measurement, the module also includes

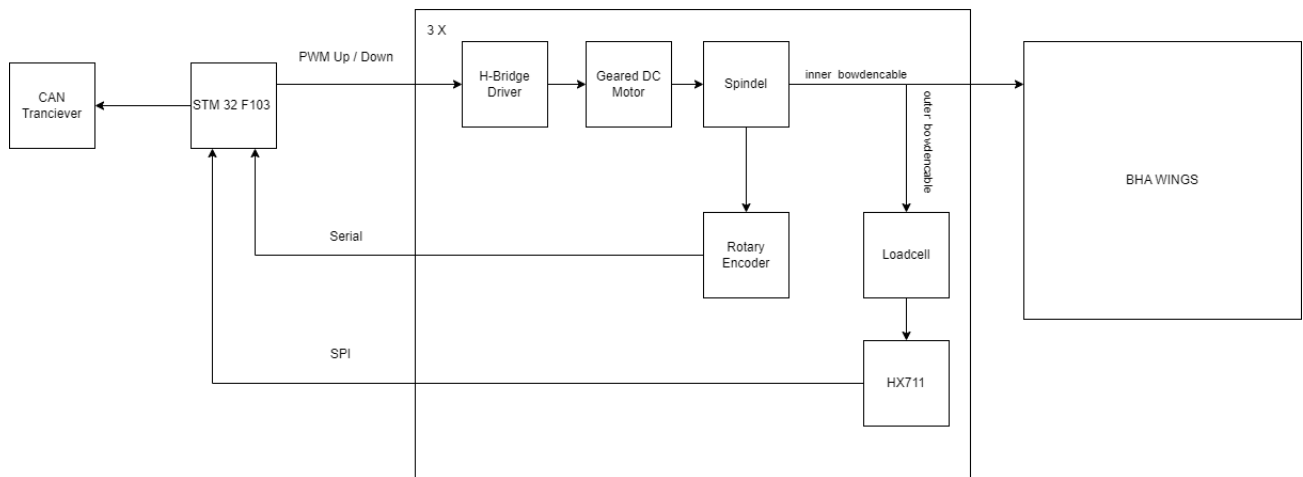


Figure 8.13: Steering module

an ADS1115 ADC with 16-bit resolution, as well as a high-precision, 10-turn potentiometer connected to a cable drum of consistent diameter. The potentiometer is powered by a regulated symmetrical power supply, and its wiper contact is connected to a hardware RC low-pass filter with a cutoff frequency of 20 Hz.

8.3.10 Clock

Given that the robot comprises multiple modules interconnected through various networks, precise timing is essential. To achieve this, an ESP8266 microcontroller equipped with an MCP2515 CAN interface and a DS3231 Real Time Clock module is utilized. This module can synchronize with a Network Time Protocol to align with the current network time. It functions as the master clock for the entire robot.

8.3.11 E-Stop Module

The E-Stop Module is comprised of an MCP2515 and an ATMEGA328P microcontroller. An emergency button, which is under continuous monitoring, is attached to the module. Upon being pressed, the module broadcasts an emergency stop CAN message throughout the network at a frequency of 10ms. This ensures that every actuator ceases its current operation immediately.

8.4 Sensor Calibration

8.4.1 IMU

Due to poor sensor quality, a noisy environment, and space limitations downhole, a unique concept was developed to calibrate the Inertial Measurement Unit more precisely. This concept involves analyzing the behavior of the drill string under bending angles, such as azimuth and inclination. A notable observation was a strong dependency between the azimuth and inclination. This dependency arises because the static drill pipe has a fixed point at the collective chuck joint. As a result, although the accelerometer readings consistently show the same acceleration, the ratios on each of the three axes differ depending on the azimuth. This phenomenon is referred to as the roll-over behavior of the drill string. Further evaluation of this behavior will be discussed in Section 10.4.6. To exploit this dependency, a calibration device will be developed. This device adjusts the inclination in a step-wise manner and performs a 360-degree azimuth rotation, also step-wise, for each step. During each iteration, the accelerometer data (acc_x , acc_y , acc_z) and the magnetometer data (mag_x , mag_y , mag_z) are recorded. The calibration device provides the actual azimuth through a rotary encoder and the inclination by the adjustment slide. This recorded data, along with the actual azimuth and inclination, are used to train a predictive model. The model processes the raw sensor data to predict the corresponding angle. Initial tests were conducted with the IMU to predict inclination using a random forest model. This model, based solely on accelerometer data, achieved an accuracy of ± 0.5 degrees. However, greater accuracy is expected in the combined version of the model, which includes both accelerometer and magnetometer data. Figure 8.14 represents the concept of how the data recorded using the calibration device will appear. Each point on the lines corresponds to a recorded value, and the model will predict the values in between, effectively generating a part of a sphere.

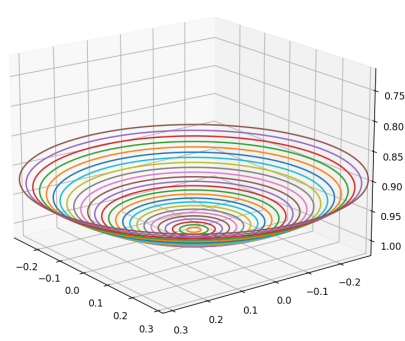


Figure 8.14: IMU Calibration Concept Visualization

The calibration device, which will be placed directly under the BHA and lowered by the top drive so that the drill bit fits into the circular cup of the calibration device, is visualized in Figure 8.15.

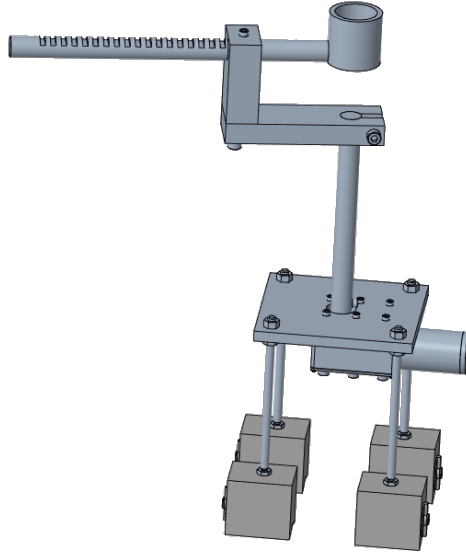


Figure 8.15: Calibration Device

8.4.2 Strain gauge

The calibration process of the strain gauges for the measurement of the WOB and the hook load are quite simple. To accurately measure forces with strain gauges an adequate bridge circuit should be chosen to for example compensate temperature influences. Since the voltage output of the strain gauges and the acting forces are proportional to each other, the calibration process of the strain gauges only needs two different measurements to accurately display the forces. One measurement must be taken in a static situation where no forces are applied, and the next measurement must be taken while a known force is applied to the strain gauge.

$$p_{prop} = \frac{F_{known} - F_0}{V_{known} - V_0} \quad (8.3)$$

With these measurements the proportionality factor p_{prop} between the acting forces and the voltage output can be calculated. The same procedure can be applied to measure acting torque on the strain gauges. If applying a force or torque is not applicable for the placement of the strain gauges, a shunt calibration method can also be used.

8.4.3 Absolute depth measurement unit

The wire spool was designed so that the maximum travel of the sledge corresponds to 10 turns. To calibrate the mechanism, it was clamped to a workbench, and the voltage difference between the fully retracted and fully deployed spool was divided by the distance. The theoretical accuracy, based on a 16-bit resolution, is approximately 0.0213mm per step. However, the actual accuracy observed, considering the system's noise, is around 0.1mm.

8.5 Development and Design of PCB

All of the PCBs and circuit boards utilized are designed and crafted within the Institute of Subsurface Energy Systems by student team members. The design process always starts with an initial sketch of all electrical components and how they should be connected. The next step involves utilizing KiCad, in which a circuit diagram has to be drawn using a developed template. This template includes the PCB size and a multi-connector to standardize connections of the PCBs and the necessary MCP2515, which enables CAN communication. As an example, the circuit diagram for the hoisting unit is presented in Figure 8.16.

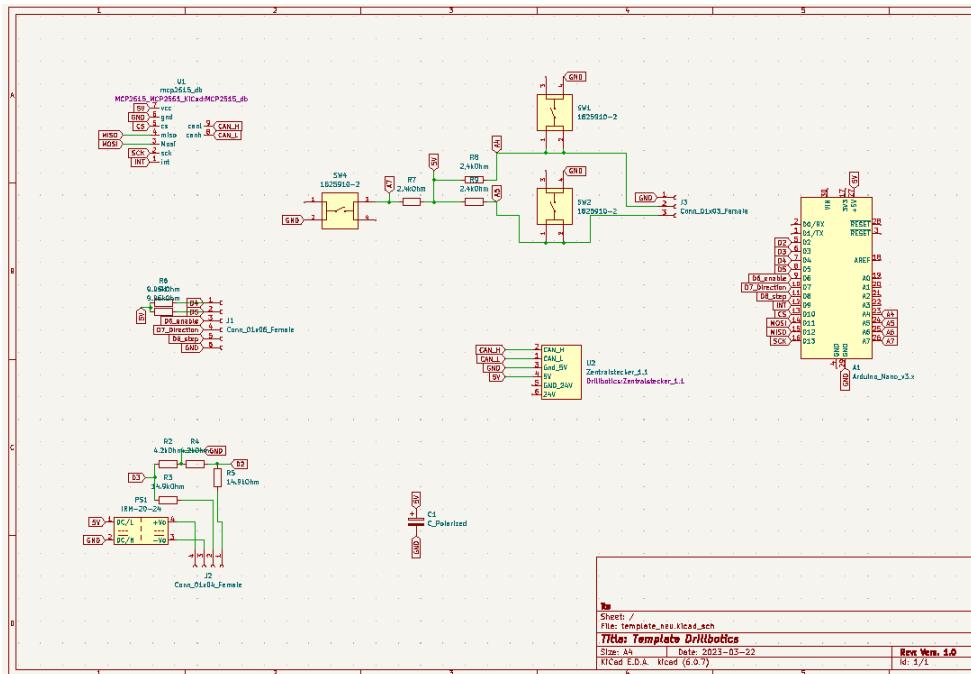
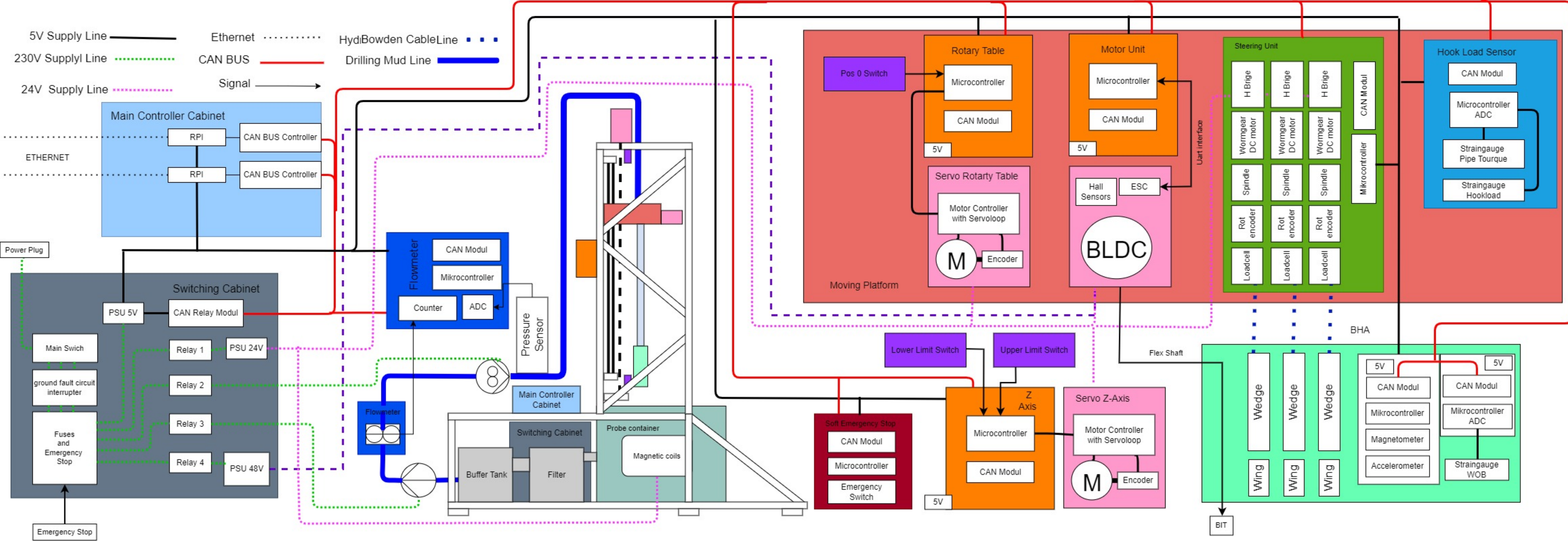


Figure 8.16: KiCad Circuit Diagram

After completing the circuit diagram and getting it approved by an advisor, the PCB design can be started, also using KiCad. The end result for the hoisting unit can be seen in Figure 8.17. With the PCB ready, the Gerber file is exported and uploaded into a program called FlatCAM, which is used to generate the CNC code. Since the traces on the circuit board will be milled out, as soon as the milling process is finished, all the individual components are hand-soldered onto the board, and initial functionality tests are performed. The resultant PCB can be seen in Figure 8.18.

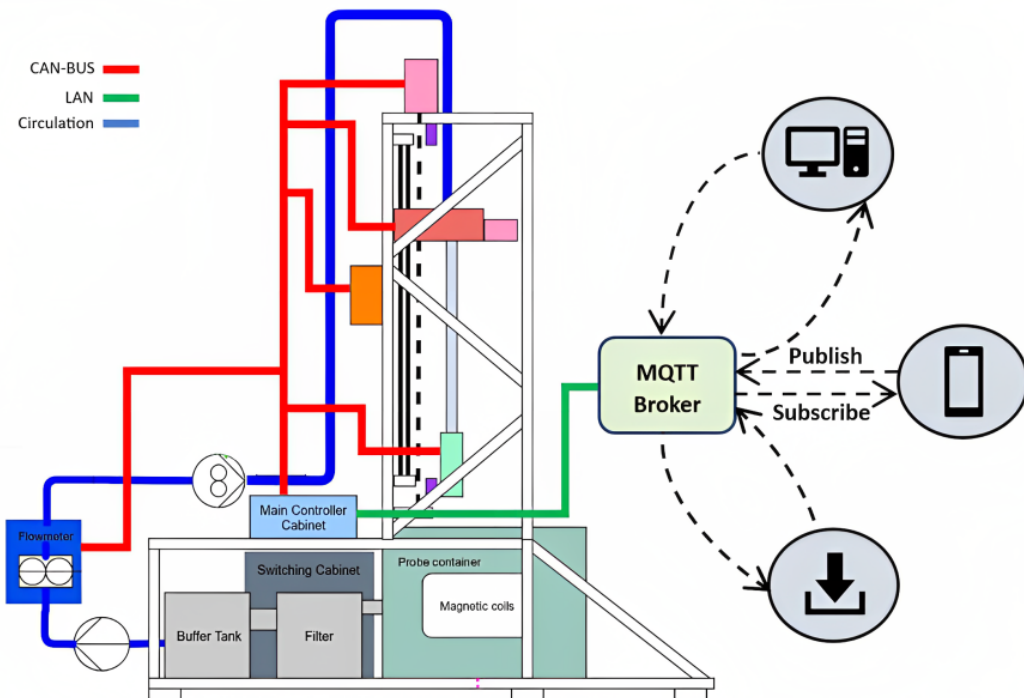


9 Network Architecture

In this chapter, a brief discussion of the rig's network architecture is presented. Notably, the majority of the algorithms that operate the machine are not located within the robot. Instead, they run on multiple external computers, enabling decentralized control of the robot. Furthermore, an overview will be provided on how these decentralized control algorithms can operate the robot simultaneously. For an initial perspective, the network can be segmented as follows:

1. Communication within the rig
2. Communication between the rig and the broker
3. Communication between the broker and the client

Figure 9.1: Network Architecture



9.1 Modular Setup and Intra-Module Communication

To preserve the scaling capability of the rig, there is no single central controller that operates all the actuators. Instead, every task and subsystem on the rig is represented by its own module. All modules are based on a uniform template, designed for easy integration into the rig. The rig currently houses 12 modules, a count that consistently increases year by year. At the core of each module is either an Arduino Nano or an STM32 micro controller, paired with an MCP2515 to facilitate CAN-BUS communication. Within the rig, all modules communicate through the CAN-Bus, allowing for a centralized node for data entry. To differentiate one module from another, each one possesses a unique set of addresses to which it responds to. An illustration of this is provided based on the Hookload module in Table 9.1. A comprehensive list is available in the Appendix 15

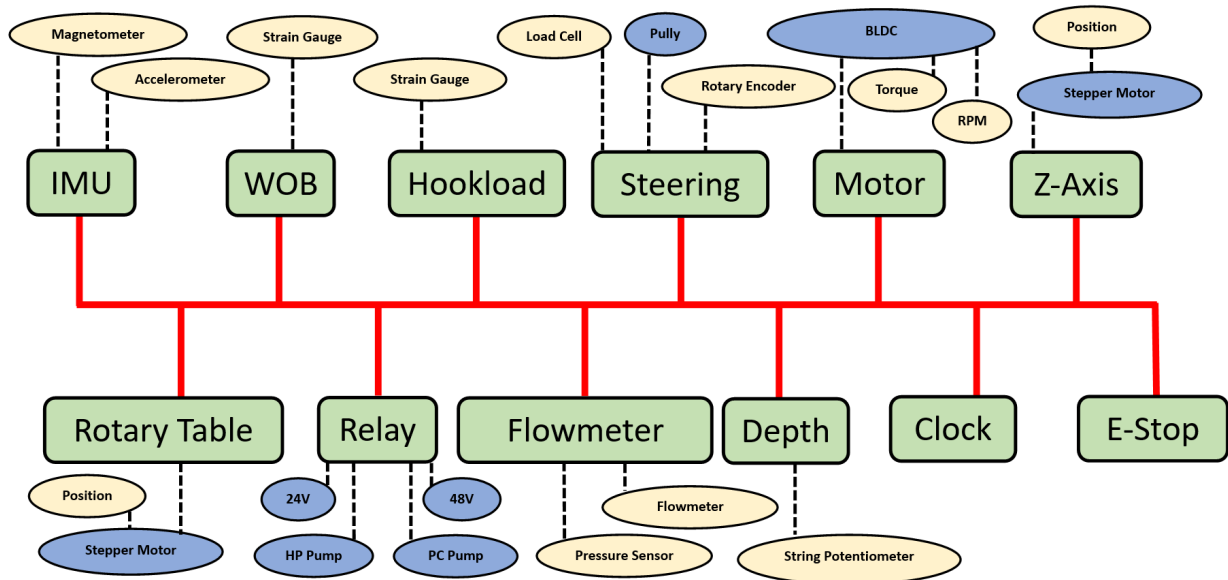
Table 9.1: Hookload Module

Hookload Module			
Address	Message	IN/OUT	Content
0x40	pong	OUT	nan
0x41	ping	IN	nan
0x42	tare	IN	nan
0x43	data	OUT	Hookload UF / Hookload F
0x43	calibration	IN	Calibration Constant / Weight conversion

In this table, the first thing to note is that the addresses are expressed as hexadecimal numbers. Next to the addresses, the 'Message' column contains the name of each message. For instance, the ping/pong messages are represented in all modules. The concept behind this was to enable the capability to ping a module. For example, when the Ping message is sent to the Hookload module, it would send 'pong' back, indicating that the module is currently active. Later on, during drilling, there is a separate client responsible for periodically sending 'ping' and checking for the 'pong' from all modules to ensure that no modules are missing. This feature was also utilized to record the response time and latency of the system in is presented in Section 9.4 The other messages can vary depending on the module. In this case, the 'Data' message would contain both the unfiltered and filtered Hookload values. The 'IN/OUT' column indicates whether the message is sent to the module or from the module. In this instance, the data is recorded via strain gauges, showcasing another functionality of the modules, namely also serving as an interface for both actuator and sensor connections. Figure 9.2 showcases the complete CAN-BUS connection to all the modules, with actuators (in blue) and sensors (in yellow) connected to the modules themselves. One important module is the clock module, which provides the entire robot

with a machine cycle. When the clock is active, it sends a CAN message every 100ms. All the modules respond by publishing their data in a predefined order. The CAN-Bus architecture also includes an additional important module that enables the connection with the MQTT Broker.

Figure 9.2: Modular Setup



9.2 CAN-Bus Translator and MQTT Broker

9.2.1 CAN-Bus Translator

As previously mentioned and visualized in Figure: 9.1, the CAN-BUS is not directly connected to the broker. Instead, an RPI located inside the main controller cabinet serves as the last connection node of the CAN-BUS. This RPI is further connected via LAN to the MQTT Broker. The translator runs on the RPI and acts like a gateway; it receives all messages from the CAN bus, converts them into a predefined data format (Refer to Appendix 15 for the detailed CAN to Broker Translation Table.), and then uploads them to the broker under a specific topic. This process is bidirectional, meaning the translator instance also receives all the messages uploaded to the broker, converts them into the CAN message format, and sends them through the CAN bus. Besides its gateway capability, the translator also provides the initial point where data can be modified or converted. For instance, if received units need to be altered, a calibration constant can be implemented for each payload passing through the Translator. A second important feature of the translator is the allocation of a timestamp. When messages come from the CAN bus, the translator assigns the current timestamp to the message before publishing it on the broker.

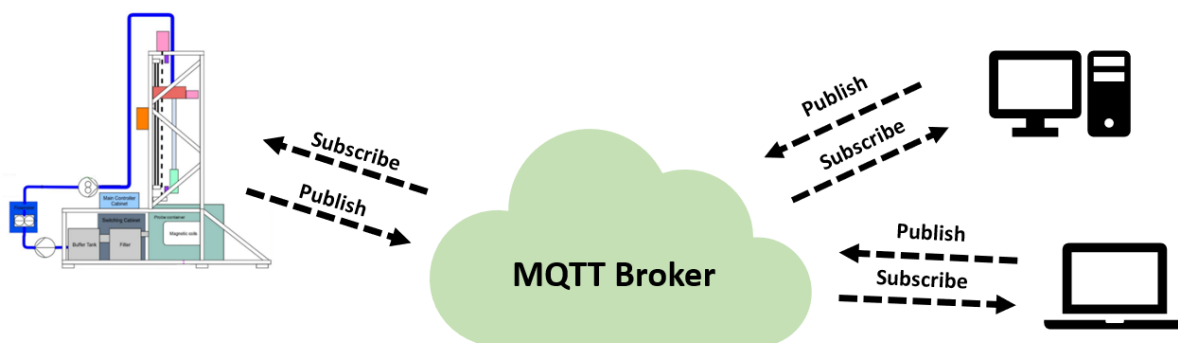
9.2.2 MQTT Broker

MQTT (Message Queuing Telemetry Transport) is a messaging protocol that is particularly popular in IoT applications. When mentioning the term "Broker" in relation to MQTT, essentially a server is being described. The role of the MQTT broker is to act as a middleman between MQTT clients. A client can be anything from a sensor to another server in a different location, or a computer running algorithms. These clients communicate with each other by publishing (uploading) messages with a specific topic to the broker or by subscribing to existing topics on the broker to receive messages. The basic concept revolves around publishing and subscribing to different topics. A topic is a string that represents a subject to which a client can publish or subscribe. One example could be "wob/data", with "wob" being the main topic representing the wob module, and "data" being the message from that module. "Publishing", in terms of MQTT, means when a client sends a message to a certain topic. "Subscribing" indicates a client's interest in a topic, and as a result, they receive all messages sent to that topic. To further prioritize messages, the broker offers a *QoS* (Quality of Service) (HiveMQ, 2019). MQTT has three levels of *QoS* that determine message delivery:

1. **QoS 0:** The message is delivered at most once, and delivery is not confirmed.
2. **QoS 1:** The message is delivered at least once, and delivery is confirmed.
3. **QoS 2:** The message is delivered exactly once by using a four-step handshake.

In summary, the broker receives messages from clients, stores them until a new message arrives, and forwards them to every subscriber. The broker is located outside the drilling rig and is connected via *LAN* to the CAN-Bus translator. The translator would then be the first client representing the rig on the broker.

Figure 9.3: MQTT Broker



9.3 Client Setup

Since the broker stores data under specified topics, all the CAN addresses must be mapped to different topics. The setup was chosen such that the main topic represents one of the 12 modules. As a simple example, consider the CAN address $0x33$. The first number after the x specifies the main topic. In this case, it is the number three, corresponding to "wob/". The number following the three, in this instance the "3", specifies the subtopic, which is "data" (please refer to Appendix 15 for a detailed overview of the CAN to Topic table). This topic will then contain a payload in the form of a JSON object, which includes a timestamp. This timestamp is assigned when passing through the translator as a reference for the corresponding record time, so when subscribing to "wob/data", the following payload will be received:

```
{
  "unfiltered": "payload",
  "filtered": "payload",
  "timestamp": "Unix"
}
```

Due to the multi-client functionality of the broker, the client setup was chosen in a way that requires 6 clients to operate the rig, ensuring the work effort is distributed fairly:

1. The **Translator** represents the first client that logs into the broker.
2. The second client runs the **Autonomous Drilling Algorithm**.
3. The third client is the **Engineering Control Interface** for manual overrides.
4. The fourth is the **Surveillance Unit**, monitoring crucial limits of the machine.
5. The fifth is the **Data Logger**, which logs all data coming from and going to the machine.
6. Lastly, the **GUI** is responsible for visualizing necessary data.

The only limitation for the clients is that data must be received in the previously mentioned JSON format and must also be published in the same format. Beyond this, a client can connect to the broker using most of the well-known programming languages. The Autonomous algorithm, described later in this Report, is entirely based on *Python*. However, other clients may operate using *C*, *Java*, *React.js*, *GO* or *MATLAB*, allowing for a very flexible control approach.

9.4 Response time and latency

9.4.1 Setup

To record the system's response time and latency, a test script was developed. Upon starting, this script would measure the time it takes for a message to be sent from the client to the rig and then back to the client. To record this time, the built-in "ping/pong" feature available in each module was utilized (refer to section: 9.1). The test was conducted under four predefined conditions:

1. No message traffic from the rig and no traffic from other clients.
2. With the Clock module on the rig running, causing all other active modules to publish their data on the clock pulse, resulting in a data stream of $6.9 \frac{kB}{s}$.
3. Traffic artificially increased to $13.8 \frac{kB}{s}$.
4. Traffic further increased to $138 \frac{kB}{s}$.

For each case, the same module was chosen. A total of 50 ping messages were published, and the corresponding time was measured.

9.4.2 Evaluation

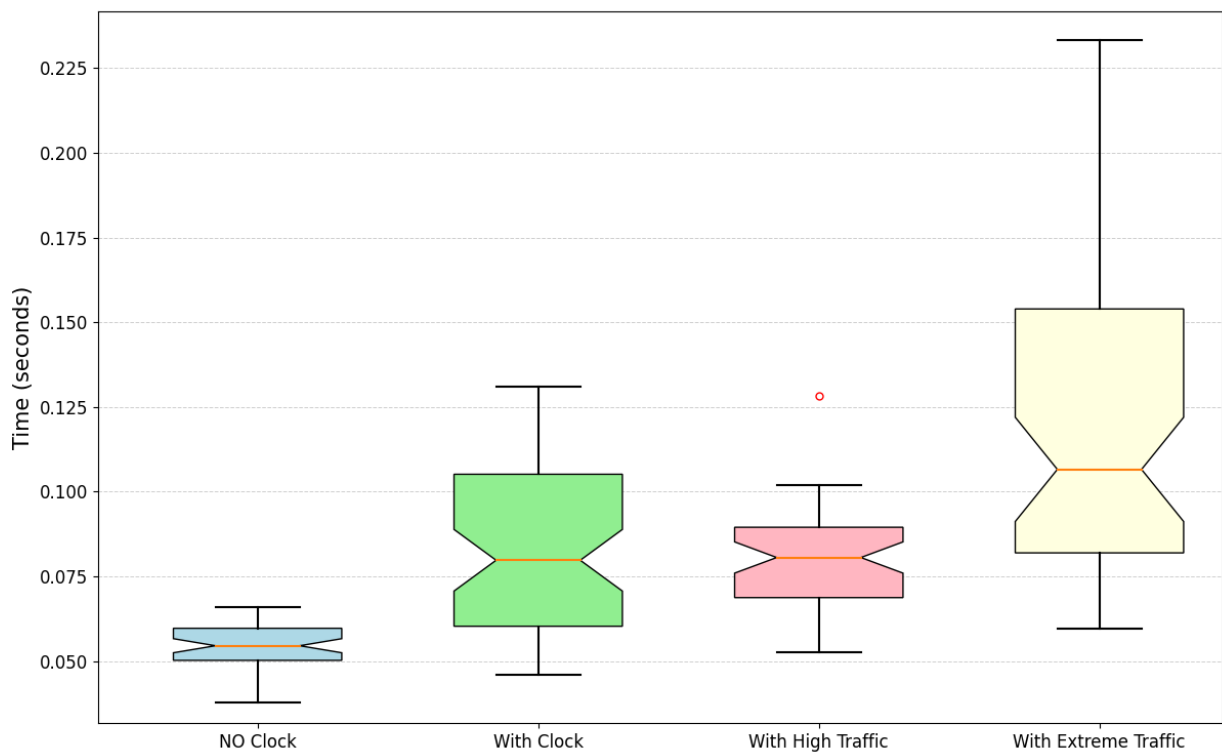
As expected, the case without any traffic and no clock performed the fastest with an average time between a ping and pong being $54.50 ms$. When the communication time within the modules is neglected, the dead time between sending a message and a physical response will be $22.75 ms$. Although not significantly fast, for the system's application, this time is sufficient. In comparison to the other cases, the "No Clock" case experienced significantly less variation. The case with the clock, representing the normal operating traffic, had an average time of $79.74 ms$, indicating an increase in transmission time. This trend is further supported by other cases showing increasing reaction time when increasing the traffic. However, with the clock running, not only was a higher transmission time recorded, but also significantly more variation in transmission time was observed.

This doesn't seem to correlate directly with the amount of messages processed since the third case, although having a higher response time of about $80.54 ms$, had significantly less variation. Indicating that within transmission path an instance could be responsible for causing this randomness. The high traffic case would also represent the amount of traffic existing when the rig is operated by 6-7 clients in full autonomous mode. The extreme traffic case, although experiencing much more variation and randomness, achieved an average

Table 9.2: Dead Time and Recorded Time for Each Case

Case	Dead Time (<i>ms</i>)	Recorded Time (<i>ms</i>)
No Traffic, No Clock	27.25	54.50
Clock	39.87	79.74
High Traffic	40.27	80.54
Extreme Traffic	53.28	106.55

response time of 106.55 *ms*. Multiple approaches were needed to record 50 ping/pong cycles since the extreme traffic caused the translator frequently to crash. However, this was to be expected since this much traffic is not anticipated during the operation of the rig. A possible solution would be to split the workload of the translator upon two RPIs: one translating everything coming from the machine and one translating everything coming from the Broker. In summary, the transmission time and accuracy to and from the rig highlight

Figure 9.4: Recorded dead time of the rig

areas for improvement. While currently sufficient for the control algorithms employed, future developments of more advanced control algorithms and models might encounter issues. Further analysis is required to determine the causes of variability in transmission time. To pinpoint areas of enhancement, as previously mentioned, one potential solution could be distributing the workload of the translator.

10 Software Architecture

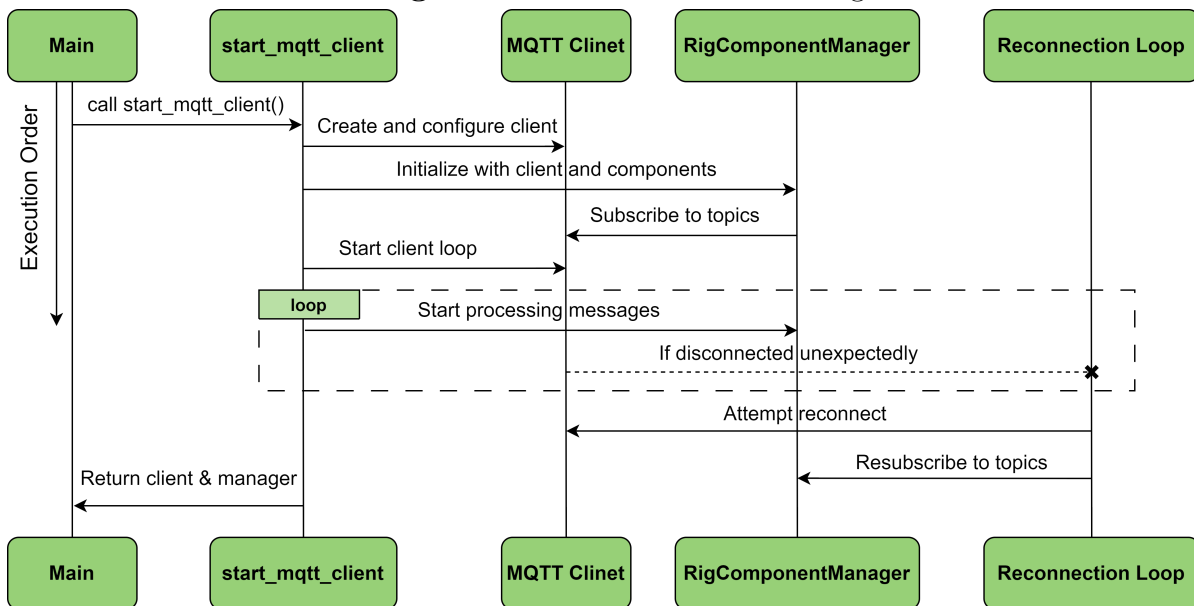
After closely examining the physical rig and its network architecture, a solid foundation was laid for the development of an autonomous control algorithm. The main objective of this development was to design a drilling algorithm that supports hands-free operation for the small scale Directional drilling rig. Once initiated with a single button press, this system targets an automation level between 9 and 10 after Parasuraman et al. (2000) . The purpose of this algorithm is to fully automate the essential procedures involved in drilling a directional well with a maximum TVD of 600 mm. This challenge translated into automating three critical processes: Drilling procedure, Survey procedure, Steering procedure. With the existing setup, the implementation of the algorithm became possible. The algorithm's design and development originate from the broker, where all the data from the rig is stored. This mandates the algorithm to first initiate a connection to the broker, ensuring efficient data retrieval, which will later be employed in the algorithm's operations. While the primary goal is hands-free operation, the system must also offer a manual override feature. This ensures that the driller has the capability to intervene whenever deemed necessary. Flexibility is built into the algorithm's architecture, allowing for on-the-fly modifications, including the incorporation of different controllers for experimental or educational purposes. Considering these requirements, the most practical architecture for such an algorithm is a state machine, which controls the robot's various states with a control panel. Even in its basic form, this setup enables manual operation of the rig. The automation element is then introduced via a "Commander" object. This component continually assesses conditions that might require a state transition, prompting the state machine to alternate states and undertake varying tasks. In summary, the main components of the algorithm include:

1. Connection Handling Object: Manages the link to the broker.
2. Digital Counterparts: Representations of all the physical rig modules.
3. Managing Object: Overseeing data transition and organization.
4. The State Machine
5. The Commander: Automates state transitions based on predefined conditions.
6. Engineering Control Interface: Allows for manual operation and intervention.
7. Data Logger: Monitors and records operational data.

10.1 Connection Handling

Connection with the Broker is achieved using the paho.mqtt library. Since a stable connection is required, the built-in keepalive value is set to default. This ensures that the client is prioritized within the broker, and even after a long period of inactivity, it is not disconnected by the broker. Given the vast amount of data expected, a Manager object is introduced. This object takes the client and all the digital counterparts of the rig as input, handing the messages over to them. The manager further establishes all subscriptions demanded by the rig components to receive the necessary data from the broker. To receive data, the built-in `on_message` function from the paho.mqtt library is used. This function runs every time a new message arrives at the client. To process these messages, the Manager object includes a `process_messages` function that runs in a separate thread, handling incoming messages and sorting them to the components.

Figure 10.1: Connection Handling



Since the stability of the connection is crucial for the operation of the algorithm, countermeasures for unexpected disconnections have been implemented. As soon as an unexpected disconnection is detected, a re-connection procedure is triggered and run in its separate thread. This ensures re-connection in the background so that ongoing calculations are not interrupted, during disconnection all operations on the rig are stopped since no modules are receiving any further commands. The client will attempt to reconnect with proper exception handling. If an exception is raised during the re-connection, a time delay is

implemented before the re-connection is tried again. After losing connection, the client is reset to default by the broker, losing the previously demanded subscriptions. To ensure the necessary topics are subscribed to, the manager object resubscribes to all topics. In several test runs, connection handling has proven to be reliable with minimal to no unexpected disconnections. If disconnected, re-connection was accomplished most of the time within the first iteration of the loop, resulting in less than 1 second of connection loss. There were no incidents where the connection was lost for more than 5 seconds. Due to the complexity faced with ensuring a stable connection, multi-threading applications and asynchronous programming became necessary in most other parts of the algorithm.

10.1.1 Multi-Threading and Thread-Safe Programming

Multi threading relates to the ability of code to run simultaneously. Instead of one code block running from top to bottom, multi threading applications can start in the middle of the main code and operate in the background, handling tasks like the aforementioned connection handling. The risk when implementing multi threaded applications into an algorithm is the potential hazard of race conditions between two threads and a phenomenon called thread starvation. A race condition occurs when two threads try to access the same instance, potentially leading to undesired output for a short period. As a countermeasure, the usual procedure is to apply a thread lock to the memory space accessed by the first thread, ensuring that the data cannot be changed while one thread is operating. Implementing thread locks should be done with caution to ensure that locked memory space is eventually released, preventing a waiting thread from being starved. If a thread enters a scenario where it waits for an extended period for memory space to be released, the thread will raise an exception and be terminated. This is in every case to be prevented. (Thread Safety (2023), Multithreading)

10.2 Digital Rig Counterparts

As previously mentioned, to ensure the algorithm's universality and adaptability, all incoming data must be stored in accessible variables. For intuitive algorithm design, each physical rig component is represented as an object. Given the repetitive nature of this task, a factory design pattern was introduced. This pattern facilitates the appropriate use of Child and Parent classes. Initially, a parent class, RigComponent, was defined. This class serves as an abstract base, laying the groundwork for components to send and receive MQTT messages. Child classes inheriting from RigComponent are mandated to incorporate an

.on_message and a .create method. Additionally, RigComponent includes a static method for exception handling, which is subsequently wrapped around all functions within the actual component call, ensuring robust exception handling on all iterations where data is read and stored. Conceptually, a component object can be compared to a shelf. It stores the most recent data points in easily accessible variables, which are continuously updated in the background. Each component contains multiple handler methods, called when their specific .on_message function is run. The .on_message function, taking the topic and payload as inputs, determines which handler to invoke based on the subtopic. The handler then stores the topic's payload in variables. Furthermore, each component has designated send methods. These were implemented to centralize the point from which messages are dispatched from the client. When a send message is activated, it's placed in a queue. A separate thread then publishes the messages following a First-In-First-Out (FIFO) principle, ensuring messages are broadcasted in their intended order. As illustrated in section 9.3, the payload of a topic can encompass multiple data points. The handler method within the specific component is responsible for unpacking this payload and allocating the data to various variables. This process represents the third and final data conversion. Table 10.1 lists all the JSON objects specific to the subtopic and indicates the variable where the data is stored for subsequent algorithmic use. These variables can be accessed at any time by invoking 'manager.Component.variable'. For instance, to access the unfiltered WOB data, one would use 'manager.Wob.data_unfiltered'. The table also offers a brief description of each subtopic and presents a summarized client publish/subscription list. In this version, only Client 1, representing the Autonomous algorithm, is shown, detailing which state machine component accesses which variables or publishes on a particular topic. For a comprehensive version, please refer to the Appendix 15.

Table 10.1: WOB Component Setup

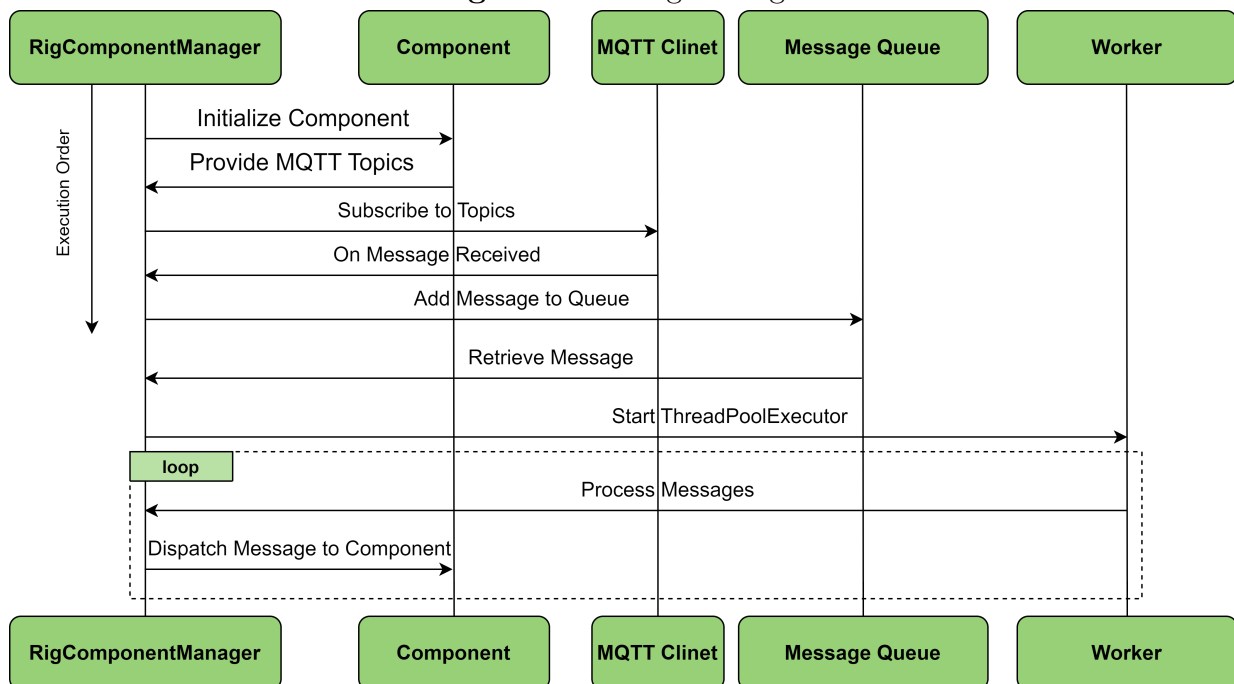
Ox30							Client 1			
wob/	Nr.	Subtopic	Json format	Variabel	Description	Software Components	main.initiation	main.survey	main.drilling	main.steering
	0	pong	[{"pong": "0", "timestamp": "Unix"}]	.pinpong .pinpong_unix	If the /ping topic is published, the module will publish /pong as feedback indicating that the module is on board.	Published by				
						Subscribed by				
	1	ping	[{"ping": "0", "timestamp": "Unix"}]		Ask if the module is responding and working.	Published by				
						Subscribed by				
	2	tara	[{"tara": "0", "timestamp": "Unix"}]	.tara .tara_unix	tare the WOB unit	Published by				
						Subscribed by				
	3	data	[{"unfiltered": "payload", "filtered": "payload", "timestamp": "Unix"}]	.data_filtered .data_unfiltered .data_unix	On this topic, the sensor data from the WOB unit will be published.	Published by				
						Subscribed by				
4	call	[{"unitconversion": "payload", "filerconstant": "payload"}]	.call_unit_conversion .call_filter_constant	this topic is used to calibrate the WOB unit	Published by					
					Subscribed by					
5					Published by					
					Subscribed by					
6					Published by					
					Subscribed by					

The following section will discuss the Manager object, responsible for directing topics to their respective components. This ensures that irrelevant topics don't consume unnecessary computational resources.

10.3 Rig Component Manager

The Rig Component Manager is a crucial element of the algorithm. It oversees the communication between the broker and rig components. Drawing from the analogy where the rig component was described as a shelf, the manager receives data packages from the broker and pre-filters to determine the intended component for the data. Once the destination of the message is ascertained, the manager object allocates a worker to relay the data to the component. During high traffic periods, the manager can allocate up to 10 different workers to sort simultaneously.

Figure 10.2: Rig Manager



In detail, the primary entry point for any new message is the `.on_message` method within the manager object. To ensure this function remains accessible, intensive computing and sorting are avoided within the `on_message`. As soon as a message arrives, the only verification performed is to check if the client ID matches that of the statemachine. Although the statemachine communicates with the broker, communication within the statemachine doesn't

need to traverse from the client to the broker and back to the same client. Therefore, the sending client ID is blocked. After this verification, all messages are queued. In the background, the `process_messages` method of the manager constantly works to keep the queue length at zero, ensuring no message accumulation. This function can call up to 10 workers that check the main topic to decide which component to involve. Later, as explained in Section 10.2, the data is saved into a variable based on the subtopic. The step-by-step functionality of the manager is visualized in Figure 10.2. Initially, the manager initializes all components and extracts the required MQTT topics from them for subscription. Once this is accomplished, the manager can receive messages, which are then transferred to a queue. From the queue, up to 10 different threads can process the messages simultaneously. The expected volume of messages received ranges between 10-15 messages per 100ms, with an average message size of 69 bytes. This translates to a required processing speed of 10kB/s. During various tests, the system demonstrated that the queue can be maintained at zero length, even when processing up to 500kB/s.

10.4 The State Machine

The core of the system is the state machine. The state machine is defined as an object containing multiple states, represented as methods. To maintain universality, the state machine algorithm does not embed the logic of each state within it. Instead, the logic is encapsulated in a separate object, which is then imported into the machine. This approach ensures that the state machine code remains clear and structured. An added advantage is that multiple logic procedures can be defined for each state, allowing for modifications to state logic without altering the state machine's layout. The state machine encompasses six states:

- | | | |
|---------------------|-------------------|-------------------|
| 1. Default state | 3. Park state | 5. Survey state |
| 2. Initiation state | 4. Drilling state | 6. Steering state |

The default and park states are integral to the state machine and cannot be replaced. This design choice serves as a safety measure. Upon entering the park state, manual control is enabled. State transitions can be initiated either manually or by adhering to a predefined procedure to activate the commander object, which embodies the autonomous drilling capability. The current state is stored in a global variable. Any change to this variable, whether internal or external, prompts the machine to switch states.

10.4.1 Default State

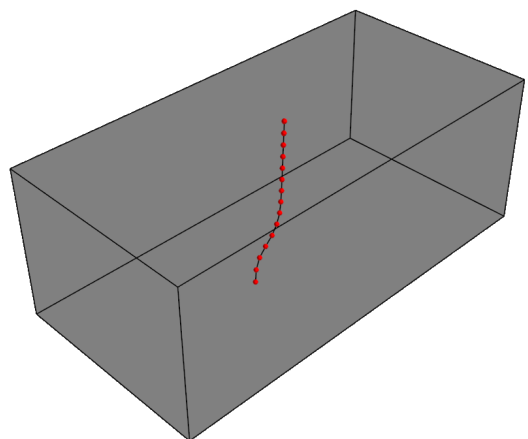
The default state is the initial state upon activating the state machine. Upon entry, the system sets a threading flag, causing the state machine to pause until a specific condition is met. The operator can either choose to control the system manually or activate the commander. In the latter scenario, the only state acknowledged initially is the Initiation state.

10.4.2 Initiation State

When the driller enters the "Initiation" state through the control panel, the system will exit the default state and enter the initiation state. This transition is made public and updated on the broker. The first message the driller will receive is to enter the desired coordinates that the system should target. Additionally, the initial motor RPM, the number of surveys, and the initial WOB-setpoint should be implemented. In later development of the algorithm an adjustment of the WOB-setpoint and the motor RPM is intended to be done by the algorithm. For the first version, this has to be implemented by the driller. However, the necessary interfaces are already in place to apply adjustments in the setpoints and will be mentioned in the following states. For the first release, this algorithm was suited for drilling into a homogeneous Bentheimer sandstone, which allows for static setpoints in WOB and RPM. As soon as all the setpoints are received, the algorithm would proceed with executing a module query, checking for missing modules using the previously described ping/pong (refer to Section 9.1) features of the modules.

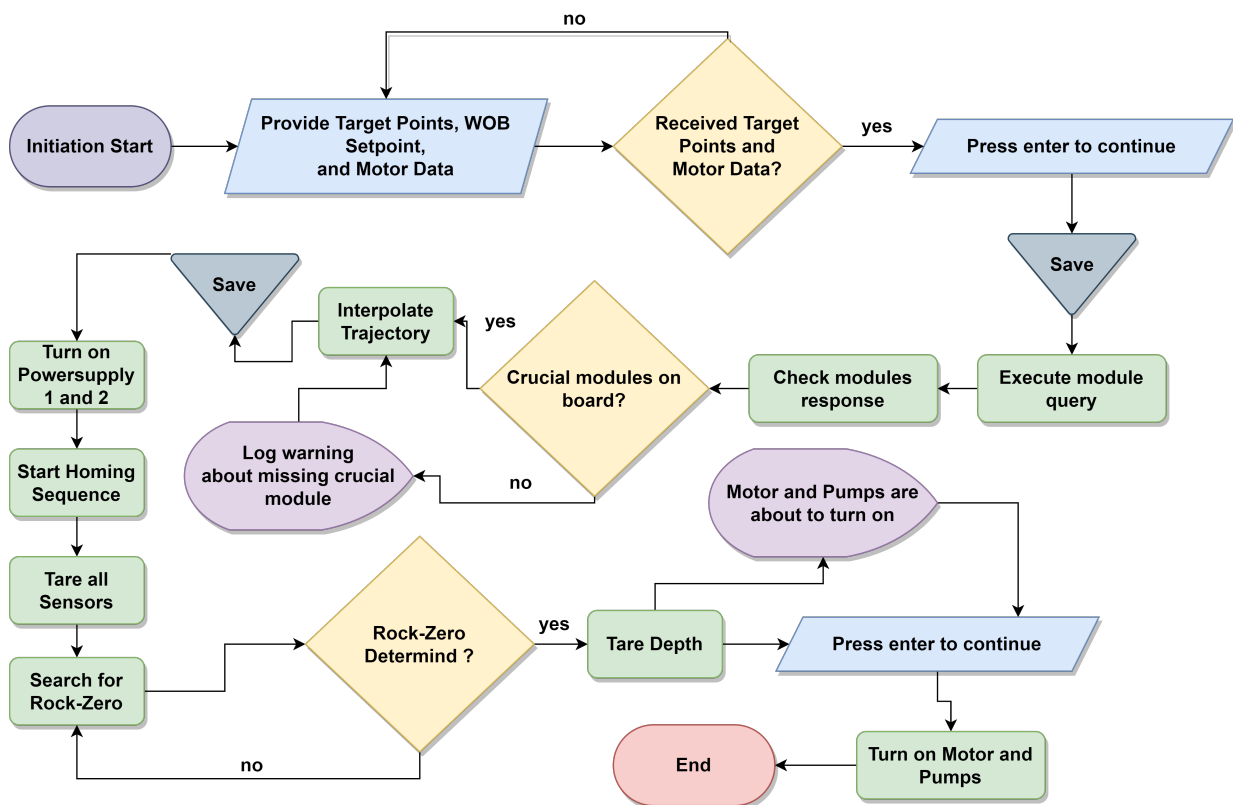
The algorithm prioritizes different modules. For instance, when crucial modules like Z-Axis or motor unit are missing, the algorithm would issue a warning, and further operation would not be possible. This, however, is not the case when modules with lower prioritization are missing. In every case when a module is missing, the driller would have to acknowledge this and prompt the system to continue anyway. Further, the algorithm would continue with calculating the trajectory from the 4 provided points (Figure 10.3). In the current setup, the interpolation is forced to fit a function through all of the 4 demanded points. In further development, target points could be prioritized, for example, to minimize the total curvature of the trajectory.

Figure 10.3: Test-Trajectory with 20 Surveys



The trajectory is interpolated in two segments: the first segment is a linear interpolation between starting coordinates and KOP. Between KOP and the first target, a spline interpolation is used with the condition that the derivative is constant between the linear interpolation and the spline interpolation. After interpolation, the cumulative length of the trajectory is calculated and split into equally spaced survey points. The number of these points is decided by the driller. After segmenting the trajectory, the length between the starting point and all survey points is determined to get the ΔL of the drill pipe, providing a reference for when a survey should be executed. During drilling, the current inserted drill pipe length will be checked and compared to the survey criteria depth. If the actual depth and survey criteria are equal, a survey will be triggered. To store the calculated data from the survey, a survey plan is created, stored into a variable, and published subsequently. If an error occurs during this process, the algorithm would raise an exception, demanding a repetition of this procedure.

Figure 10.4: Initiation Procedure



If no exception is raised, the algorithm would continue with the next phases. The first step would be activating the power supply, enabling the 24V and 48V line to the robot, which allows for control of all actuators on the rig. Subsequently, the homing procedure for the

Z-axis and the rotary table is executed to determine machine zero. After this, the WOB, Hookload, and the IMU are tared, and the "find rock zero" process starts. This process drives the Z-axis slowly downward until the hookload reaches $> 20N$. At rock zero, the current depth is set to zero, which serves as the reference point for the inserted drill pipe length. The final step would be a warning to the driller that, upon continuing, the drill motor and pumps are about to turn on. This has proven to be a very important warning since it enables the driller to alert the crew or other people around the rig.

10.4.3 Park State

The "Park" state represents the unique state from which all other states are reachable. Upon entering the Park state, the machine remains operational; for instance, the motor and pumps continue running. In this state, the driller has two options:

1. Take manual control of the robot via the control panel.
2. Switch to the drilling state and allow the commander to resume control.

During all time of the autonomous drilling process the driller can switch to the park state.

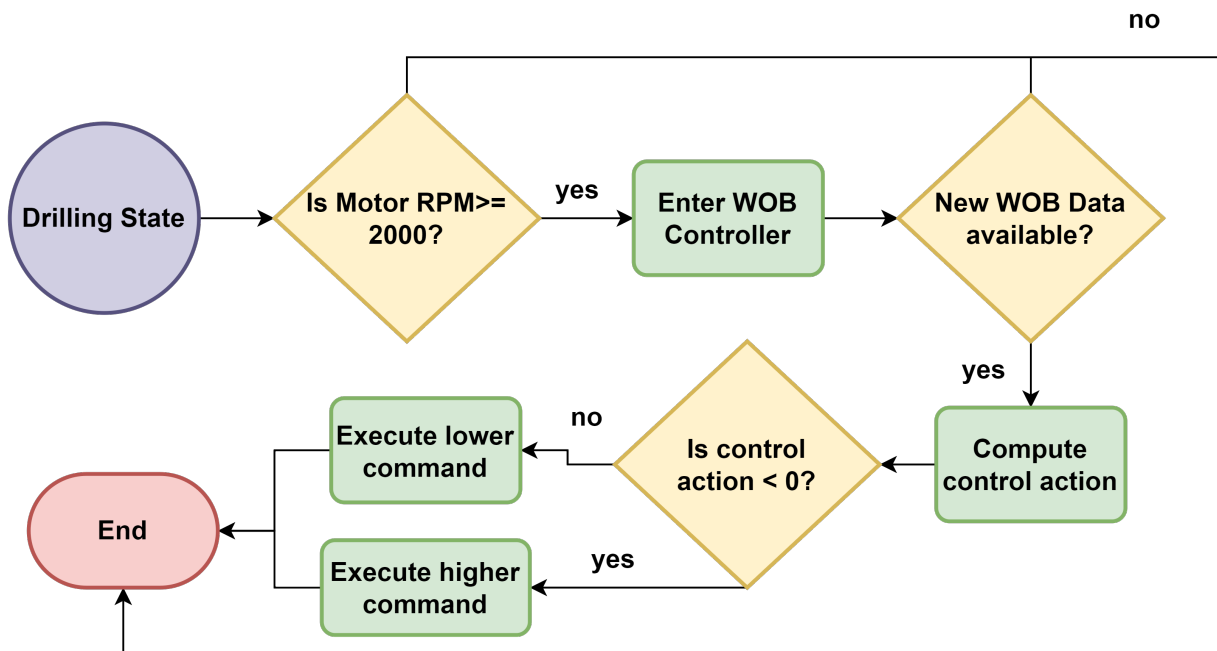
10.4.4 Drilling State

Upon entering the "Drilling" state, a sanity check is conducted to ensure that the motor is running before the Z-axis is actuated. If the current motor RPM is higher than 2000 RPM, the controller will be executed. 2000 RPM was chosen as a sweet spot since an RPM drop is to be expected when making contact with the formation. Enough room should be left, for the RPM to drop but if the RPM drop is so significant that the total RPM is less than 2000 RPM the Z-axis will also stop driving, allowing the motor to build up momentum again before proceeding. Currently, a simple PID controller is implemented, however fine tuning the controller is still in development. Nonetheless, this provides a perspective for future work, where the ideal KI , KP and KD values can be determined.

In the initial test setups, the machine will be operated with a constant forward movement speed until the controller is dialed in. During various tests, the Hookload and WOB data were observed while steering operations, indicating higher loads when steering. This led to the conclusion that, in this particular setup, a better solution would be to use the Motor torque as an input for the control, but this decisions would need further testing and considerations. In all cases, the output of the controller is used to adjust the forward speed of the Z-axis. Figure 10.5 showcases one full drilling state procedure. The loop itself is

generated by the state machine. Since the drilling state is defined as an object, it is called every time the state machine executes the state check loop. As soon as the state is not changed by the commander or by the driller, the loop will continuously enter the drilling state. Loop speed is set to 10 ms.

Figure 10.5: Drilling Procedure



During drilling, the commander object and other states would allow for the implementation of various different controllers, such as stick-slip mitigation, formation change detection, etc., which can all adjust the setpoint of the drilling controller. This was intended during the development of the algorithm. The drilling state will autonomously be paused as soon as a survey criterion by the commander is detected, which will prompt the state machine to switch states.

10.4.5 Survey State

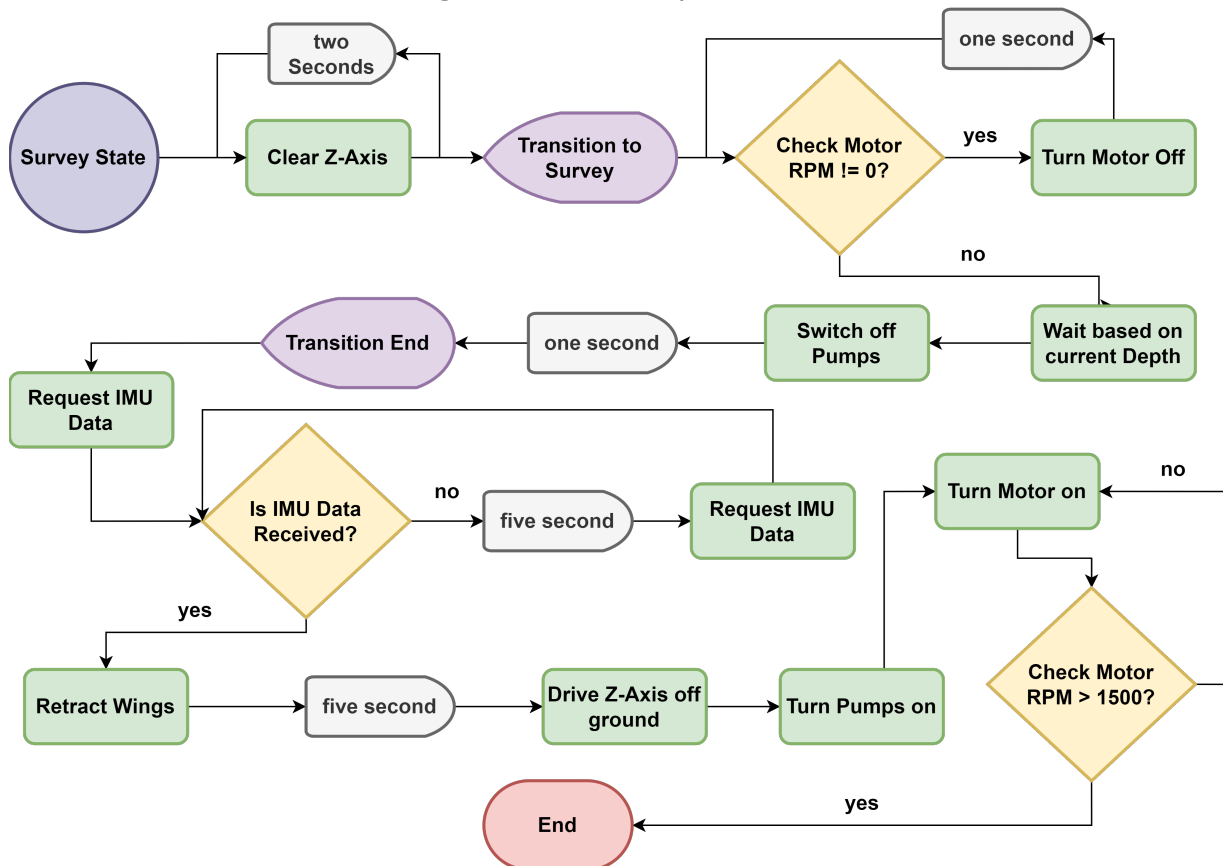
The "Survey" state represents the procedure executed during the initiation of a survey. This state is divided into two distinct phases.

In the first phase, termed the "transition to survey" phase, the groundwork is established for the subsequent measurements. Initially, the z-axis is halted and cleared to ensure there are no unintended movements. Following this, the motor is deactivated to reduce any potential vibrations during the azimuth and inclination measurements. Once the motor's deactivation

is confirmed, the pumps continue to run for a specific duration. This duration is directly related to the current depth, with the time increasing as the hole deepens. This ensures hole clearance before the primary pump is deactivated.

Upon switching off the pump, the IMU data is requested. This is a critical operation since the azimuth and inclination measurements are vital for determining the current position. This, in turn, is essential for applying the correct steering forces. The system will not proceed until this data is received. To ensure the data's reception, it is requested in a continuous loop. As soon as the data is acquired, the steering unit is instructed to retract the wings. Finally, the Z-Axis moves up by 3mm, the pumps are activated, and the motor is powered on again.

Figure 10.6: Survey Procedure



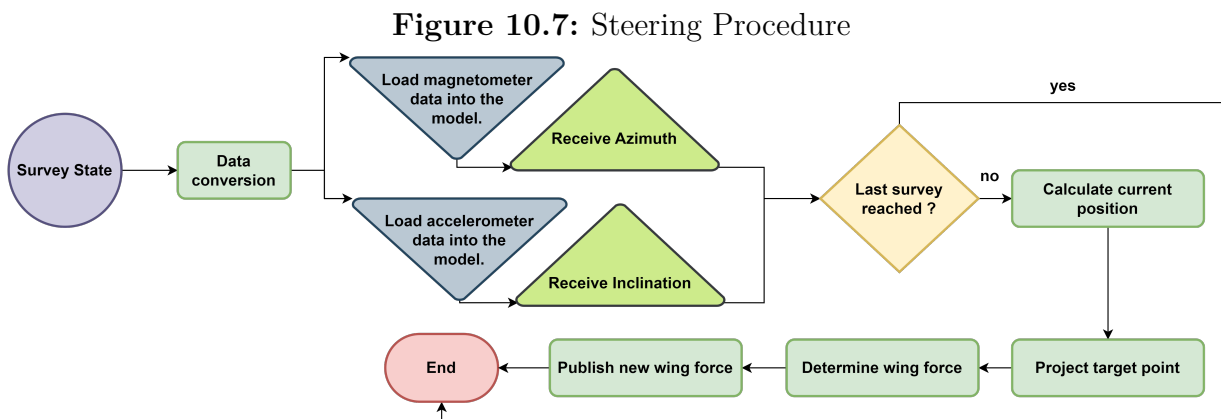
The current survey routine represents just one solution among many. During preliminary tests, different approaches were explored. Challenges arose when powering up the motor after shutting it down within the hole. High torque spikes were observed. As a counter measure the delay in the survey transition phase before the motor is shut off and the Z-axis is stationary was increased. This can be referred to as a reaming operation. The delay was

introduced after clearing the Z-Axis (refer to Figure 10.6). Further tests and evaluations are required to determine the optimal survey routine. Extended reaming intervals can result in inconsistent hole sizes, which may adversely impact the subsequent steering process.

10.4.6 Steering State

The "Steering" state marks the final state represented in the state machine. It has a setup similar to the "Survey" state, consisting of two phases. The first phase involves the actual calculation of the azimuth and inclination from the received sensor data. While different approaches can be employed to determine the azimuth and inclination, in this instance, a simple model was utilized. This model is trained to correlate the measured sensor data to an angle. The training is conducted separately for the azimuth and the inclination. For the azimuth, an algorithm was developed that continuously turns the rotary table by one degree, logging the sensor data and assigning the cumulative angle to the recorded data space. The gaps between these data points are interpolated linearly. The resulting file is then used to determine the angle of a new data point. The azimuth determination has proven reliable due to the robust electromagnetic field the rig generates around the rock sample.

The inclination model was constructed similarly. However, it exhibited significant variations during measurements, potentially due to sensor quality. Once the azimuth and inclination are determined, the algorithm proceeds to the second phase: the actual determination of the new pad forces. But before this, a sanity check is conducted to ascertain if the last survey from the survey plan has been reached.



Current Position Determination

The determination of the current position in x, y, z coordinates involves several steps. Initially the traveled distance, expressed as Δ_L has to be determined. This is achieved by evaluating the change in DP length between two consecutive survey points. Once the azimuth and inclination values are computed, the δx , δy , and δz components of the traveled vector can be determined using:

$$\delta x = \Delta_L \times \sin(\pi + \text{inc}) \times \cos(\text{azi}) \quad (10.1)$$

$$\delta y = \Delta_L \times \sin(\pi + \text{inc}) \times \sin(\text{azi}) \quad (10.2)$$

$$\delta z = \Delta_L \times \cos(\pi + \text{inc}) \quad (10.3)$$

For a complete trajectory, the new calculated vector components are added to the previous known position coordinates. This method creates a piece wise assembled trajectory in literature referred to as the tangential method. The TVD is represented by the z_{new} coordinate. Upon computation, this information is saved in the global position plan variable and dispatched to the broker:

$$x_{\text{new}} = x_{\text{old}} + \delta x \quad (10.4)$$

$$y_{\text{new}} = y_{\text{old}} + \delta y \quad (10.5)$$

$$z_{\text{new}} = z_{\text{old}} + \delta z \quad (10.6)$$

BHA Vector and Normalization

Subsequent calculations require the definition of the vector representing the Bottom Hole Assembly. This vector is defined by the difference between the last known position and the current one. The magnitude of this vector is not relevant to further calculations, and as such, the BHA vector undergoes normalization. An exception occurs when the BHA vector magnitude is zero:

$$TF_z = \begin{bmatrix} \text{last_position}['x'] - \text{prev_position}['x'] \\ \text{last_position}['y'] - \text{prev_position}['y'] \\ \text{last_position}['z'] - \text{prev_position}['z'] \end{bmatrix} \quad (10.7)$$

$$\text{norm} = \|TF_z\| \quad (10.8)$$

$$TF_z = \begin{cases} \begin{bmatrix} 0 \end{bmatrix} & \text{if norm} < 1 \times 10^{-6} \\ \frac{TF_z}{\text{norm}} & \text{otherwise} \end{cases} \quad (10.9)$$

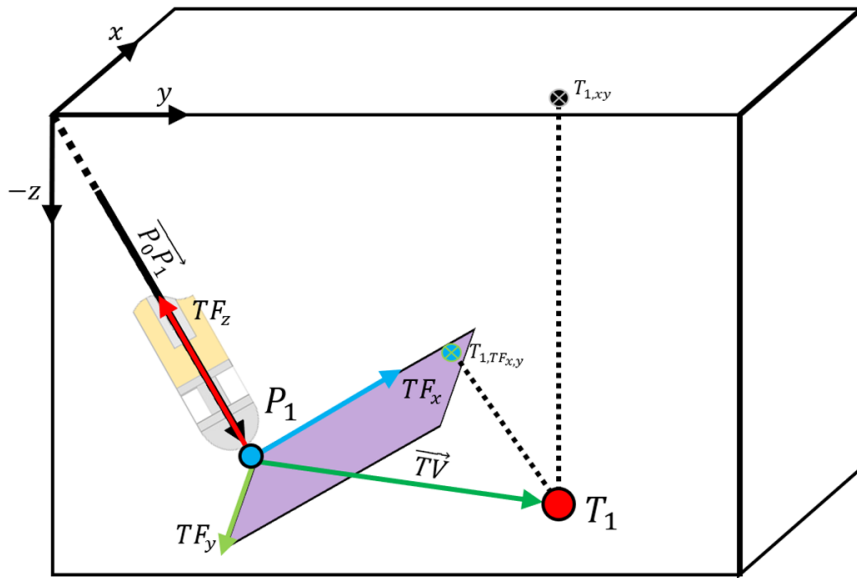
Target Vector and Projection

The further steps involve determining the Target Vector. This vector provides insights into the BHA's required direction to accurately hit the intended target point. The Target Vector is mathematically represented as:

$$T\vec{V} = P_0\vec{T}_1 - P_0\vec{P}_1 = \begin{pmatrix} T_{1,x} \\ T_{1,y} \\ T_{1,z} \end{pmatrix} - \begin{pmatrix} P_{1,x} \\ P_{1,y} \\ P_{1,z} \end{pmatrix} = \begin{pmatrix} TV_x \\ TV_y \\ TV_z \end{pmatrix} \quad (10.10)$$

To determine the direction in which the BHA has to be deflected, the Target Vector is projected within the BHA's Tool Face plane, denoted as TF_{plane} . This projection simplifies the 3D problem into a 2D one, considering pad forces exclusively act within the tool face plane. Later, this projected target vector will undergo decomposition for further insights into the required individual pad forces. Figure 10.8 represents this projection, the TF_{plane} is represented in purple, and the projected target point in blue.

Figure 10.8: Projection in TF -coordinate and reference-coordinate system

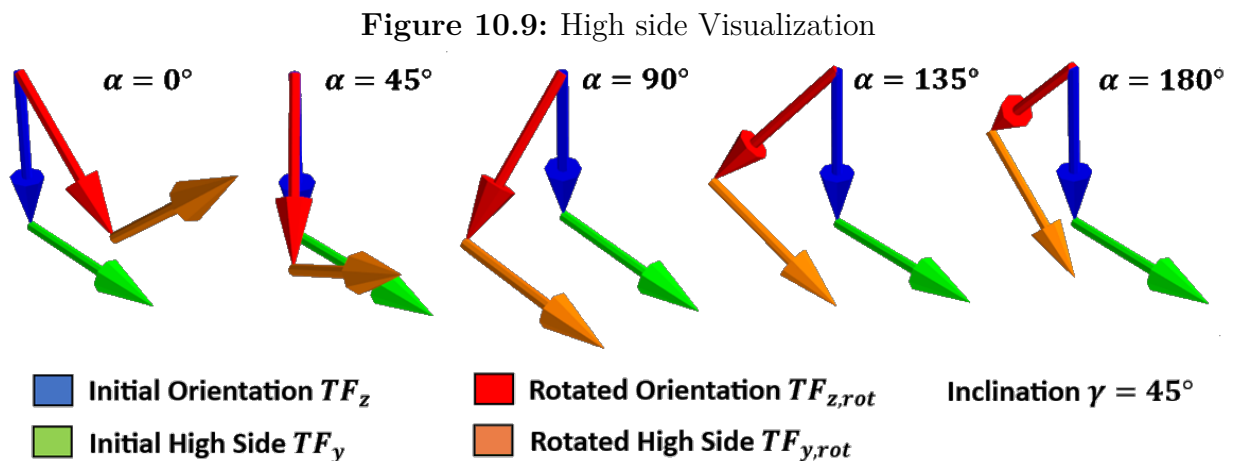


Projection is accomplished by an orthogonal projection to the plane defined by TF_z :

$$P\vec{T}\vec{V} = T\vec{V} - (T\vec{V} \cdot T\vec{F}_z) \cdot T\vec{F}_z \quad (10.11)$$

Decomposition into Pad-Forces

For the decomposition of the pad forces, several approaches were examined. A significant number of these methods overlooked the "roll-over behavior" of the DP utilized in this system. Given that the system functions with a static drillpipe and Static Bottom Hole Assembly, the azimuth induces the entire BHA to undergo a roll-over. This may lead to a loss of reference to the high side. While representing the DP and BHA as a straight line or vector might be sufficient for orientation to ascertain the current position, it could result in losing the High side pad orientation. In the preliminary algorithm designs, high inclinations weren't expected, thereby reducing the effects of the "roll-over behavior". However, subsequent tests showed that the system could achieve steeper build rates, emphasizing the importance of accounting for this behavior.



For subsequent calculations, the angle between the projected target point and the high side vector is necessary. First methodologies would reference the initial high side position of the wing at the start, which is consistently calibrated to align with the positive y-axis. This entails calculating the angle between the y-axis of the reference system and the target point. A more accurate approach would model the drillstring not merely as a line but as a tube with its high side initially oriented along the y-axis. When subjected to bending forces, such as azimuth and inclination, the tube tends to roll over its radius, leading to a drift in the high side. To determine the high side vector after applying an initial azimuth and inclination to the tube, a specific rotation sequence is essential. Initially, with the drillstring or tube oriented vertically, an azimuth rotation α is applied about the z-axis. This is followed by an inclination rotation γ about the x-axis. At this juncture, the current orientation can be established. However, to identify the high side, a unique rotation using

the inverted azimuth to rotate around the drillstring is necessary. This is achievable with Rodrigues rotation formula Rodrigues (2022). Given the orientation of the initial BHA high side vector (TF_y), the first rotation sequences can be applied using quaternion:

$$q_{\text{azimuth}} = \cos\left(\frac{\alpha_{\text{radians}}}{2}\right) + k \sin\left(\frac{\alpha_{\text{radians}}}{2}\right) \quad (10.12)$$

$$q_{\text{inclination}} = \cos\left(\frac{\gamma_{\text{radians}}}{2}\right) + i \sin\left(\frac{\gamma_{\text{radians}}}{2}\right) \quad (10.13)$$

After determining the rotations for azimuth and inclination, the two complex numbers can be combined:

$$q_{\text{combined}} = q_{\text{azimuth}} \times q_{\text{inclination}} \quad (10.14)$$

Using the complex conjugate, the rotated BHA high side vector can be ascertained:

$$TF_{y, \text{rotated}} = q_{\text{combined}} \times TF_y \times q_{\text{combined}}^* \quad (10.15)$$

For the final rotation, the high side rotates around the BHA orientation vector (TF_z), yielding the final orientation of the high side vector after applying both azimuth and inclination:

$$TF_{y, \text{final}} = TF_{y, \text{rotated}} \cos(-\alpha) + (TF_z \times TF_{y, \text{rotated}}) \sin(-\alpha) + TF_z (TF_z \cdot TF_{y, \text{rotated}}) (1 - \cos(-\alpha)) \quad (10.16)$$

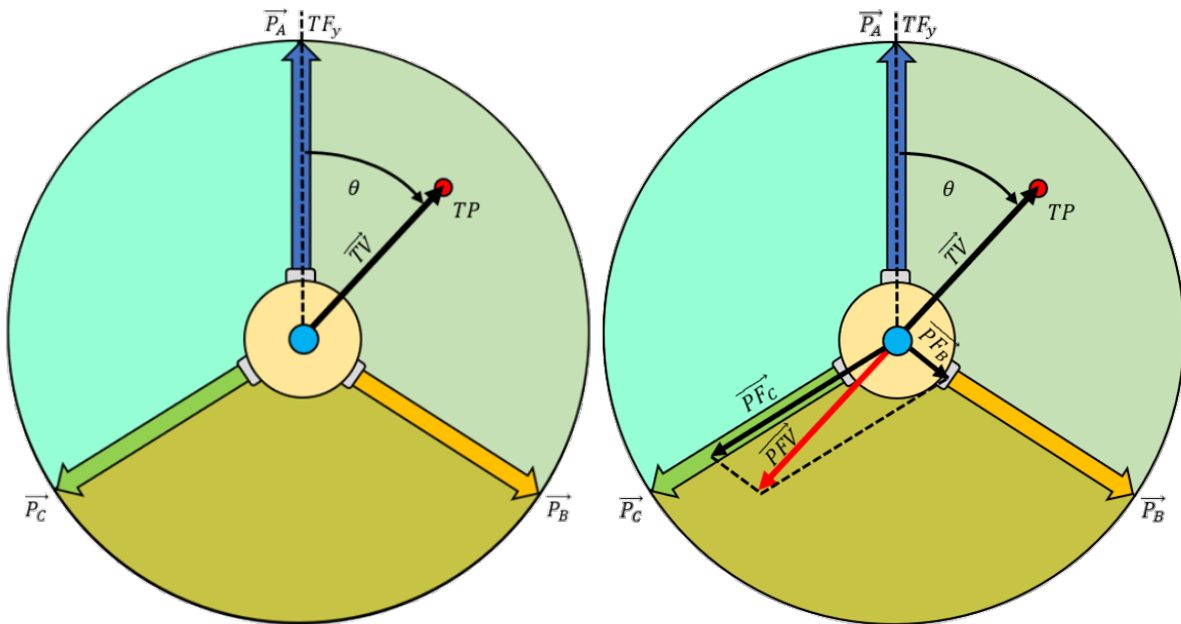
After determining the high side, the subsequent step involves calculating the angle between PTV and $TF_{y, \text{final}}$. This angle represents the steering angle within the tool face plane:

$$\theta = \cos^{-1}\left(\frac{PTV \cdot TF_{y, \text{final}}}{|PTV| \times |TF_{y, \text{final}}|}\right) \quad (10.17)$$

To determine the required force angle, the steering angle θ is augmented by 180° , resulting in θ_c , the corrected steering angle. With the force magnitude set to 1, the resulting force vector PFV is decomposed, and the activation of the active pads is expressed as a percentage of the total possible steering force. From there the new pad forces are published and the steering state ends. The utilized steering algorithm allows for the control of the correct steering direction, even though there's no adjustment based on the distance from BHA to the target. To optimize the steering capability, this distance needs to be addressed. A potential solution is to introduce a fourth adjustment variable during steering operations, in addition to the three pads. This could be the WOB set point. It's anticipated that when

drilling with a lower WOB, the build rate will be higher. This is because the total force vector acting to the formation is comprised out of the WOB which acts downward, and the pad forces which act sideways. The smaller the WOB, the more the total force is directed to the side. To ascertain the influence of the WOB on the build rate, a test setup will be planned.

Figure 10.10: Pad-Force decomposition

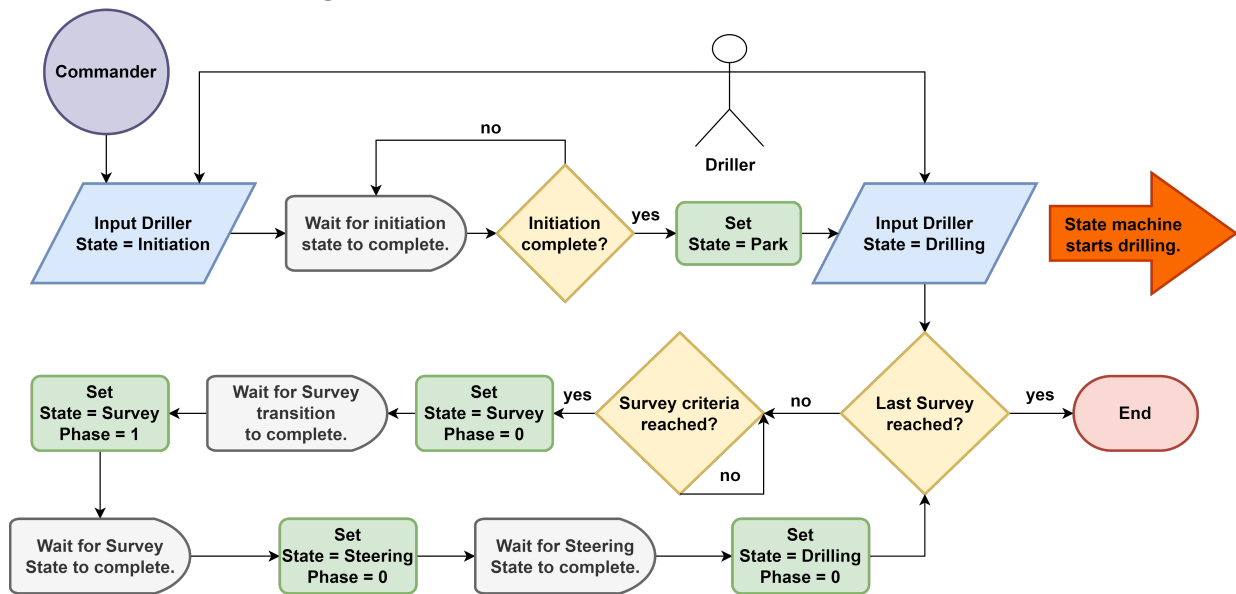


10.5 The Commander

The commander object represents the autonomous part of the drilling algorithm. To activate the commander, the driller must manually prompt the state machine to enter the initiation state. Until this point, the commander remains in a sleeping state, waiting for the state machine to release it. As soon as the initiation is finished, the commander awakens and changes the state to the "Park" state, which forces the state machine to also enter the park state. The commander then waits for a final confirmation from the driller, expressed as an initial prompt, to enter the drilling state. Upon entering the drilling state, the machine starts drilling, executing the controller on each iteration. The commander then enters its observing state, where it checks for crucial conditions that may require state changes. In future development, multiple criteria can be applied, such as safety or ROP optimization. For example, during the drilling state, the commander could observe the ROP and detect

changes in ROP, which it could use to adjust the WOB setpoint in real-time. In the current setup, the only criterion checked during the drilling state is the survey criterion. The commander checks if the current depth is greater or equal to the first survey depth. If this is true, the commander prompts the state machine to transition to surveying. This communication is done using a handshake method between the commander and the state machine. This also marks a point where the commander could observe certain criteria, as described before. In the current setup, the commander simply waits for the state machine to confirm that the transition has finished.

Figure 10.11: Automation of the State machine



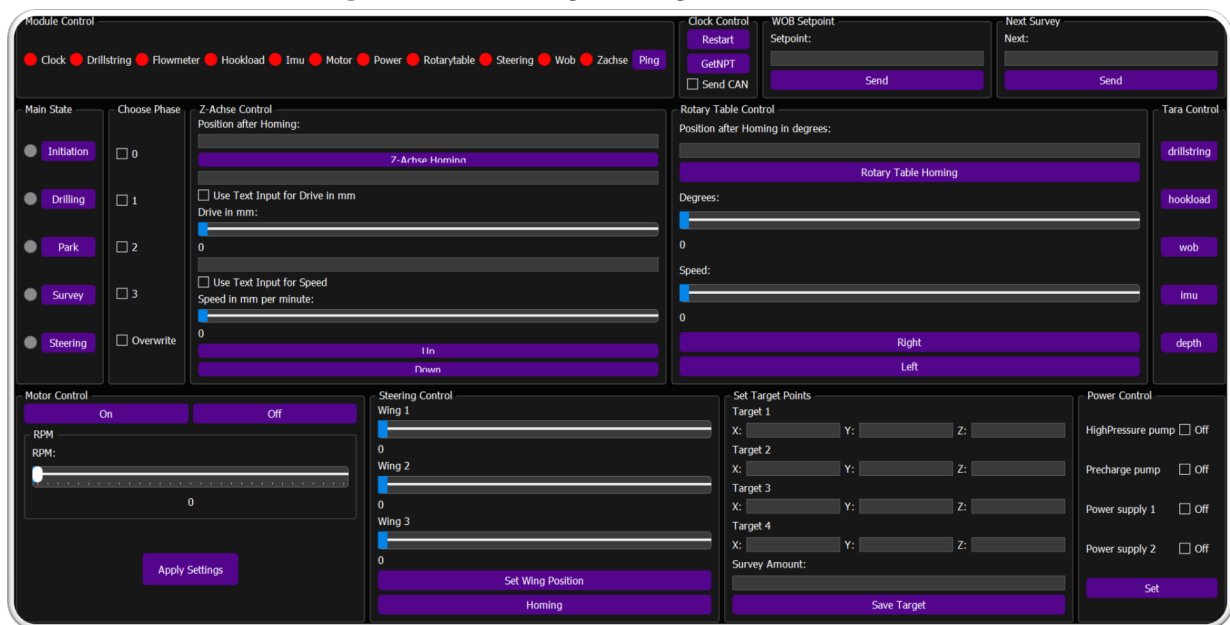
Upon receiving this confirmation, the state changes to the survey state, during which the commander waits again for the state machine to finish. As soon as the survey is completed, the commander increments the survey number and prompts the state machine to enter the steering state. The commander then waits again. After confirmation that the steering state is complete, the commander sets the drilling state again and starts observing the depth for the next survey. This process repeats until a termination criterion is reached, either by the driller or when reaching the last survey.

10.6 Engineering Control Interface:

Alongside the autonomous algorithm, a dual mode was also anticipated, allowing the machine to be operated manually. This was achieved by creating a user interface (UI) that enables

control of all the actuators on the rig. The UI also serves as the initial control interface for autonomous drilling. The UI comprises multiple input fields and buttons. When these buttons are pressed, they publish messages on the broker, allowing for interactive control. In the current setup, all actuators can be accessed via this UI, which is why it is labeled as an engineering interface. In future development, a driller-friendly UI will be developed with limited control options or narrower control ranges to ensure system safety. While the UI serves as a control panel, the graphical user interface (GUI) that displays all rig data is operated by a separate client.

Figure 10.12: Engineering Control Interface



The control panel offers a variety of different control buttons, visualized in Figure 10.12. The entire UI is subdivided into module boxes that align with other parts of the software algorithm. To highlight a few features: it's possible to ping all modules to receive feedback on which modules are active, a state control box, a box for applying the WOB setpoint, and a box for adjusting the next survey. Adjustments can be made with the commander running, in case a survey needs to be skipped. There's also a control box for inputting target points and the total number of surveys to be conducted. Other boxes are used to control the drilling motor, Z-Axis, rotary table, or each individual wing force.

10.7 GUI

The Graphical User Interface in the discussed system utilizes two programming languages for the visualization and management of data from servers and sensors, aiming to provide a comprehensive view of drilling machinery operations and enhance control efficiency. The GUI displays critical data such as the equipment's position within geological strata, real-time Revolutions Per Minute (RPM), Torque, WOB etc.. It also shows operational statuses like Parked, Initializing, Drilling, Surveying, or Steering. Metrics like Hookload and Weight on Bit (WOB) are presented for drilling process assesment, along with Pump Pressure and Flow Rate for hydraulic control. Data is fetched from the server via the MQTT protocol at one-second intervals for visualization, which aligns with the capabilities of ReactJS for rendering. ReactJS was initially used for creating a dynamic and interactive web-based interface, offering real-time insights such as torque, RPM, depth, and machine status. However, due to challenges in handling high-frequency updates and rendering, a transition to Python was implemented. Python was selected for its robustness and extensive ecosystem, better suited for managing high-frequency data transmission (25 requests per second).

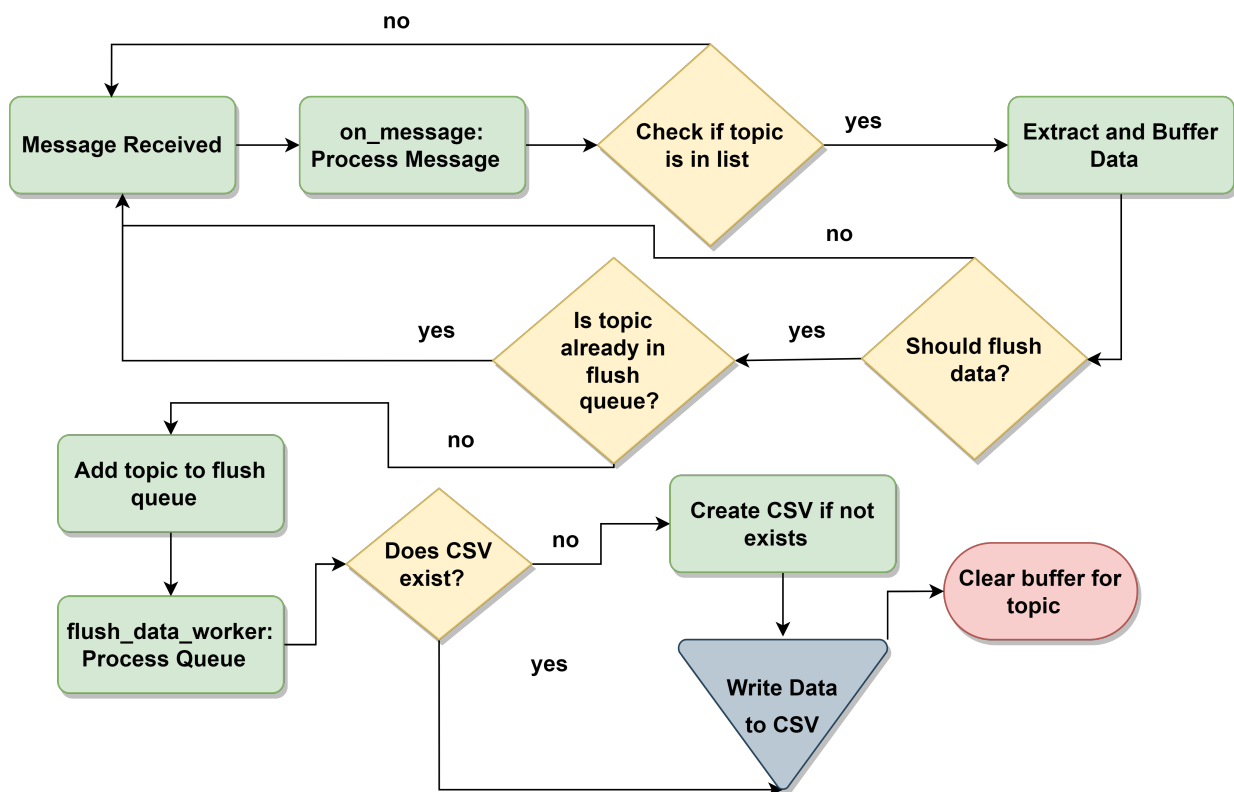


Figure 10.13: GUI

10.8 Logger

To verify results, all data originating from the rig or from any client connected to the broker is logged. The logger, implemented in Python, uses a separate client to log into the broker. From there, it subscribes to all topics and logs the corresponding data into CSV files. Given that the logger should be capable of handling significant traffic, a setup similar to the one in the autonomous algorithm was implemented. Incoming data from a topic is stored inside a buffer. When either 10 messages are found inside the buffer or 10 seconds have passed since the last buffer entry, the data is flushed into CSV files. The logger creates a CSV file for each topic/subtopic, storing them with the logging time, the payload, and the machine time, the latter representing the time the data was recorded. The logger also functions as a black box, tracking all commands sent either by the driller or by the commander. which further improves debugging of the entire Machine as well as the algorithm

Figure 10.14: Logging Process



10.9 Drilling Performance Optimizations

One objective of the competition states that the hole should be drilled as fast as possible by the autonomous drilling rig. In other words, the rate of penetration (ROP) should be as high as possible. To achieve a high ROP, it is planned to use an algorithm that optimizes the mechanical specific energy (MSE) of the drilling process. Alternatively, a machine learning approach will be followed and implemented if time is on hands as shown in **Chapter ??**.

10.9.1 Mechanical Specific Energy

The mechanical specific energy describes the amount of energy required to remove a certain volume of material during a drilling operation. The best efficiency of drilling (high ROP) is given when the minimum mechanical specific energy is reached (R. (2011)).

$$MSE = \frac{Total\ Energy\ Input}{Volume\ Removed} \quad (10.18)$$

Volume of a drill hole is simply cross-sectional area multiplied by depth of penetration (Δh) and Work Energy can be described as force multiplied by distance. In drilling there are two forces acting on the bit: Weight on Bit (axial force) and Torque (rotational force). These are additive to MSE, so there are two terms in the MSE Equation.

$$MSE = \frac{Vertical\ Energy\ Input}{Volume\ Removed} + \frac{Rotational\ Energy\ Input}{Volume\ Removed} \quad (10.19)$$

$$MSE = \frac{WOB * \Delta h}{Area * \Delta h} + \frac{Torque * 2 * \pi * Rotations\ per\ time}{Area * \Delta h}$$

The distance travelled by the bit (Δh) during a given interval is the penetration per time (ROP) divided by rotations per time. This is also known as depth of cut or as Penetration per Revolution.

$$\Delta h = \frac{Penetration\ per\ Minute}{Rounds\ per\ Minute} + \frac{ROP}{RPM} = P \quad (10.20)$$

This results in

$$MSE = \frac{WOB * \Delta h}{Area * \Delta h} + \frac{2 * \pi * RPM * Torque}{Area * ROP} \quad (10.21)$$

In this equation the MSE is a function of the WOB, the torque and the Penetration per Revolution. In order to find the minimum of the MSE, the equation is only set in dependence of one variable, the WOB. Therefore, the Torque and the Penetration per Revolution must be expressed as function of the WOB. This is possible with two assumptions. The higher

the axial force, the higher the penetration rate and the torsional force. Therefore, the MSE is only displayed as a function of the axial force, i.e. the WOB. WOB and torque have a linear relationship. With these assumptions, the penetration per revolution can be described as a quadratic function of the WOB.

$$\begin{aligned}
 Torque &= f(WOB) = A_0 + A_1 * WOB \\
 P &= g(WOB) = B_2 * WOB^2 + B_1 * WOB + B_0 \\
 P &= \frac{ROP}{RPM} \\
 MSE &= \frac{WOB * \Delta h}{Area * \Delta h} + \frac{2 * \pi * Torque}{Area * P}
 \end{aligned} \tag{10.22}$$

The parameters A_0, A_1, B_0, B_1, B_2 are determined by making test bores in which the WOB, the torque and the penetration per revolution are measured. The insertion in the function of the MSE results in the following equation.

$$MSE = \frac{WOB}{Area} + \frac{2 * \pi * f(WOB)}{Area * g(WOB)} = \frac{WOB}{Area} + \frac{2 * \pi (A_0 + A_1 * WOB)}{Area * B * WOB^2 + B_1 * WOB + B_0} \tag{10.23}$$

10.9.2 ROP Surface Plot Generation

The ROP surface plot generation is a critical process in drilling optimization. This approach involves conducting test wells to generate surface plots for different formations. Each time a new formation is drilled, the resulting data is stored in a database. This database then serves as a reference to determine appropriate setpoints for drilling parameters in similar formations in the future.

To generate a ROP surface plot, a test well is drilled in a specific formation. During this process, combinations of the drilling parameters, such as Weight on Bit and Revolutions Per Minute, are applied. The ROP is meticulously recorded for each combination of parameters, creating a comprehensive dataset that reflects how different drilling conditions affect the ROP in that particular formation.

This dataset is then used to generate a surface plot, illustrating the relationship between the drilling parameters and the ROP. These plots are crucial for understanding the optimal drilling conditions for a specific formation. Once generated, the ROP surface plot is added to a centralized database. This database becomes a valuable tool for future drilling operations, as it allows for the quick identification of the most efficient drilling parameters for any given formation, based on historical data.

The process of generating these plots and storing them in a database ensures that each new

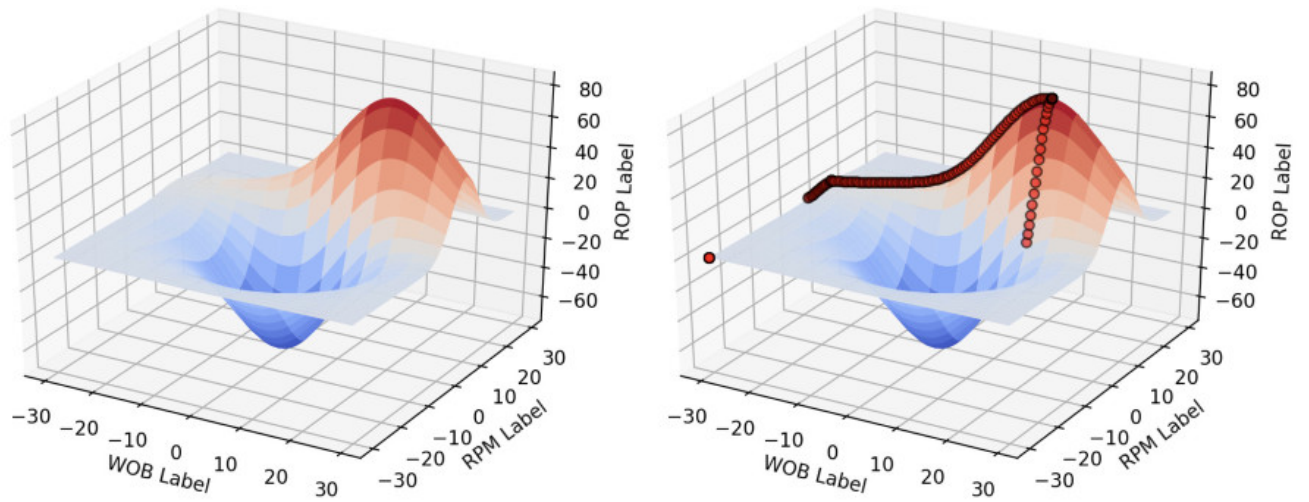


Figure 10.15: Example of a ROP Surface Plot

drilling operation can begin with a well-informed understanding of the optimal setpoints. This method significantly improves drilling efficiency and can lead to more effective and economical drilling operations.

11 Test and Evaluation

11.1 Setup

The testwell setup was designed to ensure no damage would occur to the rig, especially since the algorithm had never been fully deployed on the rig. Initial tests were conducted to observe the command timing from the algorithm and to determine where additional safety measures needed to be implemented. These tests also aimed to provide insights into the rig's drilling and steering capabilities. To conduct this test, various modifications were made to both procedures and the algorithm to minimize the variables affecting drilling performance. As previously mentioned, all controllers were deactivated. Instead, known static setpoints were introduced. The *ROP* was set to a constant $50 \frac{mm}{min}$, while the *RPM* was maintained at 2500. Pump pressure (7Bar) and flow rate ($1.7 \frac{L}{min}$) were also held constant. To avoid damaging vital components of the steering system, two downhole wings were deactivated, leaving only one wing for steering. The force exerted by this wing was also set to remain constant at 10 N. This decision was made not just for safety reasons but also to assess the deviation capability of a single wing on the Bottom Hole Assembly. With all these parameters held constant, the well was designed with a 'J' shape, featuring an early *KOP* to allow ample time for build-up. The rock sample used had a height of 600 mm. The well was situated in a single plane, eliminating the need to measure azimuth. As for the inclination survey stations where conducted each 30 mm drilled.

Table 11.1: Constants from the Testwell Setup

Parameter	Value
ROP	50 mm/min
RPM	2500
Pump Pressure	7 Bar
Flow Rate	1.7 L/min
Force exerted by wing	10 N
Rock sample height	60 cm

11.1.1 Calibration

Since the *IMU* had not been used previously, it required calibration. The *IMU* comprises both a magnetometer and an accelerometer. For this test, only the accelerometer was

calibrated because no change in azimuth was expected on the planned trajectory. A commercial accelerometer was employed for the calibration. The *BHA* was connected to this commercial accelerometer, allowing both to adjust simultaneously. When a new position was attained, the angle from the commercial accelerometer was documented, along with the corresponding output of the accelerometer inside the BHA (acc_x , acc_y , acc_z). This procedure spanned from an angle of -5° to 15° , executed in 24 steps.

The recorded data was then used to train a predictive model. Different modeling approaches were explored, with the simplest being a linear regression model. However, it didn't yield accurate results during evaluation. In contrast, the Random Forest model performed exceptionally well, with an average error in the measured angle of approximately 0.5 degrees. This accuracy was validated by comparing the model's output with the measured angle from the commercial accelerometer. Since the drilling algorithm already had the logic for angle conversion integrated, the recorded data was simply placed in the designated folder and was immediately ready for use.

Figure 11.1: Accelerometer Data and Corresponding Angle

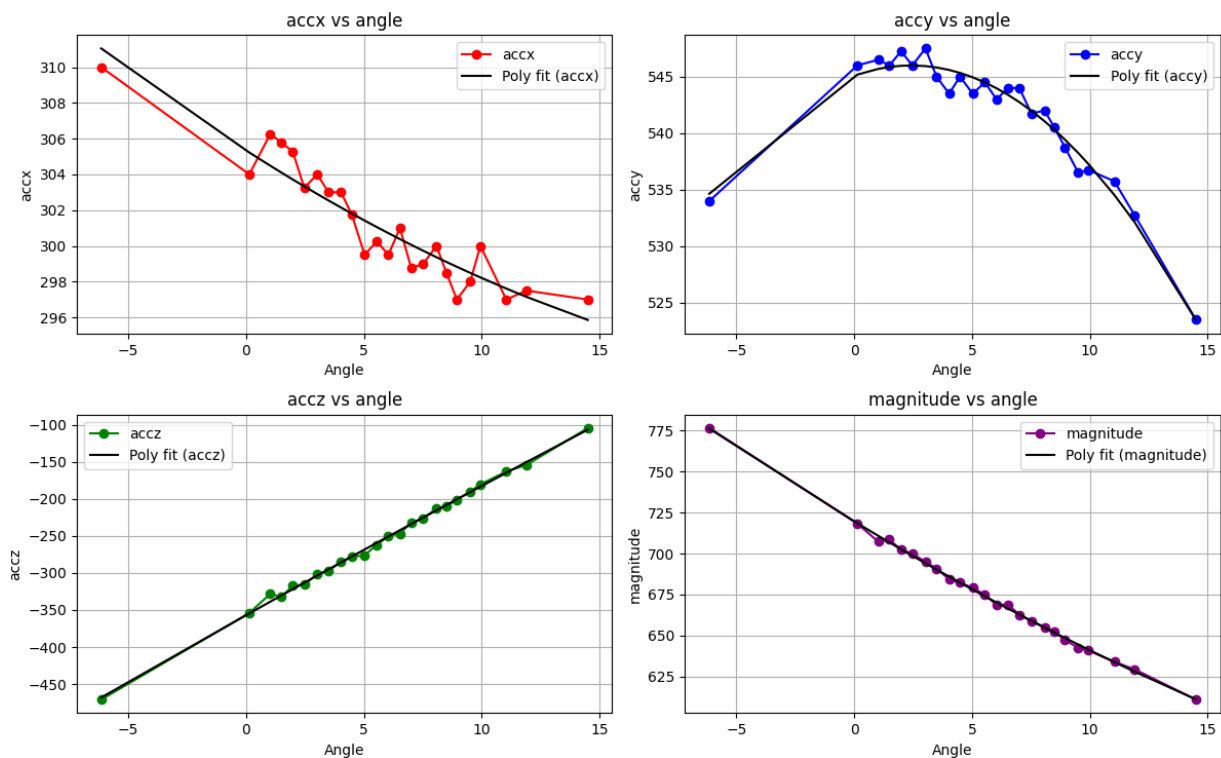


Figure 11.1 shows the acc_x , acc_y and acc_z measurements In relation to the corresponding angle, the combined magnitude of acc_x , acc_y and acc_z is shown in purple. This indicates that as the magnitude decreases, the inclination angle begins to increase. From these

readings, we can determine the orientation of the accelerometer axes. In the current setup, gravitational acceleration acts in the negative z -direction. When tilting the BHA towards the magnetic north, the positive x -axis starts to ascend, causing the gravitational force to increasingly act in the direction of the negative x -axis. In this configuration, the y -axis remains relatively constant, experiencing more or less the same level of acceleration as long there is no azimuth introduced.

An Analytic way to determine the Angle out of the accelerometer readings is given by following equation (refer to Fisher (2023)):

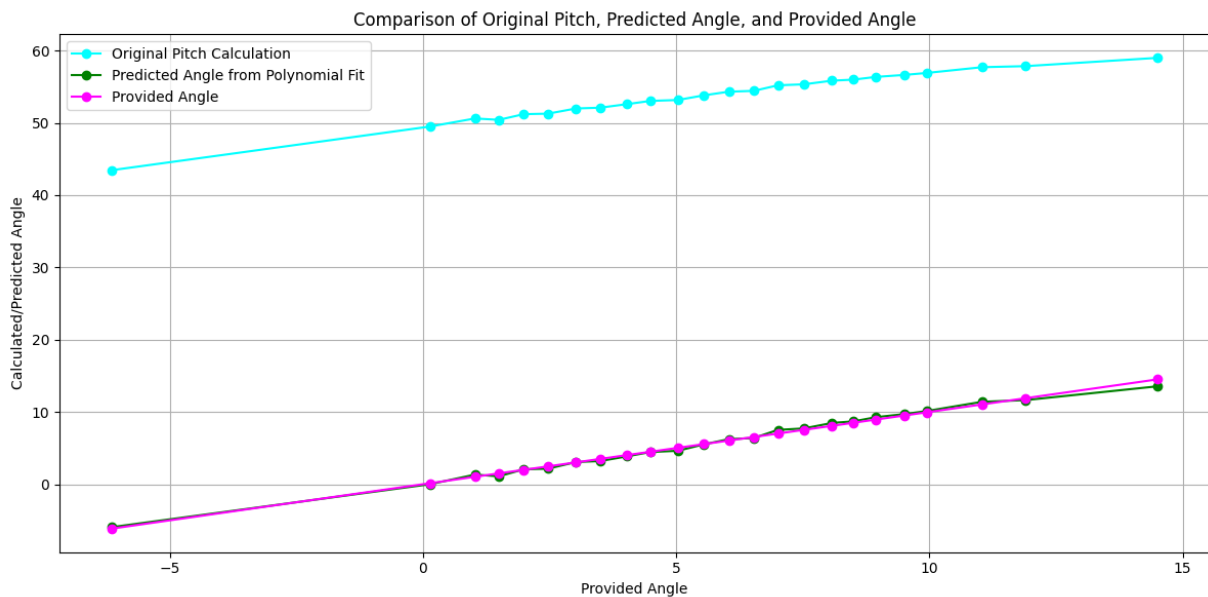
$$\theta_{\text{original}} = \arctan \left(\frac{acc_y}{\sqrt{acc_x^2 + acc_z^2}} \right) \quad (11.1)$$

However, this equation does not account for possible offsets. In the case of the implemented sensor, all three axes exhibited different offsets and variations in resolution. These irregularities can be attributed to sub optimal sensor quality. To counteract the offset in the calculated pitch angle, a 2nd-degree polynomial fit was employed. This resulted in two constants: -1.6607 for the linear part and 0.0285 for the quadratic part.

$$\text{angle} = -1.6607 \times \theta_{\text{original}} + 0.0285 \times \theta_{\text{original}}^2 \quad (11.2)$$

The following figure 11.2 shows the actual calculated angle using the unmodified analytic pitch equation, alongside the modified pitch equation and the actual measured angle.

Figure 11.2: Comparison Original Pitch and Analytic Pitch



11.2 Evaluation

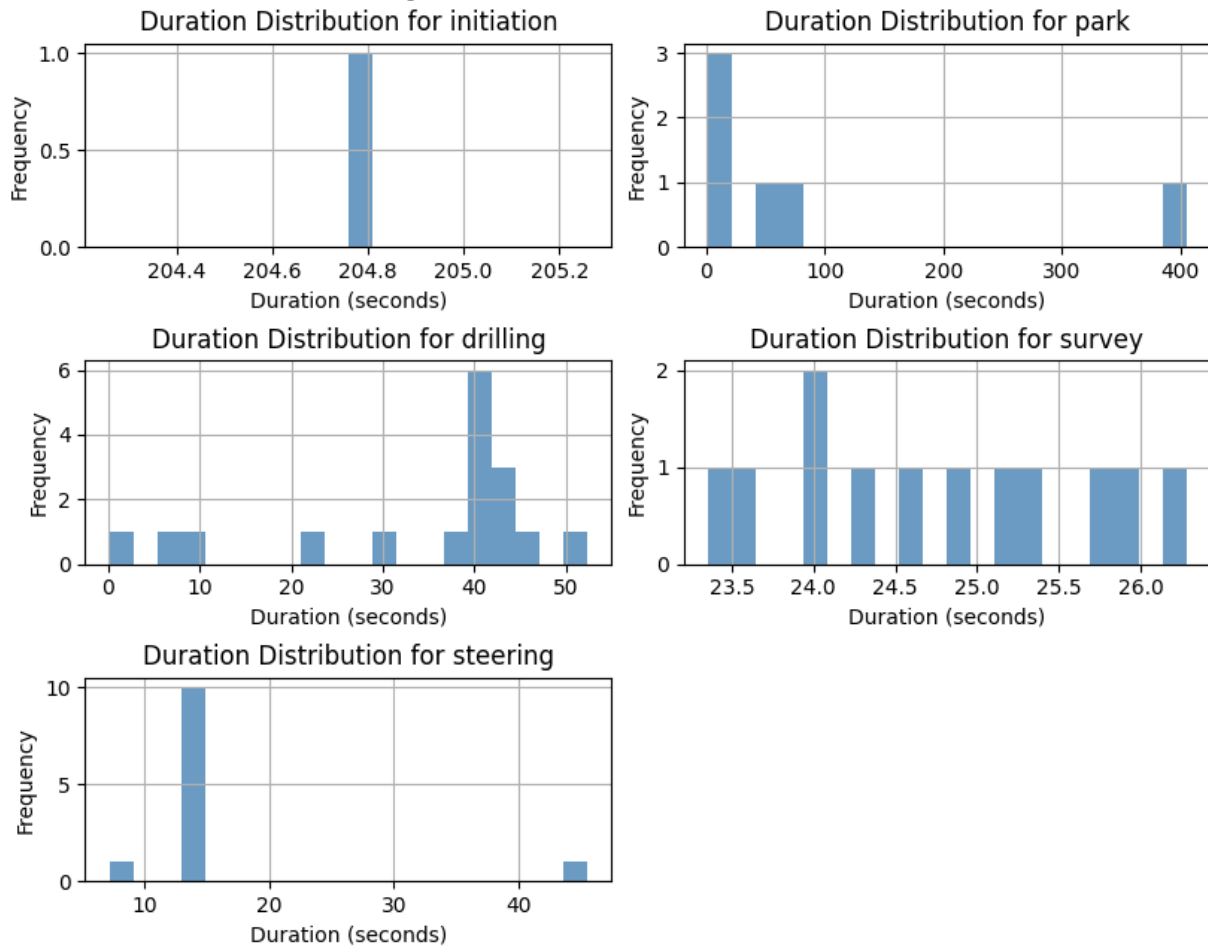
11.2.1 Initial Observations and Drilling Process

Despite encountering minor difficulties during the drilling of the test well, the results were encouraging. The initiation procedure was conducted seamlessly. The algorithm executed the homing procedure, located "rock zero," and calibrated all sensors. As expected, the initiation procedure concluded by activating the pumps and motor, then transitioning into the park state. This transition can be seen in the gantt chart 11.3 on the subsequent page. Upon the driller's command, the system entered the drilling state and switched to autonomous mode.

A total of 380 *mm* was drilled autonomously until the BHA emerged from one side of the rock sample. During the drilling, 12 surveys were conducted, recording a progressive inclination. However, by the 10th survey, a decreasing trend was observed. This was attributed to a malfunction of one wing, as indicated in the Force diagram (refer: 11.2.3). Upon further inspection, the issue was traced to a bowden cable connector that had slipped, this was later fixed easily.

11.2.2 Commander Performance and State Transitions

Examining the gantt chart 11.2.3, it's evident that the commander executed all state transitions flawlessly, and that all the surveys were conducted at regular intervals. With time plotted on the x-axis, the chart offers a detailed view of the duration for each state. For example the time required to conduct a survey remained fairly constant throughout the drilling process. However, the duration of the steering state was inconsistent (refer to Figure: 11.3), with the fifth steering state being notably prolonged. A deeper analysis of the RPM, torque, and pad force showed that an elevated pad force was in play. This resulted in an excessive motor torque during a restart, causing the RPM to plummet to zero. Fortunately, an embedded safety feature functioned as intended, attempting to restart the motor before resuming the drilling. This incident underscored a potential improvement in the steering procedure: in the current setup, the motor turns off during a survey, then the new pad forces are calculated and applied before restarting the motor. The initial aim was to ensure the drill bit was always deviated before drilling through the formation to maintain a consistent hole size. However, this method results in high torque during restart. A better approach might be to activate the motor before adjusting the pad forces.

Figure 11.3: Duration Distribution

Analyzing the duration distribution of the drilling state, varying duration's can be observed. One duration, shorter than a second, is attributed to the initial drilling state. This is where the commander detects that Survey 0 needs to be conducted. Therefore, immediately after initiating the drilling process, the commander switches to the survey state. This results in a brief duration for the first drilling state. Other duration's vary based on break intervals or errors in the z-axis motor. Refer to 11.2.3 for a more detailed description. Regarding the total time per state, Table 11.2 summarizes the time allocated to each drilling operation. When excluding the park state, the initiation procedure takes up 204.76 seconds. Considering the relatively short drilling duration, there seems to be room for improving the speed of this initiation phase, especially since a significant amount of time was spent moving the z-axis slowly to rock zero. Upon closer examination, 485.51 seconds are dedicated to non-drilling activities during the survey and steering states, while 582.55 seconds are consumed by drilling activities. Disregarding the park state, drilling makes

up approximately 45% of the total well time. It is anticipated that this percentage will increase for deeper wells, reducing the relative significance of the initial initiation time.

Table 11.2: Duration's spent in each drilling state

State	Duration (seconds)
Initiation	204.76
Park	554.52
Drilling	582.55
Survey	297.45
Steering	188.06

Further analysis of the drilling time relative to surveying revealed that for every 100 *mm* drilled, 78.28 seconds were spent conducting a survey and 49.49 seconds were spent in a steering state. This results in a NPT of 127.77 seconds for each 100 *mm* drilled.

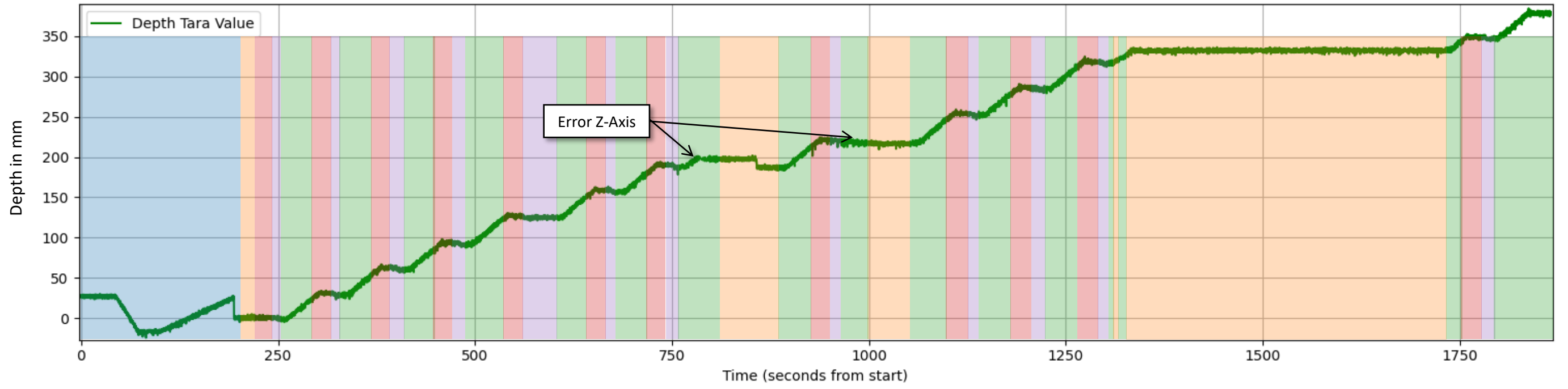
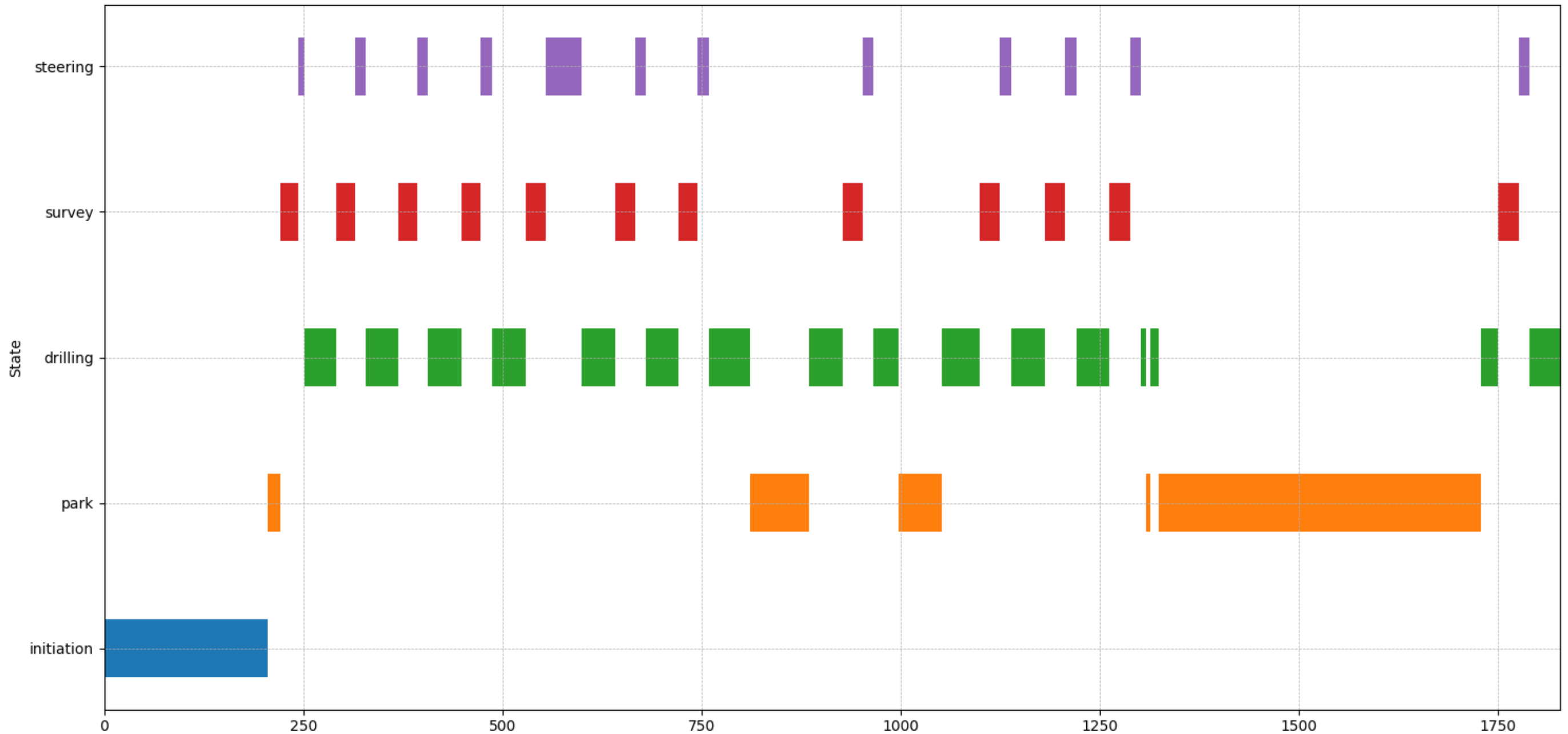
$$Time_{State,100mm} = \frac{\text{total time for a state}}{\text{total drilled distance}} * 100 \quad (11.3)$$

Another timing related observation was the planned breaks where the driller manually inputted a park state command. The commander responded as anticipated and didn't cause any trouble during manual override. The commander remained active throughout the entire park duration until the driller commanded to resume drilling. The system acknowledged this, restarted drilling, and proceeded with further surveys. The park state was activated a total of four times: twice for roughly one minute, once for a brief 5 seconds, and once for an extended period of approximately 7 minutes. None of these park interventions caused the commander to malfunction or produce timing errors.

11.2.3 Z-Axis Motor Error

Furthermore, there were evident malfunctions with the z-axis motor. Despite being in the drilling state, no drilling progress was observed due to the error state of the z-axis motor. Ideally, the machine should detect this and transition to the park state, turning off the motor to minimize unnecessary reaming. This precaution would ensure the preservation of a consistent hole size until the z-axis motor error is resolved. This also highlights the need for better error detection within the commander object. Since the z-axis travel can be observed by at least two sensors, a sanity check could be performed. If failed, the commander should raise an error and either resolve the error on its own or inform the driller. (Fixed)

State Durations Over Time (Gantt Chart)



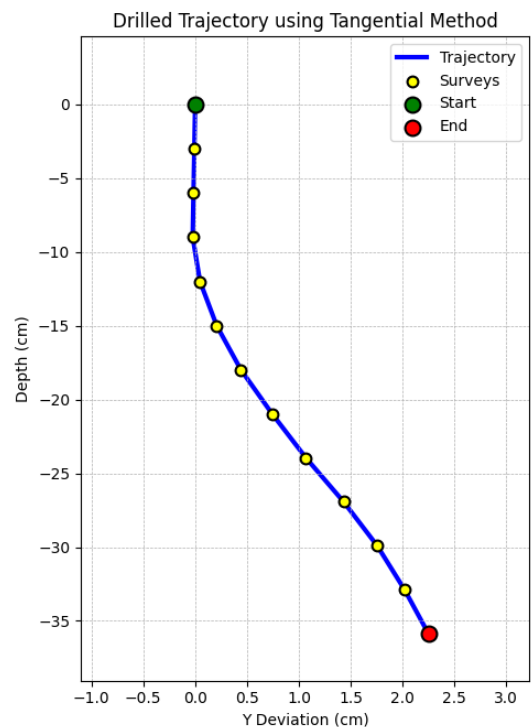
11.2.4 Trajectory

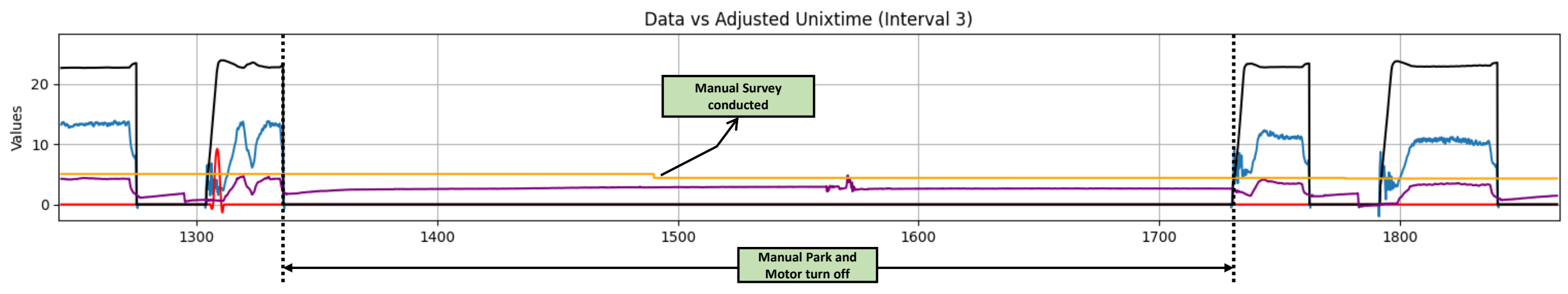
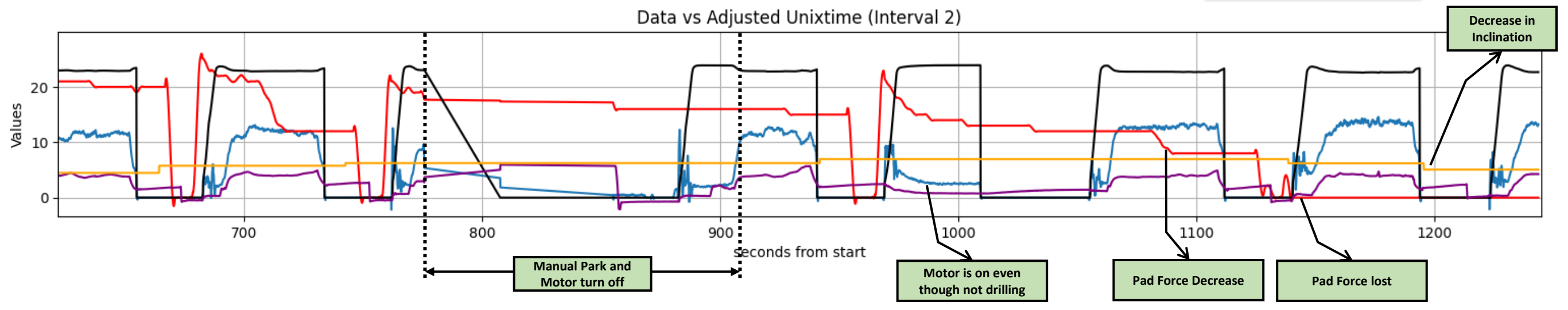
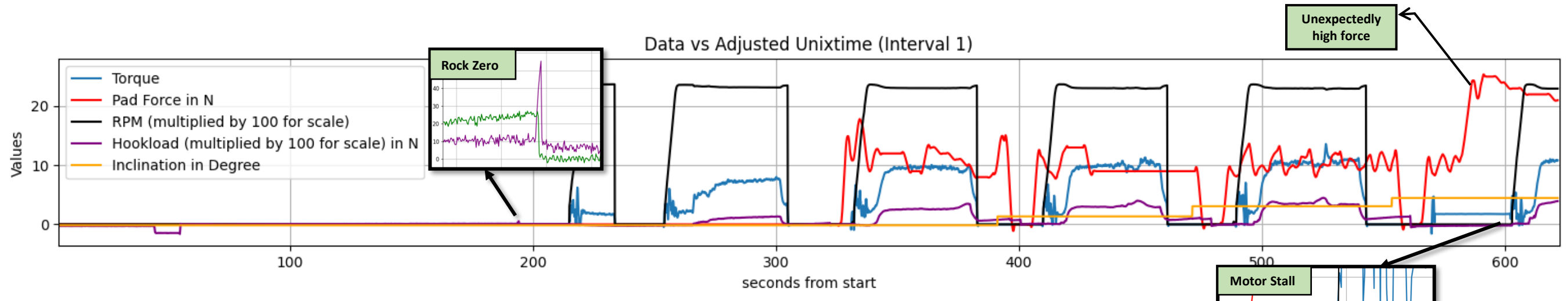
Analysis of the individual data charts from subsequent pages reveals multiple opportunities for improvement. A crucial observation is the need to adjust the controller for the pad forces to ensure they remain as static as possible. Although not directly resulting from the increased pad force, the active pad force did not rebound after retracting during the 10th survey. As a result, the inclination decreased over the subsequent drilling period, leading to a net decline of 3° from the peak inclination of 7° . The trajectory displayed in Figure 11.4 is derived using the Tangential method. This approach approximates the well path by considering the inclination and azimuth measured at the top end of each survey interval to be constant. Through this method, the trajectory achieves a Total Vertical Depth of 360 mm . Furthermore, the trajectory visualizes the horizontal shift, of 22 mm from the origin by the end of the drilling process.

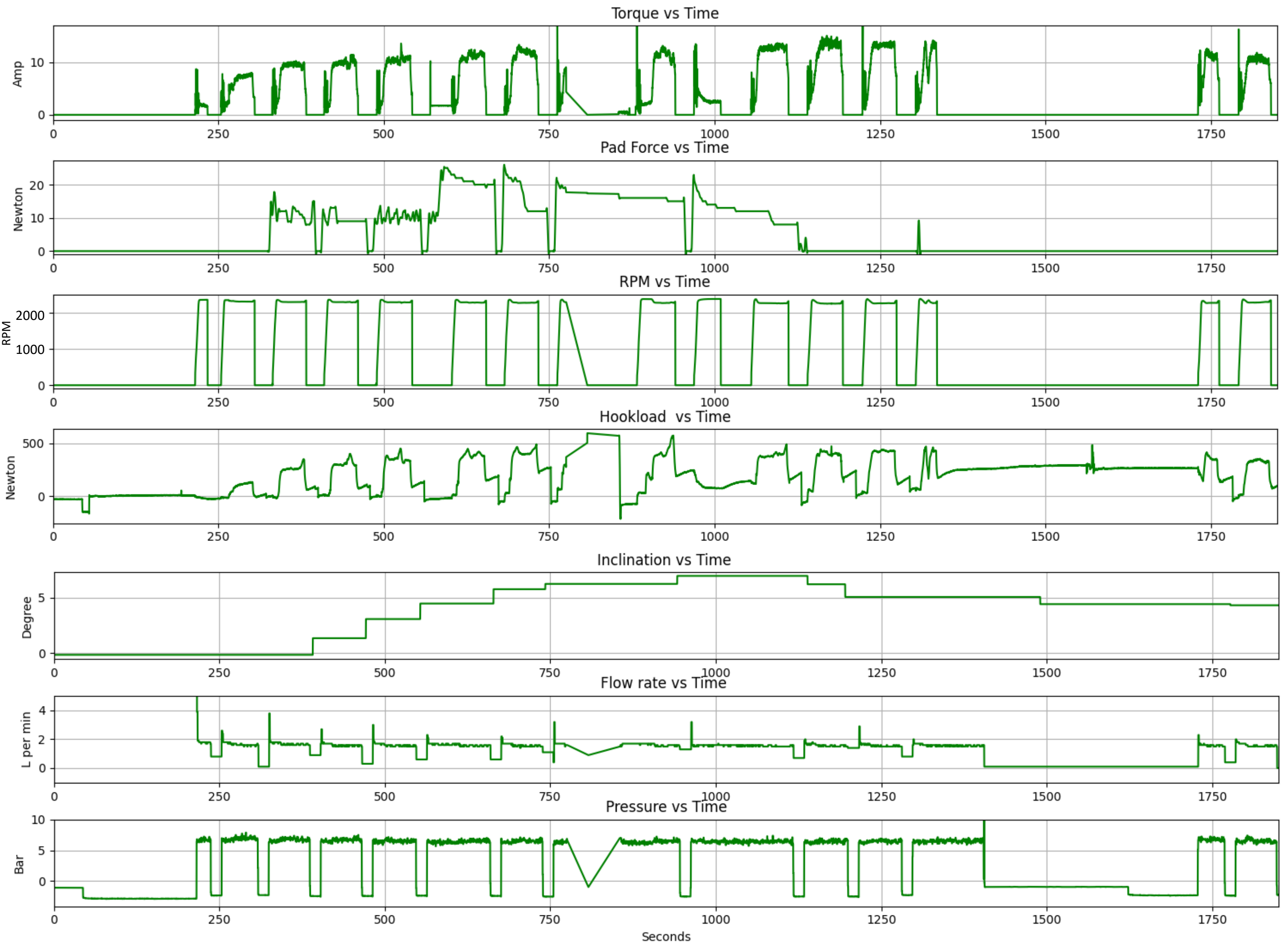
11.2.5 Additional Observations

Another observation, though not directly tied to the algorithm, was the drastic increase in pipe buckling upon activating the steering post the second survey. The resulting bending of the drill pipe compromised its stiffness, leading to an additional force deviating the *BHA* in a random direction. Although the steering controller should compensate this when having all three pads available. The vertical force needs to be sufficiently high which can not be obtained by the current drill pipe, findings indicate that the aluminum pipe should be replaced with a steel one to diminish buckling. Further inspection of the park intervals in the combined data plot 11.2.5 showed that the manual override needs enhancement. When the driller entered the park state, elements such as the motor, pumps, and pad force remained active, requiring manual deactivation. For safety reasons, transitioning to the park state should automatically turn off the motor and retract the wings. The Combined Data chart 11.2.5 reveals that even though the park state was manually activated and the motor was manually turned off, the pad force was overlooked. This oversight could pose challenges if the driller decides to manually trip out of the hole, potentially damaging the Bottom Hole Assembly.

Figure 11.4: Drilled Trajectory







12 End of Well Report

Operations Summary

The Operations Summary includes an overview of the drilling activities with specific focus on starting and ending times, drilled and measured depths, kickoff point, build-up ratio, and an overview of Non-Productive Time.

Geologic Summary

This section describes the geological aspects of the drilling site, including the types of rocks encountered and their dimensions.

Well Data Summary

The Well Data Summary presents critical drilling parameters such as RPM, WOB, pump rate, torque, measured depth, true vertical depth, and standpipe pressure. This data, collected every 100ms with a timestamp, is compiled and transferred to an CSV file for attachment to the report.

Wellbore Schematic

The Wellbore Schematic illustrates the trajectory taken during drilling, including various coordinate points.

Time vs. Depth Graph

This graph demonstrates the time taken to reach each depth, with a record of all activities within the given timeframe.

Drilling Program

This section details the drilling plan, encompassing the strategies and methodologies employed during the operation.

Mud Program

The Mud Program outlines the type of mud used for drilling, including its rheological values.

Directional Program

The Directional Program includes data collected by Bottom Hole Assembly sensors near the bit, which influences the drilling trajectory.

NPT/Incident Report

A comprehensive report on any incidents or problems encountered during drilling that led to operational delays or stoppages.

Note: This report serves as a critical tool for post-competition analysis, aiding in the creation of lessons learned and team reviews to assess successful strategies and areas for improvement.

12.1 Third-Party Interface

The system described here is a decentralized robot that can be controlled using the MQTT protocol, making it especially suitable for implementing a third-party interface. This integration can be achieved either by directly adapting the data and command structure in the target system or through an intermediary translation layer. The team is currently exploring the feasibility of implementing a translation layer compatible with the **DWIS** standard. Efforts will be made to establish closer collaboration with the **DWIS** group.

13 Further Rig Considerations

13.1 Power Consumption

The following values were recorded for the electronics of the entire drilling machine:

Device	Performance [kW]	Performance [HP]
Pump	1.6	2.16
Hoisting Motor	0.18	0.243
Rotary Table Motor	0.18	0.243
Top Drive	1	1.35
Remaining Electronics	0.1	0.135
Total	3.56	4.806

The drilling machine thereby consumes less than one fifth of the maximally allowed 25 horsepower of electrical power.

13.2 Rig Handling and Transportation

13.2.1 Design for Mobility

The rig's design prioritizes practical transportability. Key to this is the hoisting traverse, which has been engineered for easy detachment. This feature is essential for simplifying the rig's relocation and maintenance processes.

13.2.2 Quick Release Couplings

All electrical and hydraulic supply lines are equipped with quick release couplings. This significantly reduces preparation time and mitigates the risk of incorrect connections, thereby enhancing operational efficiency and safety.

13.2.3 Transport Configuration

Upon the removal of the hoisting traverse, it can be securely mounted horizontally onto the rig's support structure. This configuration is optimized for transportation, minimizing the rig's spatial footprint. In its transport mode, the rig measures:

- Height: 1600 mm (approximately 63 inches)
- Length: 2050 mm (approximately 80.7 inches)
- Width: 950 mm (approximately 37.4 inches)

These dimensions ensure that the rig remains compact and manageable during transit.

13.2.4 Weight Specifications

- **Total Weight:** The rig weighs 250 Kg (about 551 lbs.), making it relatively lightweight and easy to handle.
- **Chargeable Weight:** The maximum chargeable weight, including additional equipment, is 500 Kg (approximately 1102 lbs.).

13.3 Rock Sample Handling

In order to facilitate the placement of the rock sample into the rock sample receiver, it was decided not to incorporate an additional crane into the rig's design. This decision was influenced by the existing infrastructure at the institute's workshop, which is already equipped with a large overhead crane. This crane efficiently enables the loading and unloading of the rock sample receiver. The same logistical ease applies to the drilling simulator located in Celle.

In scenarios where the use of the overhead crane might be challenging, a mobile crane can be employed to handle the test stone. Given these existing resources and alternatives, the integration of a built-in crane into the rig was deemed unnecessary.

13.4 Rig Upscaling

13.4.1 Innovative Transmission Methods

Operating the Drillbotics® rig at a small scale presents unique opportunities to experiment with novel methods of transmitting data, fluids, and power, which might be unconventional in the oil and gas industry. Contrary to standard field applications, this rig utilizes a distinct approach where cables and fluid hoses are attached externally to the drill pipe to convey information and drilling fluid to the downhole area. Given the relatively modest depth of the borehole compared to the diameter of the Bottom Hole Assembly, this method is

quite effective. It bears resemblance to the concept of a wired drill pipe, where cables are sealed within the pipe, maintaining a direct connection. However, such technology has its limitations, especially in deeper drilling operations involving multiple connections.

13.4.2 Torque Transmission and Limitations

The torque needed to operate the drill bit is transmitted via a rotating shaft inside the static drill pipe, coated to reduce friction between the metal surfaces. This design, albeit unorthodox, faces practical challenges in field applications when upscaling the lubricant or coating, would need exceptional thixotropic properties, especially during downtimes. Additionally, the extra weight of the rotating shaft imposes increased hook load and stress on both the drill pipe and shaft, potentially leading to failure.

13.4.3 BHA Inclination and Steering

The concept for BHA inclination in the borehole is inspired by real-world applications, mirroring common push-the-bit rotary steerable systems. The BHA is equipped with extendable wings on its sides to steer in the desired direction. The key difference from field applications is in the control mechanism of these wings which is purely mechanical and actuated from the surface. Although mechanical actuation could be a potential application in the realworld, the actuation from the surface is something that would impose challenges

Note: The rig upscaling process involves exploring these innovative approaches, understanding their limitations, and drawing inspiration from real-world drilling systems to enhance the rig's capabilities.

13.5 Funding Plan and Sponsorship Update for 2023/24

13.5.1 New Organizational Structure

The TUC Drillbotics team has collaborated with the SPE Student Chapter e.V. starting from the year 2023/24. This integration within the SPE Student Chapter e.V. has been strategically decided to align with German regulations concerning funding and sponsorship acquisition. Previously, the TUC Drillbotics team relied on donations from various companies, but under the new structure, official sponsorships are now feasible.

13.5.2 Sponsorship Acquisition Phase

The report phase in the upcoming competitions will also serve as a crucial phase for sponsor acquisition. Potential sponsors are presented with various sponsorship packages, offering different levels of advertisement placements. The details of these sponsorship ranks are illustrated in **Figure 13.5.4**.

13.5.3 Current Sponsorship Status

As of this year, we are proud to announce that MICON Drilling has become the official GOLD Sponsor of the TUC-Drillbotics team. This marks a significant milestone in our team's growth and development.

13.5.4 Financial Overview

- **Projected Expenses:** For the current year, while a detailed list of expenses is yet to be finalized, our planned projects and ambitions necessitate a minimum budget of €6,000.
- **Current Funds:** As of now, our account holds a balance of €3,000.

Note: We are actively working on securing additional sponsorships and funds to meet our projected budget and support our ambitious projects for the year.



TUC Drillbotics®

learning & creation

BRONZE-SPONSOR

Base: Website, Publications*

1000 €

SILBER-SPONSOR

Base: Website, Publications*, Logo on Rig (S)

2000 €

GOLD-SPONSOR

Base: Website, Publications*, Logo on Rig (M), Logo on T-shirt

3000 €

PLATIN-SPONSOR

Base: Website, Publications*, Logo on Rig (S), Logo on T-shirt, Banner on Mast, Banner/Logo in our Digital Drilling Lab (Working Space)

6000 €

Plus Package

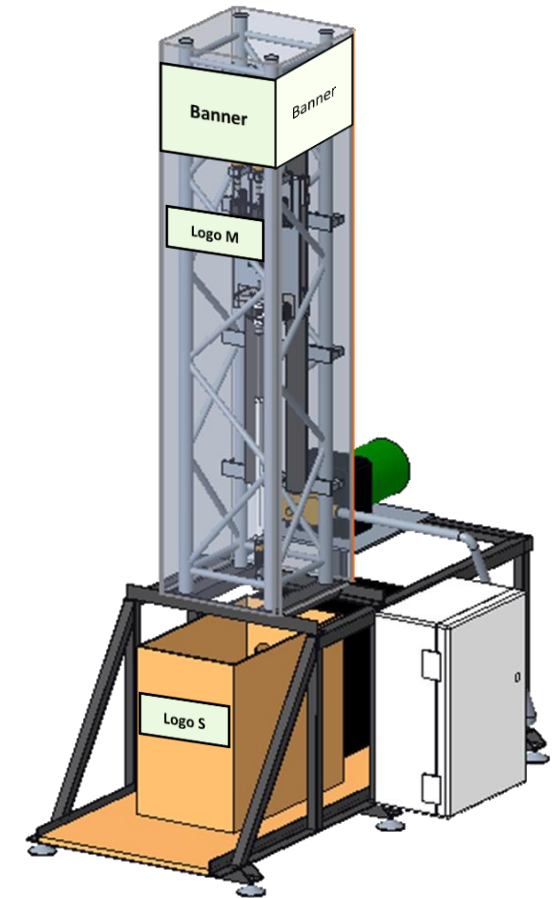
2 Year duration for 12% discount!

*Posters, Presentations, and Reports

Standard sponsoring duration is 12 months starting from October of the current year.

Logo on Rig (S) means a sticker of the logo on the base of the rig either on rock sample receiver, base chassis, or electronic cabinet.

Logo on Rig (M) means a sticker of the logo on the Mast.



13.6 Acknowledgement

We would like to thank all institutions and companies that have financed and supported the TU Clausthal Drillbotics project this year.

GOLD SPONSORS



Previous Doners



14 Safety Consideration and Risk Analysis

14.1 Safety Plan

The team's safety plan prioritizes preventing accidents among team members and individuals near the rig's operating zone. Recognizing the unpredictability of accidents, the plan emphasizes immediate response actions.

14.1.1 Safety Protocols and Training

All personnel working on the rig receive comprehensive safety briefings. No one is allowed to work alone or without supervision. Prior to any work, it must be verified that the power is off, and reactivation of power is strictly controlled to ensure the safety of personnel in the vicinity.

During testing and drilling operations, there is a strict prohibition on touching or moving close to the rig. For emergency situations, an easily accessible emergency stop switch is installed to immediately cut off the power supply.

14.1.2 Physical Barriers and Protective Measures

Physical barriers, including safety tape and acrylic glass cladding, are deployed to prevent access to moving, rotating, and pumping parts of the rig. These barriers are placed at a safe distance to ensure the protection of all personnel.

14.1.3 Communication and Emergency Response

The workspace is equipped with communication devices, allowing immediate contact with supervisors and advisors in case of an accident. This ensures prompt response and escalation of any incidents.

14.1.4 Human Factor

Human factors play a crucial role in safety management. These include potential errors, lack of attention, incorrect behavior, and inadequate training. To mitigate these risks:

- All team members undergo a comprehensive week-long training program focused on rig operations, safety protocols, and emergency response.
- Regular refresher courses are conducted to maintain high safety standards and awareness.
- A culture of safety is promoted, encouraging team members to prioritize safety and report potential hazards.

14.1.5 Risk Assessment and Continuous Improvement

- Regular risk assessments are conducted to identify and mitigate potential hazards associated with rig operations.
- Feedback from team members is actively sought and used to continuously improve safety protocols.
- Safety equipment and procedures are regularly reviewed and updated in line with industry standards and technological advancements.

14.1.6 Technical safety

Riskname	Risk Description	Risk control strategy
Drilling fluid (water) leaking	Drilling fluid leaks from hose or circulation system	Use suitable hose and circulation system (e.g. hose with appropriate pressure rating capacity). The circulation system will be checked before and while testing.
Pumps working at high pressures	Pumps and hoses where the drilling fluid is flowing through may cause serious damage to personnel and equipment if there is any kind of leaking due to the high pressures.	Pumps and valves will be pressure tested before starting any operation, 5 min at low pressure and 10 min at high pressures. At this time only authorized personnel will be allowed to be near the drilling rig. A zone will be set up for visitors or other competitors to not pass through during this time.
String wobbling	String vibration/wobbling	Start drilling at low RPM then increase gradually after reaching a certain depth e.g. 1/4". Set the limit of the RPM in algorithm. During this time the string will be observed for any non-normal operations and the vibrations will be recorded to see any abnormalities.
Bit walking	Bit drills deviated away from the trajectory plan. This risk is also associated with string wobbling.	Install a guide shoe or riser/casing at rotary table above the rock sample thus limiting the drill string wobbling. Install downhole sensors, which are accelerometer and gyro, and integrates the acquisition data with algorithm to self-control the drilling trajectory.

Drill string stuck	Drill string stuck due to unclean hole or cutting is not circulated properly from the hole	Apply minimum flow rate according to minimum cutting transport velocity estimation. Apply also minimum drill string rotation speed (RPM) according to design calculation to help hole cleaning.
Loss verticality of hole section	Drill directional hole or deviated trajectory away from the plan	Install downhole sensors (accelerometer and gyro) and integrates acquisition data with algorithm program. Apply algorithm program to maintain verticality to selfcontrol string while drilling.
Drill string buckling and twist off	The weakest part along the drill string is drill pipe. Another potential weak part is connection. Buckling and twist off could occur during the drilling.	Use high strength connection type for all parts of the drill string, particularly the drill pipe. Calculations are made to avoid going over the critical buckling load and set the WOB limit and RPM. Estimate the limit strength of drill pipe then limit the WOB and RPM to avoid the failure according to the design calculation. Set the WOB and RPM limit in the algorithm. Avoid going over the critical buckling load. In case much vibration occurs, alert (alarm) system will be active thus students can respond.

Cutting and drilling fluid spill and disposal	During the drilling, cutting, and drilling fluid will flow out of the well to the surface and must be disposed properly.	Safety containment will be installed around the rock sample and rig structure (below), thus the cutting and drilling fluid circulation (outflow) can be stored properly. The safety containment will be made from transparent material (e.g. plastic, etc.), thus the drilling process can still be observed. Additional storage containment will be installed also to store more cutting and drilling fluid circulation out of the well or rock sample. The cutting and drilling fluid outflow circulation will be recorded and disposed according to regulations (university and state regulations), particularly if there is chemical content. A general procedure will be included together with HSE procedure.
Electric cables and water hoses	Cables and hoses lying around which is a serious tripping hazard. Damaging of the equipment, tool failures and health restrictions might be consequences	Cable shafts for electric cables as well as hose guards will be laid to gather the loose components. Additionally, clearly visible warning labels will be put up to make people aware of the hazard

Table 14.1: Technical safety

14.1.7 Human safety

Riskname	Risk Description	Risk control strategy
Short circuit and/or electrical hazard	The risk is associated with electrical cable or source	Proper handling of electrical cable shall be applied, especially the avoidance from liquid (water). All electrical systems must be set up properly, soldered, installed, and connected to power source carefully and if it is possible enclosed system (use protector) and contained in one place. All the steps associated with setting up electrical must be done with safety concerns and safety protector (if applicable). Minimum safety equipment (e.g. safety glasses, gloves, etc.) must be worn during the electrical installation. No electrical connections should be made when connected to power. Every casing that has electrical components should be grounded to avoid any electrical injury to personnel.

Mechanical construction risk	During build up and/or testing, risk associated with pinch points, punctures, lacerations, cutting debris etc., could cause damage and hazard.	<p>Proper handling of material and pieces during building up the rig structure, particularly it is mandatory to wear the proper HSE equipment according to minimum standard (e.g. safety shoes, safety glasses, gloves, etc.). Students will also work from a certain height during building up the rig structure, thus precautions must be taken to prevent injuries. A certain range of zone isolation must be set thus nonrelated person will be allowed to pass the zone. A general working procedure (Standard Operating Procedure/SOP) will be set before rig construction work.</p> <p>The connection of all parts and pieces of rig structure must be checked properly during and after rig construction to confirm the solid rig structure, thus avoiding the loose pieces during the drilling or test. All the sharp edges in rig structure will be covered or protected with protector to avoid human injures. Any items that could potentially fall from any height or loosen through vibrations or high rpm should be secured with a string to some other part, to ensure that no part flies out or falls</p>
------------------------------	------------------------------------------------------------------------------------------------------------------------------------------------	----------------------------------------------------------------------------------------------------------------------------------------------------------------------------------------------------------------------------------------------------------------------------------------------------------------------------------------------------------------------------------------------------------------------------------------------------------------------------------------------------------------------------------------------------------------------------------------------------------------------------------------------------------------------------------------------------------------------------------------------------------------------------------------------------------------------------------------------------------------------------------------------------------------------------------------------------------------------------------------------------------------------------------------------------------------------------------------------------------------------------

<p>Hazard during drilling or testing</p>	<p>Accident and hazard during drilling or testing could occur.</p>	<p>The drilling automation (through algorithm and computer control) is set up thus less or even no human intervention is needed during the test. However, supervision during the test is still needed. Before the test or drilling is started, safety meeting will be held to discuss the procedure and any potential hazard. Emergency shutdown is included in algorithm program and will active in case serious hazard occurs. The emergency shutdown can also be activated manually (intervention from human) in case the self-control program does not work properly. In case there is obstacle or restriction in circulation system that causing increase of the pressure, emergency shutdown system will be activated (included in algorithm) at certain limit of pressure and relief valve is installed to release the pressure.</p> <p>A general testing procedure (Standard Operating Procedure/SOP) will be set before drilling or testing. Minimum HSE equipment standard must be worn (e.g. safety glasses, hearing protection, etc.). A certain range of zone isolation must be set thus unauthorized person will not be allowed to pass the isolation zone. A fire extinguisher will be available on location in case fire occurs due to overheating of electronic components or motor, etc.</p> <p>The hoisting system has locking mechanism to stop the movement in case lost control happens.</p>
------------------------------------------	--------------------------------------------------------------------	--------------------------------------------------------------------------------------------------------------------------------------------------------------------------------------------------------------------------------------------------------------------------------------------------------------------------------------------------------------------------------------------------------------------------------------------------------------------------------------------------------------------------------------------------------------------------------------------------------------------------------------------------------------------------------------------------------------------------------------------------------------------------------------------------------------------------------------------------------------------------------------------------------------------------------------------------------------------------------------------------------------------------------------------------------------------------------------------------------------------------------------------------------------------------------------------------------------------------------------------------------------------------------------------------------------------------------------------------------------------------------------------------------------------

Flying debris	Debris that breaks free when cleaning the hole can be unsafe during the drilling process	To maintain the debris confined in the drilling area and to avoid any flying debris to harm anyone around the drilling area, a plastic cover will be installed to protect the personnel around it.
Mobility of the rig		The mobility of rig is incorporated in the design. The rig structure will be placed above the table and wheels will be installed below the table; thus, the rig can be mobilized. A brake system will be included in wheels to prevent undesired rig movement during drilling or testing due to vibration. Proper handling system will be installed so the rig can be moved safely and in convenient way. Modular design will be considered and as far as possible applied in the rig construction, such as electrical, computer, pump and disposal storage that can be disassembled or separated. This will make the mobilization and transportation more convenient and safer.
Rig transport	Pinching of fingers due to handling the rig	To avoid finger pinching the rig will be always handled with a forklift or a portable crane. Wood pieces will be placed on the bottom and sides of the rig when securing it for transportation in case it needs to be handle with the hand to accomplish the correct position. It is prohibited to put a hand under the rig when its being lifted.

Rock sample handling	Personnel can get injured by improperly handling the rock sample	The rock sample will be lifted by a lifting crane, thus avoiding any manual handling from personnel. While lifting the rock sample safety shoes and high impact gloves are to be worn. No other work is to be performed at the time of lifting and unauthorized personnel will be instructed to step back.
----------------------	------------------------------------------------------------------	------------------------------------------------------------------------------------------------------------------------------------------------------------------------------------------------------------------------------------------------------------------------------------------------------------

Table 14.2: Human safety

14.1.8 Communication safety

Riskname	Risk Description	Risk control strategy
Communication error	Failure during data acquisition due to communication system error	Correct system communications will be controlled by someone in the personnel to ensure good data acquisition and communication between the different systems. System restart will be designed, so whenever data is failed to be acquired, by restarting the system, data acquisition can work properly.
Sensor error	Failure during data acquisition due to sensor failure	The sensors will be tested before and after installation. After each test or drilling, maintenance will be performed to confirm whether the sensors can still function properly.

Table 14.3: Communications safety

15 Appendix

15.1 A: Data and Assumptions

Based on the 2022 Drillbotics competition guidelines, some assumptions and basic information for calculation and engineering design are summarized:

Table 15.1: Drilling hole and rock data

Drilling hole and rock data	Field unit	Metric unit
Hole diameter (d_h)	1.5 in	38.1 mm
Rock strength	2-5 ksi	13.8-34.5 MPa
Cutting concentration (C_{conc})	1.5%	1.5%
Height of rock	24 in	0.6 m
Cutting density (ρ_s)	165.43 lb ft^{-3}	2650 Kg m^{-3}
Diameter cutting (d_s)	0.004 -0.04 in	0.1-1mm
ROP	0,8 ft/hr	0.24 m/hr

Table 15.2: Rig Specifications

Size	RPM	Pressure	Flow	Drill Bit ϕ	max WOB	DP Length
2m x 1m x 3m	2700 min^{-1}	8 Bar	4 L $\cdot min^{-1}$	38 mm	300N	1 m

Table 15.3: Overview of Data and Actuator

Subsystem	Actuator	Data
Circulation System	Pump Power on/off	Flow Rate, Pressure
Rotation System	BLDC Power on/off BLDC RPM RT Step Amount RT Execution Speed	BLDC Temperature BLDC RPM BLDC Torque RT Position
Hoisting System	Z-Axis power on/off Z-Axis Step Amount Z-Axis Execution Speed	Hookload WOB Measured Depth
Steering System	Surface Steering unit	Azimuth Inclination Pad Force Pad Position

Table 15.4: Drilling fluid data

Drilling fluid data	Field unit	Metric unit
Water viscosity	1 cp	0.001 Pas
Water density	8.33ppg	1000 Kgm^{-3}

Table 15.5: Drill pipe data

Steel drill pipe data	Field unit	Metric unit
Ultimate Tensile Strength	73244 psi	505 MPa
Yield strength (Y_s)	31183 psi	215 MPa
Modulus of elasticity (E)	$2.901 * 10^7$ psi	200 GPa
Weight	0.1493 lb/ft	0.2233 Kg/m
Outside diameter (d_p)	0.393 in	10 mm
Outside radius (r_o)	0.1968 in	5 mm
Inside diameter (id_p)	0.31496 in	8 mm
Inside radius (r_i)	0.15748 in	4 mm
Wall thickness (t)	0.0787 in	2 mm
Length (L_{dp})	36 in	0.91 m
Roughness	0.0006 in	0.0152 mm

Table 15.6: Stabilizer / downhole BHA data

Stabilizer/downhole BHA data	Field unit	Metric unit
Outside diameter (d_d)	1.46 in	37 mm
Diameter Flowline	0.15in	4 in
Length Flowline	3.14in	124 mm
Diameter shaft	0.19 in	5 mm
Length shaft	0.19 ft	60 mm
Length (L_{dw})	7.28 in	185 mm
Roughness	0.0039 in	0.1 mm
Inside diameter (id_d)	0.6 in	15.2 mm
Wall thickness (t)	0.1 in	2.54 mm
Length (L_{dw})	3.5 in	8.9 cm
Roughness	0.0006 in	0.0152 mm

Table 15.7: Bit data

Bit data [DSATS provided]	Field unit	Metric unit
Bit diameter	1.5 in	38.1 mm
Nozzle diameter	0.118 in	3 mm
Discharge coefficient	0.95	0.95

Table 15.8: Calculation Results

Parameter	Symbol	Calculated Result	
		Field Units	Metric Units
Critical buckling load	P _{bcr}	151.92 lbf	675.77 N
Burst limit	P _{burst}	8326.04 psi	574.06 bar
Torsional Stress limit	τ	218.25 in.lbf	24.66 Nm
Flow rate	Q	1.84 gpm	7 Lpm
Pump pressure	P _{pump}	118.76 psi	29.7 bar
Pump horsepower	HPP	0.12 HP	0.46HP

Table A.1: Inertial Measurement Unit Module

IMU Module			
Address	Message	IN/OUT	Content
0x20	pong	OUT	nan
0x21	ping	IN	nan
0x22	request	IN	nan
0x23	data accelerometer	OUT	$acc_x / acc_y / acc_z$
0x24	data magnetometer	OUT	$mag_x / mag_y / mag_z$

Table A.2: WOB Module

WOB Module			
Address	Message	IN/OUT	Content
0x30	pong	OUT	nan
0x31	ping	IN	nan
0x32	tare	IN	nan
0x33	data	OUT	WOB Filtered / WOB Unfiltered
0x34	calibration	IN	Unit Conversion / Filter Constant

Table A.3: Hookload Module

Hookload Module			
Address	Message	IN/OUT	Content
0x40	pong	OUT	nan
0x41	ping	IN	nan
0x42	tare	IN	nan
0x43	data	OUT	WOB Filtered / WOB Unfiltered
0x44	calibration	IN	Unit Conversion / Filter Constant

Table A.4: Steering Module

Steering Module			
Address	Message	IN/OUT	Content
0x50	pong	OUT	nan
0x51	ping	IN	nan
0x52	write	IN	$PF_1 / PF_2 / PF_3$
0x53	homing	IN	nan
0x54	$wing_0$	OUT	Force / Position
0x55	$wing_1$	OUT	Force / Position
0x56	$wing_2$	OUT	Force / Position

Table A.5: Motor Module

Motor Module			
Address	Message	IN/OUT	Content
0x60	pong	OUT	nan
0x61	ping	IN	nan
0x62	set	IN	RPM
0x63	data	OUT	Torque / RPM
0x64	power	IN	1 / 0

Table A.6: Z-Axis Module

Z-Axis Module			
Address	Message	IN/OUT	Content
0x70	pong	OUT	nan
0x71	ping	IN	nan
0x73	position	OUT	Position / Delta
0x74	homing	IN	nan
0x75	movex	IN	Steps / Speed
0x76	moveto	IN	Position / Speed

Table A.7: Rotarytable Module

Rotarytable Module			
Address	Message	IN/OUT	Content
0x80	pong	OUT	nan
0x81	ping	IN	nan
0x83	position	OUT	Position / Delta
0x84	homing	IN	nan
0x85	movex	IN	Steps / Speed
0x86	moveto	IN	Position / Speed

Table A.8: Relay Module

Relay Module			
Address	Message	IN/OUT	Content
0x90	pong	OUT	nan
0x91	ping	IN	nan
0x92	write	IN	0 / 1 for each Relay
0x93	data	OUT	0 / 1 for each Relay

Table A.9: Flowmeter Module

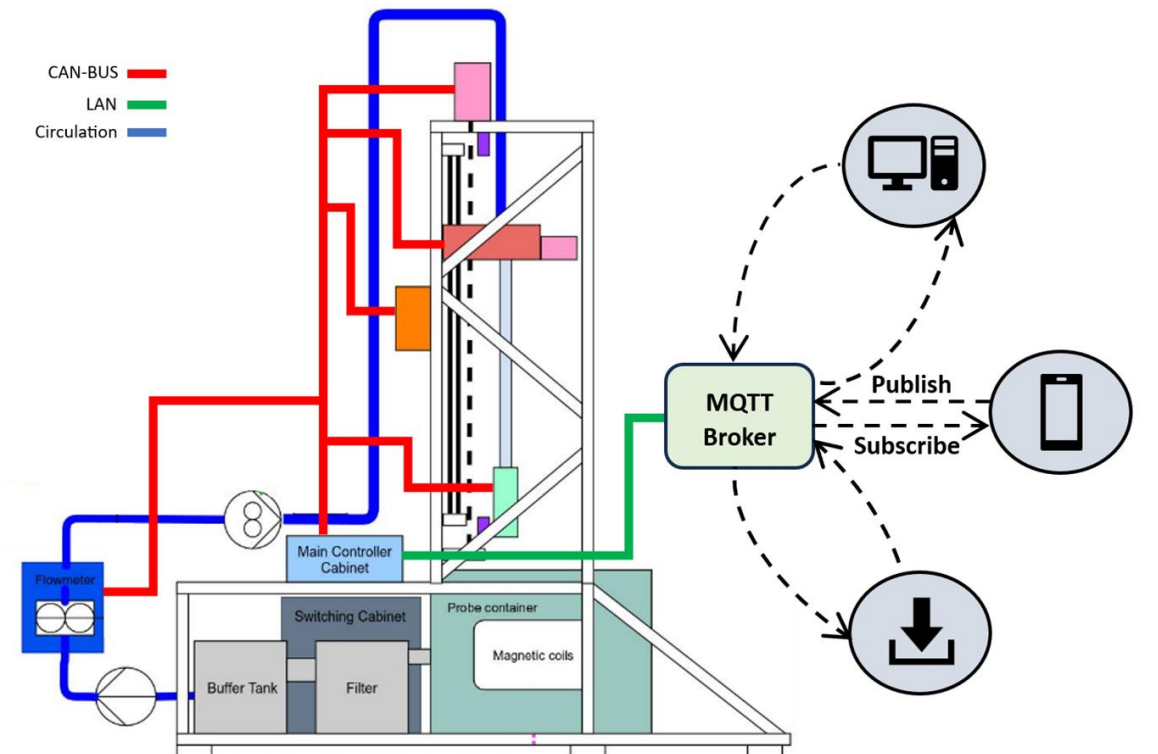
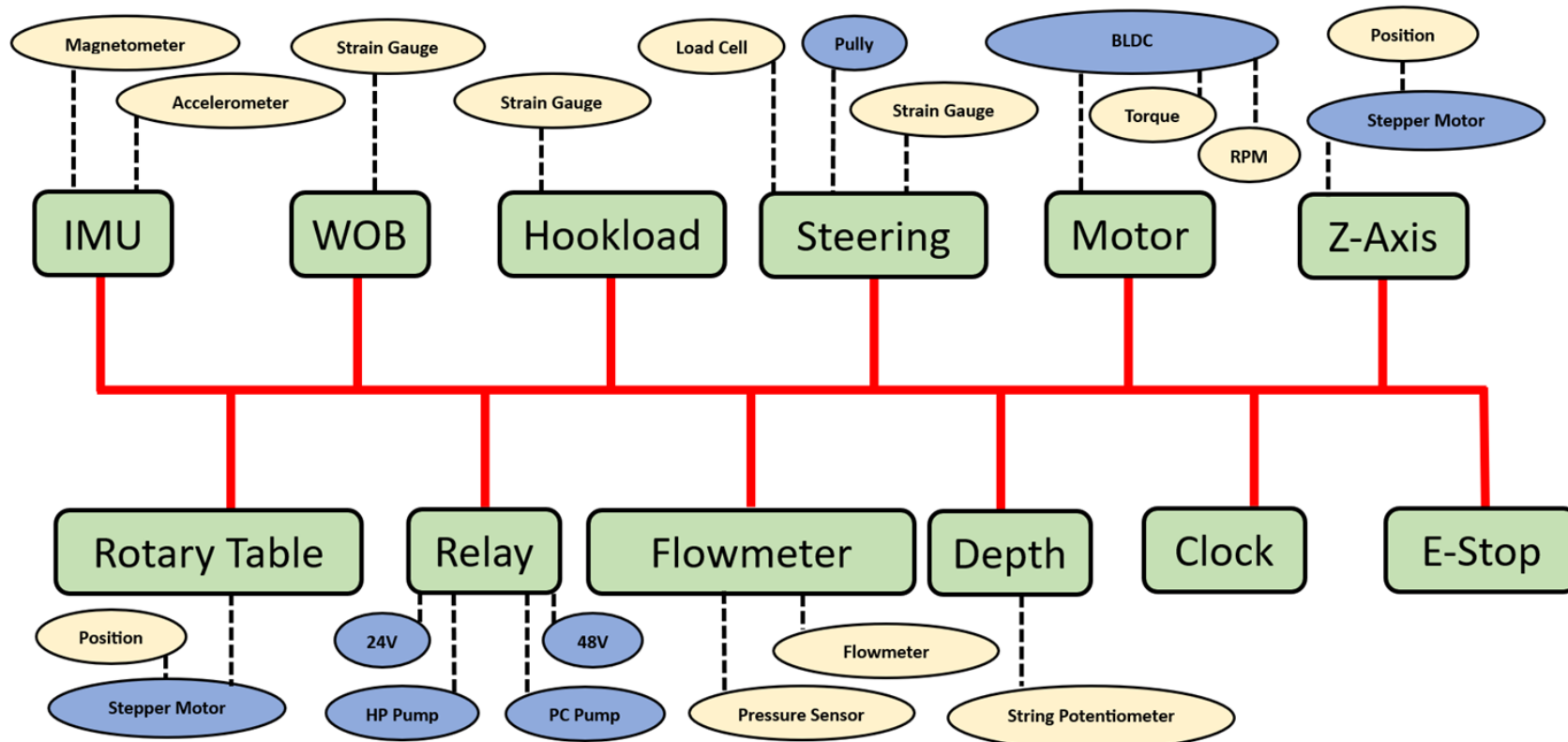
Flowmeter Module			
Address	Message	IN/OUT	Content
0xA0	pong	OUT	nan
0xA1	ping	IN	nan
0xA3	data	OUT	Pressure / Flow
0xA4	cali	IN	Unit Conversion / Filter Constant

Table A.10: Depth Module

Depth Module			
Address	Message	IN/OUT	Content
0xC0	pong	OUT	nan
0xC1	ping	IN	nan
0xC3	data	OUT	depth
0xC5	tare	IN	nan

Table A.11: Clock Module

Clock Module			
Address	Message	IN/OUT	Content
0xF0	pong	OUT	nan
0xF1	ping	IN	nan
0xF2	restart	IN	nan
0xF3	getntp	IN	nan
0xF4	setup	IN	0 / 1



A Bibliography

- [Aadnoy 2006] AADNOY, Bernt S.: *Mechanics of Drilling* -. Aachen : Shaker, 2006. – ISBN 978-3-832-24861-1
- [Fisher 2023] FISHER, Christopher J.: *AN-1057: Using an Accelerometer for Inclination Sensing*. <https://www.analog.com/en/app-notes/an-1057.html>. Version: 2023. – Accessed: [Your Access Date Here]
- [HiveMQ 2019] HIVEMQ, Team: *MQTT Essentials Part 3: Client-Broker Connection Establishment*. <https://www.hivemq.com/blog/mqtt-essentials-part-3-client-broker-connection-establishment/>, 2019, July 17. – Accessed: 13.08.2023
- [Multithreading] MULTITHREADING: *Multithreading – Wikipedia*. <https://de.wikipedia.org/wiki/Multithreading>. – Accessed: 2023-08-14
- [Parasuraman et al. 2000] PARASURAMAN, Raja ; SHERIDAN, Thomas B. ; WICKENS, Christopher D.: A Model for Types and Levels of Human Interaction with Automation. In: *IEEE Transactions on Systems, Man, and Cybernetics - Part A: Systems and Humans* 30 (2000), Nr. 3, S. 13
- [PhD u. Liu 2011] PHD, Boyun G. ; LIU, Gefei: *Applied Drilling Circulation Systems - Hydraulics, Calculations and Models*. Orlando, Florida : Gulf Professional Publishing, 2011. – ISBN 978-0-123-81958-1
- [R. 2011] R., Hamrick T.: *Optimization of Operating Parameters for Minimum Mechanical Specific Energy in Drilling*. West Virginia University Morgantown West Virginia (2011), 2011
- [Rodrigues 2022] RODRIGUES: *Rodrigues' rotation formula — Wikipedia, The Free Encyclopedia*. https://en.wikipedia.org/w/index.php?title=Rodrigues%27_rotation_formula&oldid=1122338410, 2022. – [Online; accessed 19-August-2023]
- [Thread Safety 2023] THREAD SAFETY: *Race condition — Wikipedia, The Free Encyclopedia*. https://en.wikipedia.org/w/index.php?title=Race_condition&oldid=1167011819, 2023. – [Online; accessed 14-August-2023]